

Escuela Técnica Superior de Ingeniería de Telecomunicación
Universidad Politécnica de Cartagena



(a)



(b)

Proyecto Final de Carrera

Bandpass Filters for Space Applications with Wide Spurious-Free Range



Author: José Manuel Pérez Escudero

Director: Alejandro Alvarez Melcón

Codirector: José Antonio Lorente Acosta

Codirector: Mariano Pamies Porras

Telecommunication Engineering

Author	José Manuel Pérez Escudero
Author's email	jm.perez.escudero@gmail.com
Director	Alejandro Álvarez Melcón
Director's email	alejandro.alvarez@upct.es
Co-director	José Antonio Lorente Acosta
Co-director	Mariano Pamies Porras
Title	Bandpass Filters for Space Applications With Wide Spurious-Free Range
<p>Summary</p> <p>Design of microwave fillters is an important activity, due to the fact that microwave are an integral part of a lot of communications systems; specially in spatial communications systems or terrestrial mobile systems. In the microwave field, waveguide technology still has a very large acceptance, above all in high power applications, and the cases in which the losses reduction is an important factor that has to be taken into account.</p> <p>In this project, it will be reviewed waveguide technology for bandpass filters design and new techniques which try to increase the spurious-free range will be investigated. Concretely, a new concept will be explored in order to remove such spurious band. This technique is based on the control of the coupling windows widht.</p> <p>In addition, it has been worked in the design of a bandpass filter for an antenna phase array that work at S-band. This filter has been designed in SIW (Substrate Integrated Waveguide) technology. Finally, it has been studied the use of this waveguide loaded with Ring Resonators and Complementary Split Ring Resonator (CSRR) for the realization of bandpass fiters with size reduction.</p>	
Degree	Ingeniero de Telecomunicación
Department	Tecnologías de la Información y la Comunicación
Submission date	July 2013

Agradecimientos

Primero me gustaría dar las gracias a todo el equipo docente de la UPCT, por los conocimientos transmitidos y por el apoyo cuando los exámenes no salían como debían. En general, los profesores de la UPCT son grandes personas. También quiero agradecer a Jose Antonio Lorente por su paciencia al explicarme cómo diseñar filtros con el software que iba a usar. A Mariano Pamies por supervisarme en el instituto de Fraunhofer y fuera de él, gracias por integrarme tan bien y hacerme conocer a gente tan buena como me presentaste. Gracias gente por esos coffee-breaks, salidas a comer fuera, por los partidos de fútbol de los viernes, por los viajes de autobús (nos gusta el autobús)... En definitiva, gracias a mi familia Fraunhofiana por hacerme sentir como en casa desde el primer día. A Thomas Bertuch, gracias por tu ayuda y tus ideas para seguir avanzando en el trabajo y cumplir con los objetivos, he aprendido bastante y ha sido un placer poder pertenecer a tu grupo de trabajo. Finalmente, mención especial para Alejandro Álvarez Melcón, puesto que ha sido el encargado de revisar este proyecto, porque sin él, este trabajo no habría salido adelante, por su paciencia para explicarme lo mismo una y otra vez hasta que las cosas estaban claras y por ponerme en contacto con el instituto de Fraunhofer para poder vivir una experiencia inolvidable.

A todos mis amigos que me arrastraban de casa en la época de exámenes para despejar un poco la mente, por aguantarme cuando en la época de exámenes uno se vuelve insoportable, está claro que sin esos momentos de relax jugando al billar y con unas cervezas, los estados de locura transitoria habrían sido más numerosos y por supuesto mucho peores.

A los compañeros de clase que siempre hemos permanecido unidos, me alegro de haber estudiado esta carrera además de por razones profesionales, por el hecho de haber podido conocer a gente tan maravillosa como son todos esos compañeros. Tantas horas de prácticas, clases, apuntes que se pasan de unos a otros, horas en la biblioteca resolviendo exámenes de años anteriores y sobre todo, esos momentos de cantina donde los exámenes y los estudios en sí son lo de menos...

Por último y lo más importante, he de agradecer este trabajo a mi familia. A mis hermanas por su paciencia, su ayuda y sus bromas. A mis padres, porque sin ellos no habría podido llegar donde he llegado. Todo lo que he conseguido y lo que soy es gracias a ellos, tengo que agradecerle todo lo que han sacrificado para que yo pudiese hacer lo que me gustaba. He aprendido de sus consejos y su forma de hacerme ver el mundo, que si el vaso se vacía ya habrá algo con lo que llenarlo. En esta vida sólo hay que tener paciencia y constancia para conseguir todo lo que uno se propone. En definitiva, porque cuando he vivido momentos difíciles ellos son los que siempre han estado y estarán ahí. Estoy seguro que si no fuese por ellos habría abandonado y ahora no estaría escribiendo esto.

*Dedicado a
mi familia*

Contents

1	Introduction	1
1.1	Brief history of microwave filters	1
1.2	Motivation	2
1.3	Description and organization of the work	4
2	Design of Waveguide BandPass Filters	7
2.1	Types of filter	7
2.1.1	Types of filter depending on passband	9
2.1.2	Types of filters depending on their transfer function	11
2.2	Chebyshev Filter	12
2.3	Low-Pass Prototype	14
2.3.1	Chebyshev Lowpass Prototype Filter	15
2.4	Frequency and elements transformation	15
2.5	Bandpass Filter Model	17
2.5.1	Bandpass filter based on impedance inverters	18
2.5.2	Transmission Line Model and Impedance Inverter Model	20
2.6	Synthesis Dimension	23
2.6.1	Iris width	23
2.6.2	Cavity length	24
2.7	Summary to design waveguide bandpass filters	26
3	Technique to reduce spurious in waveguide BandPass filter	27
3.1	Introduction	27
3.2	Spurious reduction using non-uniform coupling windows	27
3.3	Spurious reduction using non-uniform cavities	35

4	More Illustrative Examples of Spurious Reduction	39
4.1	Filters using constant coupling windows thicknesses	39
4.2	Filters using non-uniform coupling windows thicknesses along the filter	45
4.3	Filters using non-uniform cavity width	48
4.4	Filters using both non-uniform coupling windows and non-uniform waveguide widths .	53
5	Design of SIW BandPass filter	57
5.1	SIW technology considerations	57
5.2	Transformation from SIW to Waveguide	59
5.3	Transition between Substrate Integrated Waveguide and μ Strip	60
5.3.1	Transition using a tapered μ Strip line	60
5.3.2	Transition using an impedance inverter	63
5.4	Experimental results	63
6	Techniques for size reduction	69
6.1	Substrate Integrated Waveguide loaded with Ring Resonator	69
6.2	Substrate Integrated Waveguide loaded with Complementary Split-Ring Resonator . .	71
6.2.1	Substrate Integrated Waveguide simetrically loaded with Complementary Split Ring Resonator	71
6.2.2	Substrate Integrated Waveguide Asimetrically loaded with Complementary Split Ring Resonator	76
6.3	Intedigital Filter using μ Strip technology	78
7	Conclusions and future work	83
8	Appendix	85
8.1	Table of Dimensions	85
8.1.1	Table of the first coupling window	85
8.1.2	Table of the second coupling window	87
8.1.3	Table of the third coupling window	88
8.2	Code of Matlab to compute the impedance inverters	89

List of Figures

1.1	Ninth order waveguide filter.	1
1.2	Bandpass filter mask	4
2.1	Filter as two-port network.	8
2.2	Ideal Response of Low-Pass Filter.	9
2.3	Ideal Response of High-Pass Filter.	10
2.4	Ideal Response of Band-Pass Filter.	10
2.5	Ideal Response of Band-Stop Filter.	10
2.6	Elliptic Filter.	11
2.7	Bessel Filter.	12
2.8	Butterworth Filter.	12
2.9	Type I Chebysev Filter.	13
2.10	Low-Pass Prototype.	14
2.11	Transformation from lowpass prototype to high pass prototype.	16
2.12	Transformation from lowpass prototype to band stop prototype.	17
2.13	Transformation from lowpass prototype to band pass prototype.	17
2.14	Waveguide Bandpass Filter Structure.	18
2.15	Band pass filter containing impedance inverters.	18
2.16	Quarter-wave impedance transformer acting as impedance inverter.	18
2.17	Shunt inductance equivalent circuit for an impedance inverter.	19
2.18	Series capacitance equivalent circuit for an admittance inverter.	19
2.19	Impedance Inverter.	20
2.20	Admittance Inverter.	20
2.21	Transmission line and impedance Inverter filter model.	21
2.22	Short-circuit transmission line as resonator.	21

2.23	Structure for the computation of the iris dimensions.	23
2.24	Flux Diagram to compute iris width.	24
2.25	Structure to compute the length of the resonator by method one.	24
2.26	Equivalent circuit of one coupling with two different waveguides.	25
3.1	Structure for the computation of the spurious frequency	30
3.2	Influence of the thickness of the iris in the spurious frequency	30
3.3	Response of the reference filter. (a) Response of the filter inside the passband. (b) Response of the filter out of the passband, showing the spurious band.	32
3.4	Response of the filter with thicknesses of (2, 8, 11)mm (a) Response inside the passband and (b) Response of the filter out of the passband	33
3.5	Response of the filter with thickness of (12, 9, 1)mm (a) Response of the filter inside the passband and (b) Response of the filter out of the passband.	34
3.6	Structure of the new type of filter, containing non uniform waveguide cavity widths.	36
3.7	Structure of the coupling window for the computation of the iris dimension with two cavities that have different widths.	36
3.8	Equivalent circuit of the structure of the coupling window for the computation of the iris dimension if the cavities attached have different widths.	36
4.1	Geometry of designed referenced filter.	41
4.2	Response of the filter that uses constant thicknesses of 8 mm along the filter. (a) Response inside the passband. (b) Response of the filter out of the passband.	43
4.3	Response of the filter that uses constant thicknesses of 10 mm. (a) Response inside the passband. (b) Out-of-band response of the filter.	44
4.4	Response of the filter that uses thicknesses of (11, 8, 2) mm along the structure. (a) Response in the passband. (b) Response of the filter out of the pass band.	46
4.5	Response of the filter that uses non-uniform thicknesses of (12, 10, 8, 6, 4, 2) mm. (a) Response in the passband. (b) Response of the filter out of the pass band.	48
4.6	Response of the filter that uses thicknesses of (1, 11, 1) mm along the structure. (a) Response in the passband. (b) Response of the filter out of the passband.	49
4.7	Response of the filter that uses thicknesses of 1 mm along the structure and different width for the third cavity. (a) Response inside the passband. (b) Response of the filter out of the passband.	51

4.8	Response of the filter that uses 1 mm thicknesses along the structure, and a different width for the first and the fifth cavities. (a) Response in the passband. (b) Response of the filter out of the passband.	52
4.9	Response of the filter that uses 1 mm thicknesses along the structure and a different width for the second and the fourth cavities. (a) Response in the passband. (b) Response of the filter out of the passband.	53
4.10	Response of the filter that uses thicknesses of (12, 9, 1) mm and different width for the second and the fourth cavities. (a) Response in the passband. (b) Response of the filter out of the passband.	55
4.11	Response of the filter that uses thicknesses of (12, 9, 1) mm, and different width for the second cavity. (a) Response in the passband. (b) Response of the filter out of the passband.	56
5.1	Structure of SIW.	58
5.2	SIW and the equivalent rectangular waveguide	60
5.3	μ Strip-to-SIW transition	61
5.4	Structure to compute the optimum width of the taper	62
5.5	Simulations Results of Fig. 5.4	62
5.6	Transition using an impedance inverter	64
5.7	Structure of filter	64
5.8	S parameters of filter SIW	65
5.9	Phase of filter SIW	66
5.10	Comparison between the filter manufactured and fullwavesimulation	66
5.11	Comparison between the filter manufactured and fullwavesimulation with ϵ_r modified .	67
5.12	Final filter that has been manufactured with ϵ_r modified	67
6.1	SIW cavity loaded with Ring Resonator	70
6.2	S parameter of SIW cavity loaded with Ring Resonator	71
6.3	Structure of Complementary Split Ring Resonator and its equivalent-circuit model . .	72
6.4	Configurations of CSRR unit cell: (a) face-to-face, (b) back-to-back, (c) side-by-side reversely oriented and (d) side-by-side equally oriented	72
6.5	Simulations of different Configurations of CSRR unit cell: (a) face-to-face, (b) back-to-back, (c) side-by-side reversely oriented and (d) side-by-side equally oriented	73
6.6	Structure of two order CSRR to calculate coupling coefficient	74

6.7	Response of two CSRR coupled	74
6.8	Structure of Complementary Split Ring Resonator Filter	75
6.9	S parameter of Complementary Split Ring Resonator Filter	75
6.10	Phase of Complementary Split Ring Resonator Filter	76
6.11	Structure of Complementary Split Ring Resonator Filter asimetrally loaded	77
6.12	S parameter of Complementary Split Ring Resonator Filter asimetrally loaded	77
6.13	General configuration of interdigital bandpass filter	78
6.14	Structure of Interdigital Filter	80
6.15	S parameter of Interdigital Filter	81
6.16	Phase of Interdigital Filter	81

List of Tables

2.1	Element values for Chebyshev lowpass prototype filter ($g_0 = 1, \omega_c = 1, L_{Ar} = 0.1$ dB).	16
3.1	Table of the impedance inverters	29
3.2	Table of dimensions (millimeters)	29
7.1	Table of the comparison between different technologies	84
8.1	Table of the first coupling window	86
8.2	Table of second coupling window	87
8.3	Table of third coupling window	88

Chapter 1

Introduction

1.1 Brief history of microwave filters

In 1864 the existence of radio waves was predicted by James Clerk Maxwell. In 1888, Heinrich Hertz demonstrated such a existence by building a spark gap radio transmitter. Thus began the era of wireless communications, however work on microwave filters began only a short time before the Second World War. Major advances and applications were made at various laboratories in the United States during the World War years of 1941 and 1945. The first technology used in microwave filters was the waveguide technology, which was born to meet the needs of radar and electronic countermeasures, nevertheless, soon found civilian applications such as use in microwave links [1].

Fig. 1.1 shows a photograph of a ninth order waveguide filter.



Figure 1.1: Ninth order waveguide filter.

1.2 Motivation

This project consists of two parts:

First one explain the design strategy of microwave filters. Design of microwave filters is an important activity, due to the fact that microwaves are an integral part of several communications systems; specially in spatial communications systems or terrestrial mobile systems. In the microwave field, waveguide technology still has a very large acceptance, above all in high power applications, and the cases in which the losses reduction is an important factor that has to be taken into account.

Although the design of waveguide filters is a subject that has reached a huge technology maturity [2],[5], [9] there are still some characteristics and aspects that can be improved and from which communications systems would be able to profit. Waveguide filters are based on distributed elements, distributed elements are those where the physical dimension of the component(e.g transmission line) affect the attributes of the circuit (resistance, capacitance and inductance). These elements are used at high frequencies where the wavelength approaches the physical dimension of the circuit.However, one of the main problems that has every filtering structure based on distributed elements is the appearance of spurious in harmonic frequencies from fundamental frequency. Although it is impossible to avoid this phenomenon due to the periodic nature of the elements that are part of the structure of the filter, in the past, some techniques have been researched to try to palliate it. For instance, regarding bandpass filters on waveguide technology, the integration of lowpass filters in the same irises of bandpass filters was proposed in [6]. Using waveguide technology too, but instead of bandpass filter in lowpass filter, a quasi-periodical structure with the aim to reject the spurious from the main mode (TE_{10}) was proposed in [7]. Other researches also have developed similar techniques for lowpass filters, but in this case, on microstrip technology [8].

In this context, this work proposes a new strategy to try to reduce the spurious level in waveguide bandpass filters. The new strategy is based on act upon the thicknesses of the coupling windows that are used as impedance inverter between the different resonators of the filter. The new concept proposed leads to new easier structures of irises than the structures used, for example, in [6]. In traditional designs, thicknesses of the coupling windows are determined *a priori* using practical considerations of convenience for the manufacturing of these irises. Once the irises are fixed, all the thicknesses of the coupling windows remain invariant along the structure.

In the new strategy, I propose to modify the thicknesses of the coupling windows along the filter, with the aim to reduce the level of the spurious that have been generated. The idea is supported by the fact that windows with different thickness can be designed with the same coupling in the fundamental

band, nonetheless, they offer different loads in the harmonic frequency. The different load offered to harmonic frequency from each resonator is the effect that is intended to exploit, in order to achieve the reduction of the spurious levels of the filter.

Besides, waveguide filters are very expensive, difficult to integrate with other technology, and whose size is one of the mainly disadvantages of the waveguide technology, insomuch as they are very large and heavy. Therefore, according to the application may be not possible to use this kind of technology.

This second part of this project where the size of the filter is really important comes motivated by a project that has been developed at Fraunhofer Institute for High Frequency Physics and Radar Techniques (Fraunhofer FHR).

Concretely, AESA antenna demonstrator for civil S-Band applications has been developed at Fraunhofer Institute. This active array antenna is an inexpensive approach to phased-array technology but presents a main problem. This current antenna demonstrator has no mechanism to reduce the effect of interferences what reduce the proper performance of the antenna demonstrator.

Nonetheless, after doing some experimental measurements, it has been determined that this out-of-band interferences need to be mitigated. To do that, a bandpass filter should be included in the front-end. Actually, it is needed a bandpass filter and a limiter, these two devices can guarantee the AESA antenna keep-alive condition.

However, not any kind of filter is useful. We need a bandpass filter that accomplish the following challenges:

- Very restricted filter dimensions (length ≤ 59 mm and width ≤ 45 mm)
- Low insertion losses
- Good matching
- Maximum rejection (for the given size)
- Spurious reduction

A bandpass filter mask is shown in Fig. 1.2.

Because of the dimensions problem of the waveguide that has been discussed previously, it is necessary to use other technologies such as microstrip, stripline and other planar technologies. However, planar technology may present so many losses that would not be convenient for this application. An emerging technology called Substrate Integrated Waveguide is between both of them and it is made

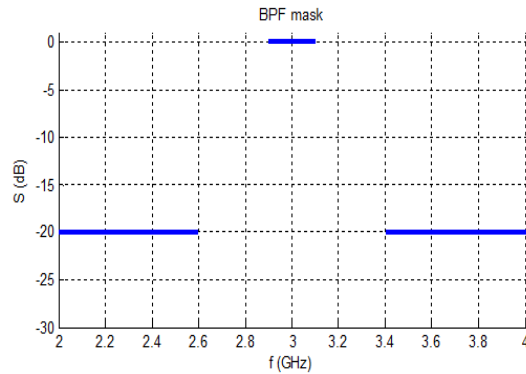


Figure 1.2: Bandpass filter mask

of a piece of substrate with metalization in both sides, and via holes short both metalization. This way, a waveguide is confined inside the structure. The idea is to implement a low-losses filter with size reduction. Such a thing can be possible to obtain with this technology, although in our particular case, not only SIW technology has been used but it has also been combined with other technologies, i.e. metamaterial resonators, which allow to reduce the insertion loss of the filter, and reduce the size considerably.

1.3 Description and organization of the work

Below, it will be explained the content of every chapter in which the project has been divided.

Chapter 2

This chapter contents theoretical concepts and some useful practical concepts relatives to filter design.

Concretely, in this chapter the procedure to design a bandpass filter will be explained, independently of the technology employed. It will be explained the main kind of filters that exist according to the pass band and transfer function. It will be introduced the concept of lowpass prototype, and the transformation from this prototype to the bandpass model.

Finally, the last part of this chapter consists of the explanation and practical method to compute the dimensions of the filter in waveguide technology.

Chapter 3

Firstly, in this chapter a new hypothesis to remove spurious will be introduced. This initial hypothesis says that the coupling windows load in a different way the harmonic frequencies. Then, it will be explained the strategy followed to prove this initial hypothesis. Some examples will be shown, including some designs with non-uniform coupling windows, with the aim to prove the effectiveness

and limitations of the technique that has been proposed.

Chapter 4

This chapter contents more illustrative examples for the reduction spurious technique.

Chapter 5

Due to the big size of waveguide filter, may be desired to use other technologies. In this chapter, it will be presented a real case in which a low-losses filter with reduced size is needed. This case is based on an antenna demonstrator that has been developed at Fraunhofer Institute. The chosen strategy to reduce the size of the filter is SIW technology. Due to this, it will be explained some basic concepts in order to design this kind of filter and it will be shown some examples, including both simulations and measurements.

Chapter 6

Despite of the results achieved in Chapter 4, the filter dimensions are still rather large for the intended application. Therefore, other technologies are taken into account, the first technology consists of using a SIW cavity loaded with a Ring Resonator. The second one consists of using SIW transmission line but this time loaded with Complementary Split Ring Resonator.

Chapter 7

In this last chapter the obtained results in this project are commented and conclusions are formulated. Finally, future research which could be derived from this project are proposed.

This work has been developed in collaboration with the Fraunhofer Institute, under the supervision of Dr. Mariano Pamies and Dr. Thomas Bertuch.

Chapter 2

Design of Waveguide BandPass Filters

In this section, it will be explained how a waveguide filter works and the basic procedure to design this type of structures. The first thing that must be taken into account is the response of the filter and in which frequency band it will work. This means that we need to decide if it will be either a low-pass, band-pass, high-pass filter or band-stop filter [9]. Another characteristic is the transfer function, different filters exist depending on the band which will be suppressed and their different responses, i.e Chebyshev, Butterworth, Bessel and Elliptical. In this project, I will describe more deeply the Chebyshev response [10] because the filters that will be designed henceforth in this project are band-pass filters whose response obeys to the classical equi-ripple Chebyshev function. After the explanation of the Chebyshev response it will be explained how the low-pass filter prototype is built, and then the frequency transformation to produce the final bandpass characteristics. It will be explained the band-pass model based on impedance inverters [12] and it will be shown the structure of the filter using waveguide technology, since it is the technology that will be used in the project for the physical realization of the filters. Finally, it will be explained the way to calculate the physical geometry of the filter, starting with the theoretical desired response.

2.1 Types of filter

Filters can be defined as two-port networks, as shown in Fig. 2.1, that allow the transmission of certain frequencies and the suppression (or at least high attenuation) of other frequencies. Usually, filters are characterized by the scattering parameters (S) expressed in dB values. The most common set of specifications of typical filters are defined as:

- **Bandpass bandwidth**

The bandwidth is either the difference between the upper cutoff frequency and the lower cutoff



Figure 2.1: Filter as two-port network.

frequency, or in the case of a low-pass filter, it is the interval from zero to the upper cutoff frequency. In the case of a high-pass filter it is the interval from its lower cutoff frequency to infinite. Also, it can be seen as the interval frequency in which $|S_{21}| = 1$ (therefore all the energy is transmitted); as well as $|S_{11}| = 0$ (therefore, no energy is reflected).

- **Insertion Losses**

Losses introduced in the bandpass bandwidth by the filter are known as insertion losses. Also, it can be defined as the ratio, in dB, of incident power P_i to transmitted power P_t .

$$IL = 10 \log_{10}\left(\frac{P_i}{P_t}\right) \quad (2.1)$$

It can be related with $|S_{21}|$ as $IL = 20 \log_{10} |S_{21}|$ dB.

- **Ripple**

It can be interpreted as the variation of the amplitude of the signal within the bandpass bandwidth. This may also appear within the suppressed band depending on the response of the filter.

- **Stopband Attenuation**

Stopband is a band of frequencies through which the attenuation is above the required stopband attenuation level.

- **Return Losses**

Losses introduced by the filter due the impedance mismatch are known as return losses. They can be defined as the ratio, in dB, of incident power P_i to reflected power P_r .

$$RL = 10 \log_{10}\left(\frac{P_i}{P_r}\right) \quad (2.2)$$

Return losses are related with $|S_{11}|$ as $RL = 20 \log_{10} |S_{11}|$ dB. All filters satisfy the next relationship linking RL, IL and dissipative Losses:

$$|S_{21}|^2 + |S_{11}|^2 + \text{Power Losses} = 1 \quad (2.3)$$

If the filter is lossless the relationship is $|S_{21}|^2 + |S_{11}|^2 = 1$.

- **Group Delay**

Group Delay ($\tau(\omega)$ measured in seconds) is a value that indicates the delay that each spectral component suffers as it travels through the filter. This parameter can be obtained from the phase of the (S_{21}) as:

$$\tau(\omega) = \frac{\partial \Phi(\omega)}{\partial \omega} \quad (2.4)$$

where $\Phi(\omega)$ is the phase of the (S_{21}) parameter.

In most communication applications it is desirable that the phase response of the filter is a linear function of frequency, so that the filter has constant group delay. Therefore, there is not dispersion leading to spread spectrum of the signal, which produces phase distortion and increases BER (Bit Error Rate) in digital communications.

2.1.1 Types of filter depending on passband

Now it will be explained the different types of filters according to their passbands [9]. As it was said previously, there are four main different types of filters that can be classified as follows:

- **Low-Pass filter**

Low-pass filters allow only low frequencies to be transmitted. Actually, they allow only the interval from zero to an upper cutoff frequency to pass from the input port to the output port. The basic form of the transfer function for this type of filters is shown in Fig. 2.2.

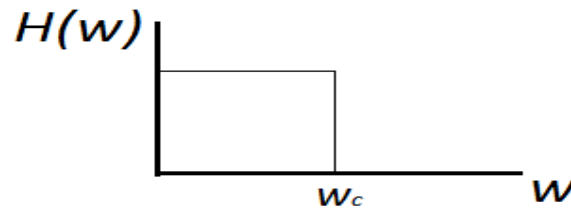


Figure 2.2: Ideal Response of Low-Pass Filter.

- **High-Pass filter**

High-pass filters allow only high frequencies to be transmitted. Actually, they allow only the interval from a lower cutoff frequency to infinite to pass from the input port to the output port. The basic form of the transfer function for this type of filters is shown in Fig. 2.3.

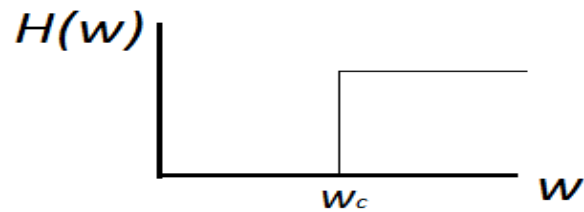


Figure 2.3: Ideal Response of High-Pass Filter.

- **Band-Pass filter**

Band-pass filters allow only the interval from a lower cutoff frequency to an upper cutoff frequency to be transmitted from the input port to the output port. The basic form of the transfer function is shown in Fig. 2.4.

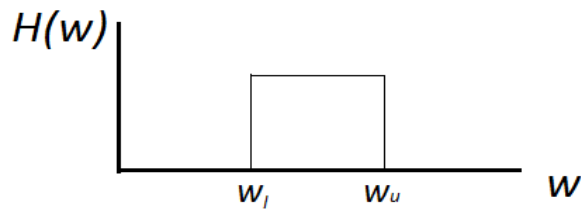


Figure 2.4: Ideal Response of Band-Pass Filter.

- **Band-Stop filter**

Band-stop filters allow all frequencies except the interval from a lower cutoff frequency to an upper cutoff frequency to be transmitted from the input port to the output port. The basic form of the transfer function is shown in Fig. 2.5.

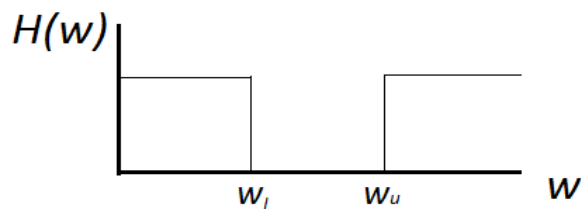


Figure 2.5: Ideal Response of Band-Stop Filter.

2.1.2 Types of filters depending on their transfer function

As stated previously, filters can be classified according to their response or transfer function. The goal of this section is not to go deeply into the different types of responses, and they will only be described briefly with the objective to be able to distinguish them in the future. Thereafter, it will be described the Chebyshev transfer function in more detail [10]. Some of the more widely used types of filter responses are the followings:

- **Elliptic Filter**

This type of filter presents a very steep response with equiripple in both the passband and the stopband. To obtain equiripple in both passband and stopband, elliptic filters must have both poles and zeros. This filter response has the form defined by the formula (2.5).

$$|H_c(\omega)| = \frac{1}{1 + \epsilon^2 U_N^2(\omega)} \quad (2.5)$$

where $U_N^2(\omega)$ is the nth-order Jacobian elliptic function. Graphically an example of an elliptic filter response can be seen in Fig. 2.6.

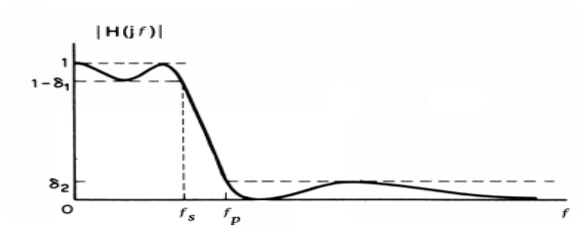


Figure 2.6: Elliptic Filter.

- **Bessel Filter**

Bessel filters achieve the desired filter response but with a constant time delay in the passband. Its transfer function is defined as (2.6).

$$|H(s)| = \frac{\theta_N(0)}{\theta_N(s/w_o)} \quad (2.6)$$

where $\theta_N^2(\omega)$ is the nth-order Bessel polynomial. Graphically Bessel filter has the transfer function shown in the Fig. 2.7.

- **Butterworth Filter**

Butterworth filters are defined by the property that the magnitude response is maximally flat

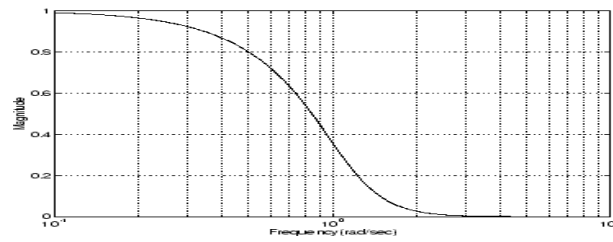


Figure 2.7: Bessel Filter.

in the passband. Another property is that the magnitude is monotonic in the passband and in the stopband. Its transfer function can be calculate with the formula (2.7).

$$|H_c(\omega)| = \frac{1}{1 + (j\omega/j\omega_c)^{2N}} \quad (2.7)$$

where N is the order of the filter. Graphically Butterworth filter has the transfer function shown in Fig. 2.8.

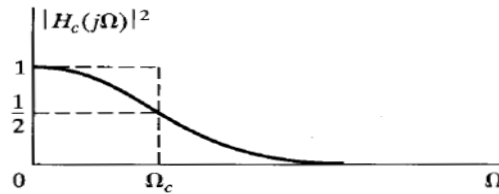


Figure 2.8: Butterworth Filter.

- **Chebyshev Filter**

This type of filters will be explained more deeply in the next section, since they are the filters to be designed in this work. Therefore, by now it is only necessary to mention that this filter presents a steep response whose bandpass has certain specified ripple.

2.2 Chebyshev Filter

The maximally flat filter is the simplest filter and its response may not be good enough to meet rejection requirements. In some applications, it is needed to achieve a steeper response, using a low order filter. In this sense Chebyshev is the response that offers the best trade-off between complexity and rejection capabilities.

It is important to know that there are two different types of Chebyshev filter responses: In type I, Chebyshev filter has the property that magnitude of the frequency response is equiripple in the

passband and monotonic in the stopband. On the other hand, type II Chebyshev filter has the property that the magnitude of the frequency response is equiripple in the stopband and monotonic in the passband. The two types of Chebyshev filter will be discussed in the next paragraphs:

- Type I Chebyshev filter

Fig. 2.9 shows the frequency response of the type I Chebyshev filter whose transfer function has the form:

$$|H_c(\omega)|^2 = \frac{1}{1 + \epsilon^2 V_N^2(\omega/\omega_c)} \tag{2.8}$$

where V_N is the N th-order Chebyshev polynomial defined as:

$$V_N(x) = \cos(N \cos^{-1} x)$$

From this equation is easy to obtain a recurrence formula in which V_{N+1} can be obtained from $V_N(x)$ and $V_{N-1}(x)$ by applying trigonometric identities. The equation follows that:

$$V_{N+1}(x) = 2x V_N(x) - V_{N-1}(x)$$

It should be noted that $V_N(x)^2$ varies between zero and unity for $0 < x < 1$. For $x > 1$, $\cos^{-1} x$ is imaginary so $V_N(x)$ behaves as a hyperbolic cosine and consequently increases monotonically. On the other hand, $H_c(\omega)^2$ ripples between 1 and $\frac{1}{1+\epsilon^2}$ for $0 < \omega/\omega_c < 1$ and decrease monotonically for $\omega/\omega_c > 1$. From another point of view, ripple is often given in dB so the relationship between ϵ and the ripple is $Ripple(dB) = 20 \log_{10}(\sqrt{1 + \epsilon^2})$. The specifications of a given transfer function consists in selecting ϵ , that is the allowable passband ripple, ω_c that is the passband cutoff frequency and the order of the filter N . Graphically the transfer function of type I Chebyshev filter is shown in Fig. 2.9.

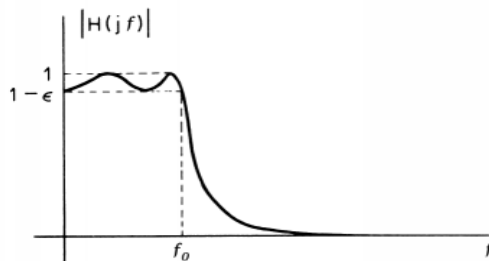


Figure 2.9: Type I Chebyshev Filter.

- Type II Chebyshev filter

Now it will be explained type II Chebyshev filter. Basically, type II Chebyshev filter can be related to a type I filter through a transformation. If it is replaced the term $\epsilon^2 V_N^2(\omega/\omega_c)$ by its reciprocal and also it is replaced the argument of V_N by its reciprocal, it is obtained:

$$|H_c(\omega)|^2 = \frac{1}{1 + [\epsilon^2 V_N^2(\omega_c/\omega)]^{-1}} \quad (2.9)$$

What it is normally done, is to perform the design of type I Chebyshev filters and then apply the transformation explained above these lines to convert the filter to a type II Chebyshev transfer function.

2.3 Low-Pass Prototype

Microwave filters of types high-pass, band-pass and band-stop are based on low-pass filter prototypes. Then, the design is completed through some frequency and elements transformations. Frequency and elements transformation will be discussed in the next sections. This section is only focused on explaining the elements of this lowpass prototype and how their values are computed [12].

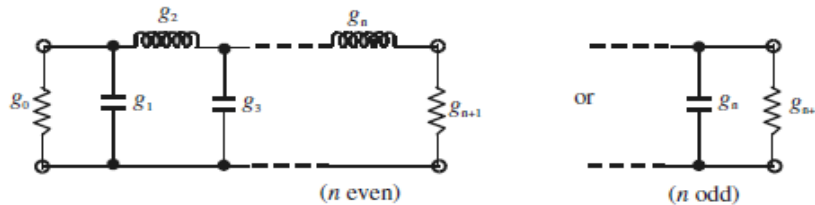


Figure 2.10: Low-Pass Prototype.

A typical low-pass prototype circuit can be seen in Fig. 2.10. This prototype is in general defined as a lowpass filter whose elements values are normalized. Therefore the left-hand load resistance is equal to one ohm and it is denoted by $g_0 = 1$. It is also assumed that the passband edge occurs at $\omega' = 1$. It can be noted that the elements of odd order, namely $g_1, g_3, g_5 \dots g_n$ are shunt capacitances, while the elements of even order, namely $g_2, g_4, g_6 \dots g_n$ are series inductances. Finally, the last element is different weather the order of the filter is odd or even. If the order is odd, the last element of the filter g_n is a shunt capacitance. Otherwise, the last element g_n is a series inductance (for n even). The right-hand load resistance ($r = g_{n+1}$), is again normalized to one ohm for all cases except that of Chebyshev response with n even.

2.3.1 Chebyshev Lowpass Prototype Filter

For Chebyshev Lowpass prototype filter with a fixed passband ripple and cutoff frequency $\omega_c = 1$, the elements can be computed as follows [12]:

$$g_0 = 1 \quad (2.10)$$

$$g_1 = \frac{2a_1}{\gamma} \quad (2.11)$$

$$g_k = \frac{4 a_{k-1} a_k}{b_{k-1} g_{k-1}} \text{ for } k = 2 \dots n \quad (2.12)$$

$$g_{n+1} = \begin{cases} 1 & n \text{ odd} \\ \coth^2(\beta/4) & n \text{ even} \end{cases}$$

where:

$$\beta = \ln(\coth(\frac{L_{AR}}{17.37})) \quad (2.13)$$

$$\gamma = \sinh(\frac{\beta}{2n}) \quad (2.14)$$

$$a_k = \sin(\frac{(2k-1)\pi}{2n}) \text{ for } k = 1 \dots n \quad (2.15)$$

$$b_k = \gamma^2 + \sin^2(\frac{k\pi}{n}) \text{ for } k = 1 \dots n \quad (2.16)$$

For the required passband ripple L_{AR} dB and the minimum stopband attenuation (L_{AS}), the degree of the filter can be computed as:

$$n \geq \frac{\cosh^{-1} \sqrt{\frac{10^{0.1 L_{AS}} - 1}{10^{0.1 L_{AR}} - 1}}}{\cosh^{-1}(\omega_s)} \quad (2.17)$$

where

$$L_{AR} = -10 \log(1 - 10^{RL/10}) \quad (2.18)$$

and RL is the minimum passband return loss.

On the other hand, for some passband ripple L_{Ar} and for filter degrees of $n = 1 \dots 9$, the typical element values are already tabulated. The value of the elements for Chebyshev lowpass prototype with $L_{AR} = 0.1$ dB are shown in Tab. 2.1 [2]:

2.4 Frequency and elements transformation

A lowpass filter prototype can be converted into any other filter, namely high-pass filter, band-pass filter or band-stop filter. This is done by scaling their impedance and frequency values. The prototype is also modified slightly. Although it will be only explained the bandpass transformation, all prototypes are shown next with the aim to know how their basic structures are. Fig. 2.11 shows the high-pass

n	g_1	g_2	g_3	g_4	g_5	g_6	g_7	g_8	g_9	g_{10}
1	0.3052	1.0								
2	0.8431	0.6220	1.3554							
3	1.0316	1.1474	1.0316	1.0						
4	1.1088	1.3062	1.7704	0.8181	1.3554					
5	1.1468	1.3712	1.9750	1.3712	1.1468	1.0				
6	1.1681	1.4040	2.0562	1.5171	1.9029	0.8618	1.3554			
7	1.1812	1.4228	2.0967	1.5734	2.0967	1.4228	1.1812	1.0		
8	1.1898	1.4346	2.1199	1.6010	2.1700	1.5641	1.9445	0.8778	1.3554	
9	1.1957	1.4426	2.1346	1.6167	2.2054	1.6167	2.1346	1.4426	1.1957	1.0

Table 2.1: Element values for Chebyshev lowpass prototype filter ($g_0 = 1$, $\omega_c = 1$, $L_{Ar} = 0.1$ dB).

prototype, stop-band prototype is shown in Fig. 2.12 and Fig. 2.13 shows the band-pass prototype [3].

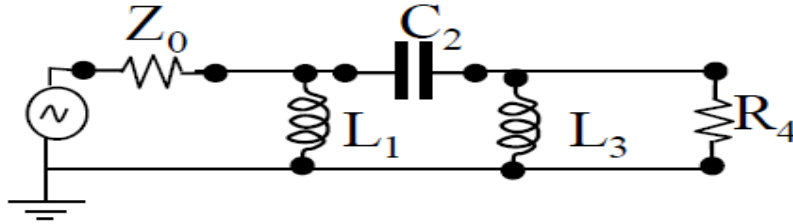


Figure 2.11: Transformation from lowpass prototype to high pass prototype.

In the following it will only be explained the bandpass transformation, because this is the type of filter used in this project. Thus, if the edge frequencies of the passband are ω_1 and ω_2 , the formulas for the frequency scaling are the following:

$$\omega' = \frac{1}{w} \left(\frac{\omega}{\omega_0} - \frac{\omega_0}{\omega} \right) \quad (2.19)$$

where $\omega_0 = \sqrt{\omega_1 \omega_2}$ is the center frequency of the bandpass filter and w is the so called fractional bandwidth whose formula is:

$$w = \frac{\omega_2 - \omega_1}{\omega_0} = \frac{\text{bandwidth}}{\omega_0} \quad (2.20)$$

Using this transformation for the series reactances and the shunt susceptances, the new filter elements can be determined as follows:

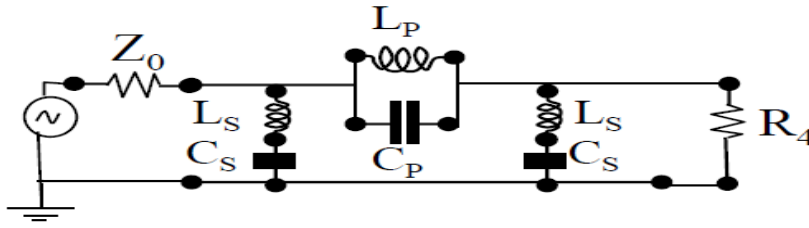


Figure 2.12: Transformation from lowpass prototype to band stop prototype.

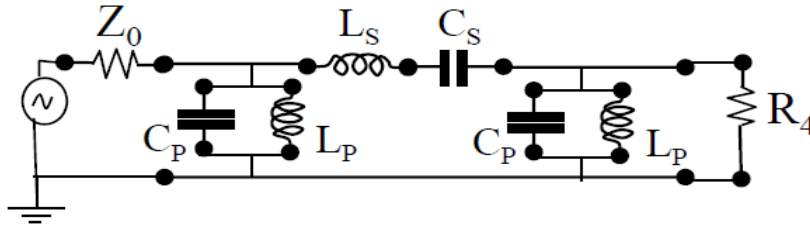


Figure 2.13: Transformation from lowpass prototype to band pass prototype.

- L_K is transformed to a series LC circuit where:

$$L'_K = \frac{L_K}{w \omega_0} \quad (2.21)$$

$$C'_K = \frac{w}{\omega_0 L_K} \quad (2.22)$$

- C_K is transformed to a shunt LC circuit where:

$$L'_K = \frac{w}{\omega_0 C_K} \quad (2.23)$$

$$C'_K = \frac{C_K}{w \omega_0} \quad (2.24)$$

2.5 Bandpass Filter Model

In this project, the filters that are going to be designed are bandpass filter realized in rectangular waveguide technology. The band-pass filter structure realized with this technology can be seen in Fig. 2.14.

The filter is composed of an input port and an output port; the length of the input/output port does not affect the behaviour of the filter (it only affects to the total phase of the signal). In this figure, W is the width of the iris and t is the thickness of the iris.

The irises are the coupling windows that divide one resonator from the adjacent one. Finally, L is the length of the resonator and it is tuned to obtain the resonance at f_0 . All the resonators have

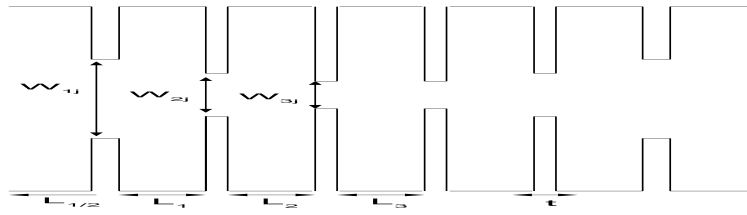


Figure 2.14: Waveguide Bandpass Filter Structure.

to be tuned at the same frequency, for synchronously tuned filter topologies. In a practical structure there are (n) resonators being (n) the order of the filter.

2.5.1 Bandpass filter based on impedance inverters

The filter structure of Fig 2.14 can be modeled with impedance inverters and LC resonators [12]. The conceptual operation of the impedance and admittance inverters is to transform series-connected elements to shunt-connected elements and viceversa. Therefore, bandpass filters can be modeled as shown in Fig. 2.15.

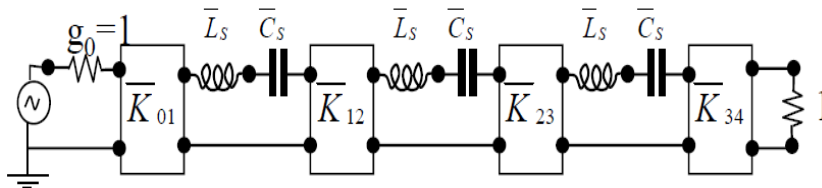


Figure 2.15: Band pass filter containing impedance inverters.

In this figure $\bar{K} = \frac{K}{Z_0}$ is the normalized value of the impedance inverter K . One of the most used equivalent circuits of an impedance inverter is based on the quarter-wave impedance transformer, as shown in Fig. 2.16. The input impedance of the quarter-wave transformer, looking at the input is:

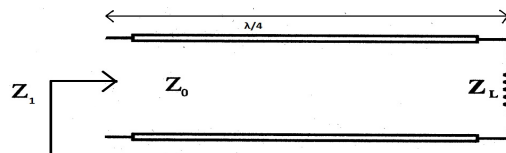


Figure 2.16: Quarter-wave impedance transformer acting as impedance inverter.

$$Z_{in} = Z_0 \frac{Z_L + j Z_0 \tan(\beta l)}{Z_0 + j Z_L \tan(\beta l)} \quad (2.25)$$



Figure 2.17: Shunt inductance equivalent circuit for an impedance inverter. Figure 2.18: Series capacitance equivalent circuit for an admittance inverter.

$$K = |Z_0 \tan(\phi/2)|$$

$$\phi = \tan^{-1}(2X/Z_0)$$

$$X/Z_0 = \frac{K/Z_0}{1-(K/Z_0)^2}$$

$$K = |Z_0 \cot(\phi/2)|$$

$$\phi = -\tan^{-1}(2B/Z_0)$$

$$B/Z_0 = \frac{K/Z_0}{(K/Z_0)^2-1}$$

since the length (l) of the transmission line is $l = \lambda_g/4$, then

$$\beta l = \frac{2\pi}{\lambda_g} \frac{\lambda_g}{4} = \pi/2 \quad (2.26)$$

thus $\tan(\pi/2) = \infty$ and $Z_{in} = \frac{Z_0^2}{Z_L}$.

Other equivalent circuits for impedance inverters are based on lumped elements. Two of them are based on either a shunt inductance or a series capacitance, and they can be observed in Fig. 2.17 and Fig. 2.18 [3].

In general, impedance inverters can be defined as a two-port network whose impedance seen looking at the input port is $Z_{in} = \frac{K^2}{Z_L}$, if Z_L is the impedance at the output port. In the previous relation (K) is the constant of the inverter (the characteristic impedance when using a quarter-wave line). Thus, for example, if Z_L is an inductive load, Z_{in} will become of capacitive type, and vice versa. This can be seen as a phase shift of -180° on the reflection coefficient. This phase shift in the reflection coefficient represents a phase shift of ± 90 degrees in the transmitted voltage wave. Hence, the inverter introduces a phase shift of ± 90 degrees in the S_{21} parameter. The $ABCD$ matrix of the ideal impedance inverter is expressed by the following formulas [3]:

$$\begin{bmatrix} A & B \\ C & D \end{bmatrix} = \begin{bmatrix} 0 & \mp jK \\ \pm 1/jK & 0 \end{bmatrix}$$

Likewise, admittance inverters can be defined as a two-port network whose admittance seen looking at the input port is $Y_{in} = \frac{J^2}{Y_L}$, if Y_L is the admittance seen looking at the output port. In this case J is the constant of the admittance inverter. Similarly, the admittance inverter introduces a phase shift of ± 90 degrees to the S_{21} parameter. The $ABCD$ matrix of the ideal admittance inverter is expressed

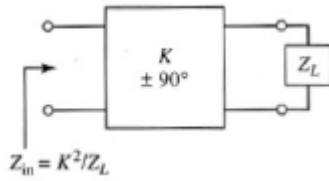


Figure 2.19: Impedance Inverter.

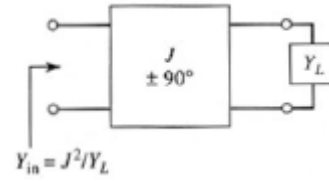


Figure 2.20: Admittance Inverter.

by the following formulas:

$$\begin{bmatrix} A & B \\ C & D \end{bmatrix} = \begin{bmatrix} 0 & \pm 1/jJ \\ \mp jJ & 0 \end{bmatrix}$$

Their operation from a graphical point of view is shown in the Fig. 2.19 and Fig. 2.20.

On the other hand, LC resonators are characterized by two parameters:

- Resonant frequency ω_0 : all the resonators are tuned at the same frequency (ω_0) in synchronously tuned topologies.
- Slope parameter X_i : that can be defined as [12]

$$X_i = \frac{\omega_0}{2} \frac{dX}{d\omega} \text{ when } \omega = \omega_0 \quad (2.27)$$

then, for the particular case of an LC resonator:

$$X_i = \omega_0 L_i = \frac{1}{\omega_0 C_i} = \frac{\omega'_1}{w} L'_i \quad (2.28)$$

where (w) is the fractional bandwidths, and it was defined in eq.(2.20), L_i is the lowpass element and L'_i is the corresponding element after the bandpass transformation.

2.5.2 Transmission Line Model and Impedance Inverter Model

Finally, one approach to design a bandpass filter is to start with an equivalent circuit that represents the filter with impedance inverters and transmission line resonators as shown in Fig. 2.21 [9]. In this case waveguide resonators are modeled with transmission lines, while the coupling inductive waveguide windows are modeled by ideal impedance inverters.

An isolated resonator can be characterized with the transmission line equivalent circuit shown in Fig. 2.22. The resonant condition in general can be written as

$$Z_1 + Z_2 = 0 \quad (2.29)$$

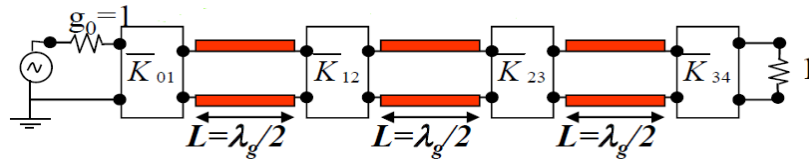


Figure 2.21: Transmission line and impedance Inverter filter model.

where Z_1 is the input impedance in an interface looking at the right, and Z_2 is the input impedance at the same interface looking at the left. For the short-circuited transmission line resonator shown in Fig.2.22 this conditions leads to

$$Z_{in} + 0 = 0; \quad (2.30)$$

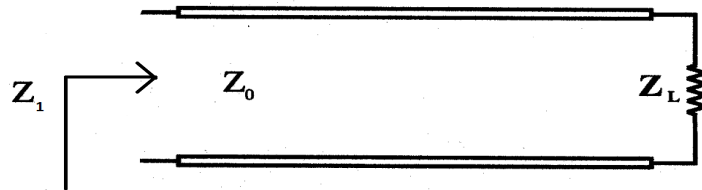


Figure 2.22: Short-circuit transmission line as resonator.

Therefore,

$$Z_{in} = j Z_0 \tan(\beta l) = 0 \quad (2.31)$$

The condition $\tan(x) = 0$ is fulfilled when $x = n\pi$ for $n = 0, 1, 2, \dots$. Since the argument of the tangent function has to be a multiple of π , $\beta l = \frac{2\pi}{\lambda} l = n\pi$, then the length of the transmission line to meet the resonance is obtained as:

$$l = n \frac{\lambda}{2} \quad (2.32)$$

In addition to the resonant frequency, the resonator will be fully characterized with the calculation of the slope parameter of the transmission line resonator. Now, focusing on the case of a waveguide resonator, $\beta_g = \frac{2\pi}{\lambda_g}$. Taking into account the resonant condition (2.32), $l = \frac{\lambda_{g0}}{2}$ and the slope parameter definition (2.27), it is obtained the expression (2.33).

$$X = \frac{\omega_0}{2} \frac{\partial Z_0 \tan(\pi \frac{\lambda_{g0}}{\lambda_g})}{\partial \omega} \text{ when } \omega = \omega_0 \quad (2.33)$$

The relationship between the frequency and the wavelength is:

$$\lambda = \frac{2\pi c}{\omega} \quad (2.34)$$

and the wavelength for the dominant (TE_{10}) mode in the waveguide λ_g is:

$$\lambda_g = \frac{\lambda}{\sqrt{1 - (\frac{f_c}{f})^2}} \quad (2.35)$$

Finally, the slope parameter is computed as:

$$X = \frac{\omega_0 Z_0}{2} \frac{\partial}{\partial \omega} \left(\tan \left(\frac{\pi \omega}{\omega_0} \sqrt{\frac{1 - (\frac{\omega_c}{\omega})^2}{(\frac{\omega_c}{\omega_0})^2}} \right) \right) \quad (2.36)$$

The derivative is calculated when $\omega = \omega_0$; then it is obtained the slope parameter as:

$$X = \frac{\pi}{2} Z_0 \left(\frac{\lambda_{g0}}{\lambda_0} \right)^2 \quad (2.37)$$

Then, the values of normalized impedance inverters are related to the elements of the lowpass prototype as follows [9]:

$$\frac{K_{01}}{Z_0} = \sqrt{\frac{R_A L'_1}{g_0 g_1}} = \sqrt{\frac{R_A w X_1 / \omega'_1}{g_0 g_1}} = \sqrt{\frac{R_A w X_1}{\omega'_1 g_0 g_1}} \quad (2.38)$$

$$\frac{K_{i,i+1}}{Z_0} = \sqrt{\frac{L'_i L'_{i+1}}{g_i g_{i+1}}} = \sqrt{\frac{w X_1 / \omega'_1 w X_{i+1} / \omega'_1}{g_i g_{i+1}}} = \frac{w}{\omega'_1} \sqrt{\frac{X_i X_{i+1}}{g_i g_{i+1}}} \quad (2.39)$$

$$\frac{K_{n,n+1}}{Z_0} = \sqrt{\frac{R_B L'_n}{g_n g_{n+1}}} = \sqrt{\frac{R_B w X_n / \omega'_1}{g_n g_{n+1}}} = \sqrt{\frac{R_B w X_n}{\omega'_1 g_n g_{n+1}}} \quad (2.40)$$

where R_A is the resistance of the generator and R_B is the load resistance at the output of the filter. For this design their values are equal to one because they are normalized.

If all transmission lines have the same characteristic impedance and the same resonant frequency then they have the same slope parameters, therefore, the previous formulas can be simplified as follows:

$$\frac{K_{01}}{Z_0} = k_{01} \sqrt{R_A x w} \quad (2.41)$$

$$\frac{K_{j,j+1}}{Z_0} = w x k_{j,j+1} \quad (2.42)$$

$$\frac{K_{n,n+1}}{Z_0} = k_{n,n+1} \sqrt{R_B x w} \quad (2.43)$$

where $k_{i,i+1} = \frac{1}{g_i g_{i+1}}$ is the coupling and $x = X_i = X_{i+1}$.

2.6 Synthesis Dimension

The final step in the design of a filter is to convert the circuit parameter values into dimensions of the physical implementation. Fig. 2.14 shows the structure of a waveguide filter that will be studied in this work, and all the relevant dimensions. This section will explain the steps needed to calculate the dimensions of the filter, i.e the width of the iris w (that will control the coupling between resonators) and the length of the cavity L (that will control the resonant frequency of the resonator) for a fixed thickness t . This process will be repeated for each resonator and each coupling window with the aim to obtain the transfer function that has been specified in the requirements.

2.6.1 Iris width

Once the normalized value of the impedance inverter that will be synthesized (K/Z_0) is known, the module of the transfer parameter (S_{21}) that is necessary in the simulation of the structure of Fig. 2.23 can be obtained with the next known relationship [9]:

$$|S_{21}| = \frac{2Z_0}{K + \frac{Z_0^2}{K}} = \frac{2}{\frac{K}{Z_0} + \frac{Z_0}{K}} \quad (2.44)$$

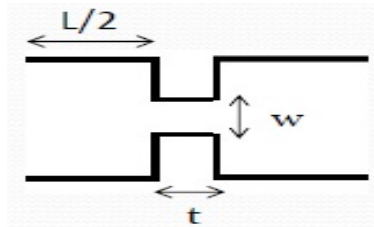


Figure 2.23: Structure for the computation of the iris dimensions.

In the Fig. 2.23, $L/2$ is the distance from the ports to the coupling window. To compute the iris width this distance can be any value because it does not modify the module of the scattering parameter S_{21} . This distance only modifies its phase and now we are interested only in its module. Fig. 2.24 shows the main steps of this computation. Therefore, according to the Fig. 2.24 the procedure for this calculation is as follows; firstly, using a full-wave electromagnetic simulation software it is obtained the response of the simulation of the structure of Fig.2.23, and the value of S_{21} is extracted. Secondly, the simulated $|S_{21}|$ is compared against the target $|S_{S21}|$ given by the formula (2.44). Then, the width of the iris is changed until the value of $|S_{21}|$ that is obtained with the simulation of the structure equals the target value of $|S_{21}|$ that has been obtained theoretically (see formula 2.44).

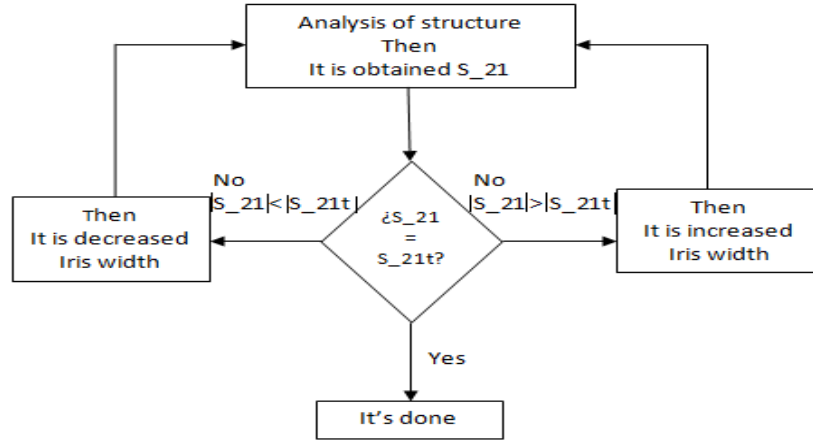


Figure 2.24: Flux Diagram to compute iris width.

2.6.2 Cavity length

Cavity length can be computed by two methods:

- Method one

Method one is based on the structure that can be observed in Fig. 2.25 [4]. If cavities were loaded

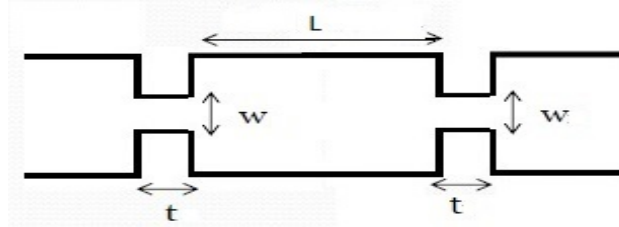


Figure 2.25: Structure to compute the length of the resonator by method one.

by a short-circuit then the length of the cavity would be $l = \lambda_g/2$. Therefore the phase would be $\beta l = \frac{2\pi}{\lambda_g} \frac{\lambda_g}{2} = \pi$. Nonetheless, irises are considered as two complex impedances, therefore the phase is modified and the central frequency is shifted. In order to tune the desired resonant frequency, the length of the resonator has to be modified. In this case the electrical length is:

$$\beta l = \frac{2\pi l}{\lambda_g} = \pi - \alpha_1/2 - \alpha_2/2 \quad (2.45)$$

where α_1 is the length extension in degrees of the resonator because of the port one and α_2 is the length extension in degrees of the resonator because of the port two. Thus, length of the resonator is:

$$l = \frac{\lambda_{g0}}{2\pi} (\pi - \alpha_1/2 - \alpha_2/2) \quad (2.46)$$

The relationship between the phase of S_{11} and α is $\alpha = \pi - \phi$ where ϕ is the phase of S_{11} . Therefore, length of the resonator can be computed as:

$$l = \frac{\lambda_{g0}}{4\pi}(\phi_1 + \phi_2) \quad (2.47)$$

where ϕ_1 is the phase of S_{11} for first iris and ϕ_2 is the phase of S_{11} for the second iris. This formula takes into account that the cavity is affected by two irises.

- Method two

The structure of Fig. 2.23 can be analyzed by means of an equivalent circuit. Analyzing this equivalent circuit, we will be able to determine the phase that would be obtained at the output of the circuit if the length of the resonator was $L/2 = \lambda_g/4$, that is to say ideally. Then, this phase will be used to compute the length of the cavities L , tuning the length so that the resonant frequency is ω_0 . This equivalent circuit can be seen in Fig. 2.26. First of all, with the aim to

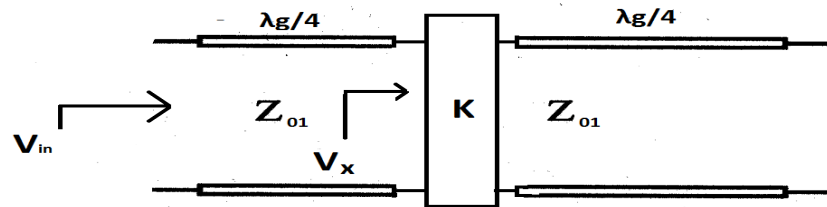


Figure 2.26: Equivalent circuit of one coupling with two different waveguides.

determine the phase of S_{21} , it is necessary to know the formula of the voltage in a transmission line. Incident voltage wave in a transmission line is computed by the formula (2.48).

$$V_{in} = V e^{-\beta_g l} \quad (2.48)$$

where $(\beta_g l)$ is the phase of the voltage wave. If the inverter is a quarter-wave transmission line, then $(l = \lambda_g/4)$. The phase of the voltage at the output is shifted with respect to the voltage at the input by a factor $-\beta l = -\frac{2\pi}{\lambda_g} \frac{\lambda_g}{4} = -\frac{\pi}{2}$. Therefore, the phase of S_{21_x} is -90° . That is because the impedance inverter introduces a phase of $\pi/2$.

Using above result, we now calculate the phase of the transmission coefficient S_{21} in the structure of Fig. 2.26. Taking into account the two pieces of transmission lines, of length $(\lambda_g/4)$, connected at the input/output of the inverter, the phase of the complete structure is $\text{Ph}(S_{21}) = -\pi/2 + \pi/2 - \pi/2 = -\pi/2$.

Therefore, the procedure to compute the length is to modify the positions of the ports of the structure shown in Fig. 2.23 so that the phase of S_{21} is equal to -90° , at the desired resonant

frequency. One thing to take into account is that the position of the port is the same at both side of the iris, because the structure is considered to be symmetric.

Both methods can be implemented with any electromagnetic simulation software, which allows the full wave simulation of waveguide devices, such as FEST3D [13]. This is the program which we have used in this project. Other alternatives, very popular in the electromagnetic scientific community are HFSS, REMCOM, CST, etc.

2.7 Summary to design waveguide bandpass filters

1. Computation of the order of the filter: From the insertion-loss specification and the desired attenuation, it is computed the necessary order of the filter by an iterative way. If the filter is to exhibit a Chebyshev response, the formulas to be applied are the following [5]:

$$A_{dB}(\omega') = \begin{cases} 10 \log_{10}(1 + \varepsilon \cos^2(n \arccos(\omega'/\omega'_1))) & \omega' \leq \omega'_1 \\ 10 \log_{10}(1 + \varepsilon \cosh^2(n \cosh^{-1}(\omega'/\omega'_1))) & \omega' \geq \omega'_1 \end{cases}$$

being n the minimum order of the filter which satisfies the specified attenuation, with $\varepsilon = 10^{L_{AR}/10} - 1$ y $L_{AR} = -10 \log_{10}(1 - 10^{RL/10})$.

2. Computation of the lowpass prototype element values: Once it is computed the order of the filter, it is possible to compute the values of the lowpass prototype elements by means of the formulas (2.10), (2.11) and (2.12) [12].
3. Computation of impedance inverters: With the lowpass prototype coefficients, it is computed the impedance inverters applying the formulas (2.38), (2.39) and (2.40) [9].
4. Computation of iris width: Compute the scattering parameter S_{21} by the formula (2.44). Then, run the iris structure of Fig. 2.23 with an electromagnetic simulation software and extract the S_{21} value. Then, modify and optimize the width of the coupling windows until the target S_{21} value is obtained.
5. Procedure to compute the cavity length:
 - Calculate the length of the resonator by means of the computation of the position of the port of the Fig. 2.23 for which the phase of S_{21} is equal to -90° (Method two of 2.6.2).
 - Calculate the length of the resonator using a full wave software to simulate the structure of the Fig. 2.25 and the, use the formula (2.47) (Method one of 2.6.2).

Chapter 3

Technique to reduce spurious in waveguide BandPass filter

3.1 Introduction

The strategy for the design of the filter that has been followed in this chapter is based on the hypothesis that different thicknesses for the coupling windows cause different loading effects to the spurious frequency. The iris can be adjusted so that the coupling, at the fundamental frequency, is the same for all the thicknesses considered. However, all these irises will represent different loading effects to the spurious frequency. Because of these different loading effects, it is expected that the spurious appears at different frequencies. In this way, spurious from some cavities may interact destructively with the spurious of the other cavities and a higher rejection is expected.

Finally, I include three design examples. The first one is a simple filter that can be used as a reference filter. The second one is a filter that uses small thicknesses in the external coupling windows and larger thicknesses for the inner irises. The final illustrative example uses the inverse process; the most external coupling windows use large thicknesses, while the inner irises use small thicknesses. The purpose to include these examples is to observe the influence of using windows with non-uniform thicknesses in the spurious response of complete filters.

3.2 Spurious reduction using non-uniform coupling windows

With the aim to illustrate the technique to reduce the spurious based on controlling the non-uniform thicknesses of the coupling windows along the filter, it will be shown the developments upon a specific filter example. The filter that will be designed is a waveguide bandpass filter of fifth order, its

fundamental frequency is 11 GHz and its bandwidth is 100 MHz. This filter presents minimum return losses equal to $RL = -25$ dB with classic Chebyshev response. The coupling windows will be rectangular inductive windows because of simplicity.

The technique that has been proposed for the reduction of the spurious is based on an initial hypothesis: non-uniform coupling windows, which present the same coupling in the fundamental band, load the harmonic frequencies in a different way. This property allows to introduce different thicknesses for the coupling windows of the filter to try to avoid the constructive combination of the harmonics of the different resonators. Since the constructive combination of the harmonic frequencies is avoided, it is expected to reduce the spurious levels.

To prove the initial hypothesis, a systematic procedure has been applied and it is explained below. Firstly, the coupling windows will be characterized as impedance inverters as shown in Fig. 2.23.

Then, the width of the window (ω) is adjusted to obtain the same value of the impedance inverter when the thickness (t) is varied from 1 mm to 12 mm.

Once the normalized value of the impedance inverter that will be synthesized (K/Z_0) is known (according to the synthesis equations ((2.38),(2.39) and (2.40)), the module of the transfer parameter (S_{21}) that is necessary in the simulation of the structure of Fig. 2.23 can be obtained with the relationship (2.44)[9] (reader is referred to section 2.6.1 for more details).

To perform the study, we will use the notation (ω_{ij}, t_{ij}) to refer to the width and thickness, respectively, of the coupling windows of the filter. The first subscript (i) refers to the position of the iris in the filter. For the filter that is going to be designed $i = 1, 2, 3$, considering that the filter is a symmetrical filter of fifth order. The second subscript (j) refers to the number of different thicknesses that have been taken in the analysis. In this study we will select up to twelve different thicknesses ($j = 1, 2, \dots, 12$).

Once the values (ω_{ij}, t_{ij}) that synthesize a given impedance inverter are known, it is necessary to compute the lengths of the resonators for a fixed resonant frequency. The technique was explained in section 2.6.2. It is based on the structure of Fig. 2.23 too. This structure is simulated with a full wave technique, acting on the positions of the reference planes, until the phase of the transmission parameter that is obtained is $Ph(S_{21}) = -\pi/2$ at the design frequency (11 GHz) (reader is referred to section 2.6.2 for more details). At this moment half of the length of the loaded resonator by the correspondent iris will have been obtained ($L_{ij}/2$) [12] (see Fig. 2.23).

It is important to realize that at the end of this procedure, we have a set of irises and resonators with geometries $(\omega_{1j}, t_{1j}, L_{1j})$, so all of them synthesize the first inverter of the filter, and all the cavities have the same central resonant frequency (11 GHz), but with coupling windows of different

thicknesses. The same applies to the irises and resonators related to the second inverter of the filter $(\omega_{2j}, t_{2j}, L_{2j})$, and with the irises and resonators related to the third inverter of the filter $(\omega_{3j}, t_{3j}, L_{3j})$.

We show in Table 3.1 the values of the normalized inverters needed for the design of the filter of our example, together with the required value of the transmission parameter ($|S_{21}|$) that is obtained with the equation (2.44). Table 3.2 includes the geometric data for all the irises and resonators designed using the procedure described previously. The table includes the data of the irises corresponding to the three impedance inverters of the filter ($i = 1, 2, 3$) and for all the thicknesses of the irises ($j = 1, 2, \dots, 12$). The final step is to check out the spurious frequency for every iris designed. The

	$\frac{K}{Z_0}$	$S_{21}dB$
ω_{1j}	0.1918	-8.6352
ω_{2j}	0.0285	-24.8822
ω_{3j}	0.0200	-27.9661

Table 3.1: Table of the impedance inverters

t_j	ω_{1j}	ω_{2j}	ω_{3j}	L_{1j}	L_{2j}	L_{3j}
1	8.109	4.259	3.779	8.265	9.485	9.507
2	8.918	5.121	4.642	7.954	9.2696	9.363
3	9.580	5.885	5.393	7.648	9.108	9.220
4	10.13	6.539	9.220	7.359	8.943	9.073
5	10.59	7.113	6.626	7.070	8.774	8.922
6	11.00	7.626	7.141	6.780	8.608	8.768
7	11.34	8.087	7.008	6.514	8.435	8.614
8	11.65	8.502	8.033	6.249	8.267	8.459
9	11.90	8.878	8.418	5.970	8.099	8.305
10	12.13	9.224	8.771	5.727	7.933	8.150
11	12.33	9.536	9.095	5.489	7.770	7.998
12	12.51	9.824	9.393	5.260	7.608	7.847

Table 3.2: Table of dimensions (millimeters)

best way to perform this computation is to use the structure of a single doubly terminated coupled resonator, as shown in the Fig. 3.1.

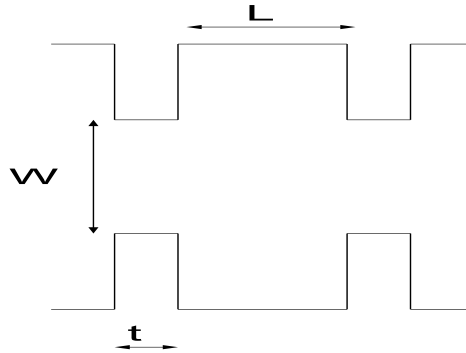


Figure 3.1: Structure for the computation of the spurious frequency

We place all the designed irises (ω_{ij}, t_{ij}) in the coupling windows, with the total length that has been computed (L_{ij}) to maintain the same resonant frequency at 11 GHz (see table 3.2). For all the cases, the structure is simulated in a large frequency range, and the spurious frequency is measured.

We have done the procedure described previously for all the three inverters of the filter that has been proposed as example. For all the optimized geometries, the first spurious frequency has been measured using the configuration of Fig. 3.1. The resonant frequencies of the first spurious for the three inverters are shown in Fig. 3.2.

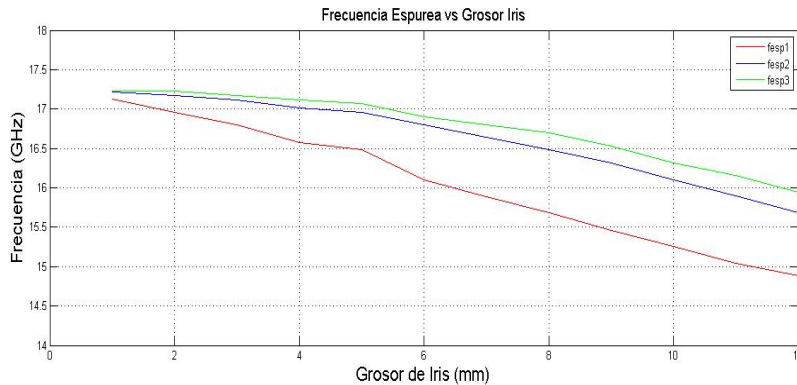


Figure 3.2: Influence of the thickness of the iris in the spurious frequency

From the results that have been obtained, we are able to conclude that it is possible to achieve a wide control in the spurious resonant frequency, modifying the thickness of the coupling windows (t_{ij}). In fact, we can observe that for very thin windows, the spurious frequency for all the three inverters is produced near to 17.2 GHz. If the thickness of the window is increased, the spurious resonant frequency for the first iris drops to 14.9 GHz. The effect is similar if the resonator is loaded with the other inverters, although the effect is less strong than in the previous case, and the spurious frequency is reduced to 15.7 GHz for the second inverter, and 16 GHz for the third inverter. The results show

stronger influence if the resonator is loaded with the input inverter. This observation indicates that the spurious frequency of the first resonator will be able to be adjusted acting on the thickness of the input inductive window in a more effective way.

These results confirm that synthesizing the inverters of the filter with non-uniform coupling windows, it will be possible to introduce different displacements for the different spurious frequencies, so that it is possible to avoid the constructive combination of the spurious band.

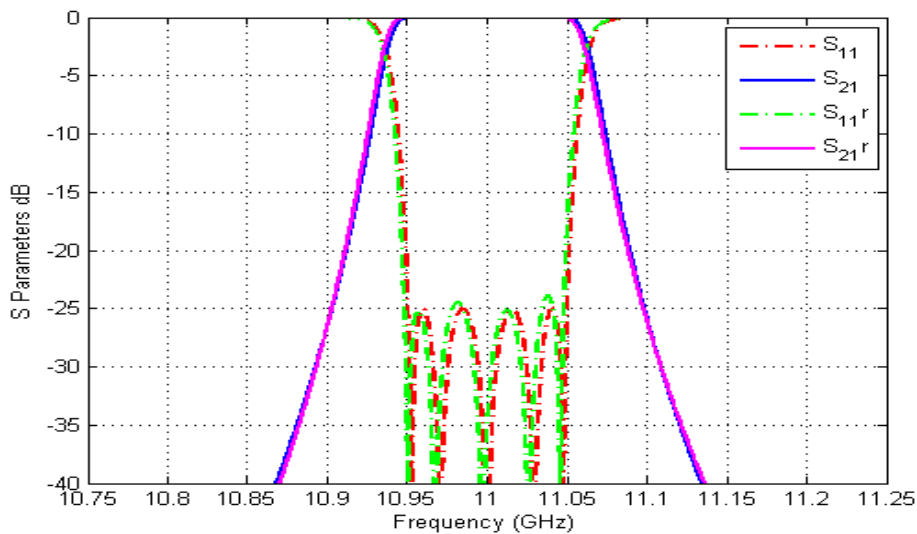
With the aim to check out the effectiveness of the proposed idea, first we will take as reference filter one that has been designed with the same thickness of 2 millimeter for all the coupling windows. The filter has been designed with the procedure described in the previous section (characterization of the isolated impedance inverters, see Fig. 2.23), using the software FEST3D [13]. Fig. 3.3(a) shows the simulated results obtained in the passband, and table 3.2 includes the dimensions for the windows and the length of the resonators (taking into account that $t_{ij} = 2$ for all the irises). As can be seen, the filter that has been designed meets the initial requirements perfectly.

To check out the behavior of the reference filter in the spurious band, its response is shown in Fig. 3.3(b) from 9 GHz until 20 GHz. It can be observed that a spurious band appears very sharp above 17 GHz.

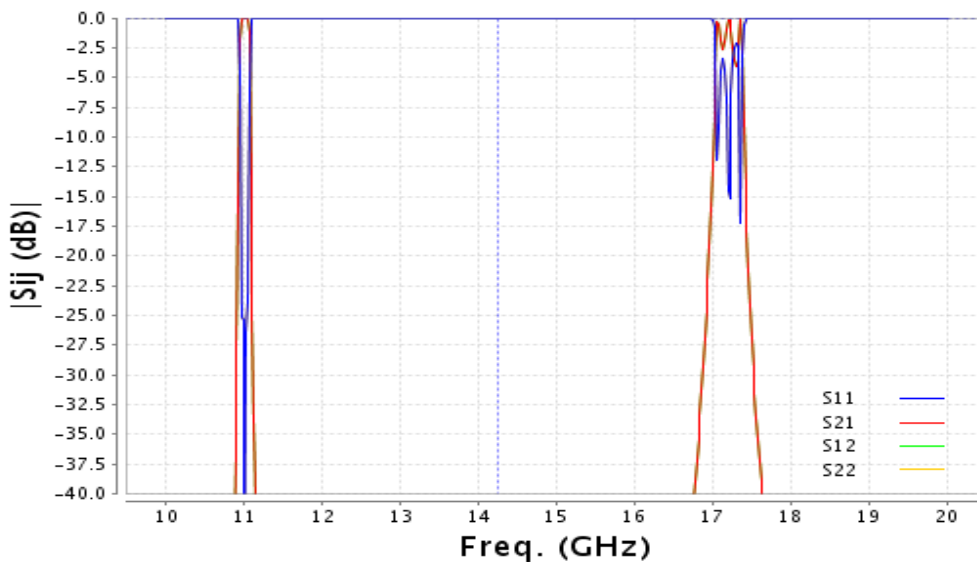
With the aim to prove the effectiveness of the technique that has been proposed in this work, first another filter was designed using smaller thicknesses for the external windows ($t_{1,2}$) and bigger thicknesses for the internal windows ($t_{2,8}$, $t_{3,11}$). In this way, when the filter is dimensioned, all the coupling windows have similar widths (ω_{ij}). The dimensions of the filter are included in Table 3.2 ($\omega_{1,2}, L_{1,2}$; $\omega_{2,8}, L_{2,8}$; $\omega_{3,11}, L_{3,11}$). The response of the filter in the pass band is shown in Fig. 3.4(a), where it can be seen that the filter presents the desired transfer function, very similar to the reference filter. On the other hand, Fig. 3.4(b) shows the behavior of the filter out of the pass band of the filter, to study the spurious behavior.

We can observe that the use of bigger thicknesses of the windows has shifted the spurious to lower frequencies (closer to the passband). However, the goal of the reduction of the spurious levels has not been achieved. In fact, there is a wider spurious band than the initial one, and closer to the passband (starting around 16 GHz).

Since the previous strategy does not achieve the initial goal, the strategy is now changed in the election of the thicknesses of the coupling windows. Now, the idea is to choose a very wide external window ($t_{1,12}$), whereas the internal windows will be thinner ($t_{2,9}, t_{3,1}$). This election of the thicknesses of the windows cause a big difference between the input window ($\omega_{1,12}$), that is now very open, and



(a)



(b)

Figure 3.3: Response of the reference filter. (a) Response of the filter inside the passband. (b) Response of the filter out of the passband, showing the spurious band.

the internal window ($\omega_{3,1}$) that is now very close. The response of the filter within the pass band is shown in Fig. 3.5(a).

The dimensions obtained after the design process are shown in Table 3.2 ($\omega_{1,12}, L_{1,12}$; $\omega_{2,9}, L_{2,9}$; and $\omega_{3,1}, L_{3,1}$). In the results shown, it is possible to observe that the design in the pass band is not as precise as for the filters designed previously. The filter is not as good as the other because

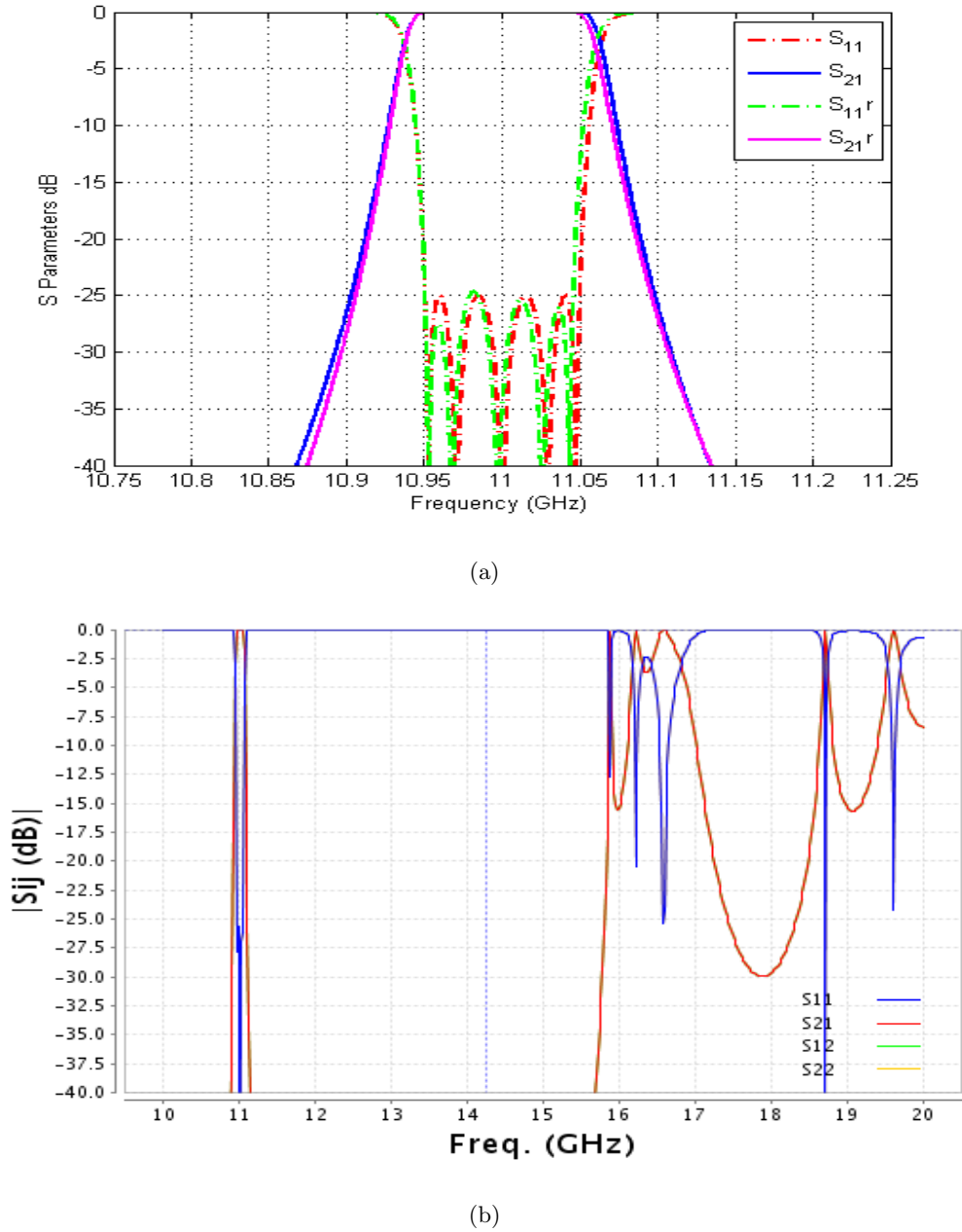
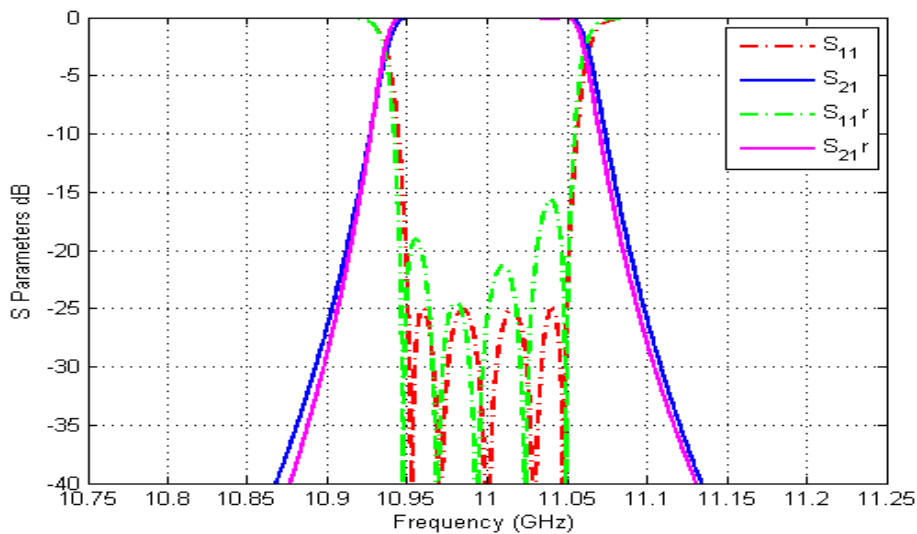
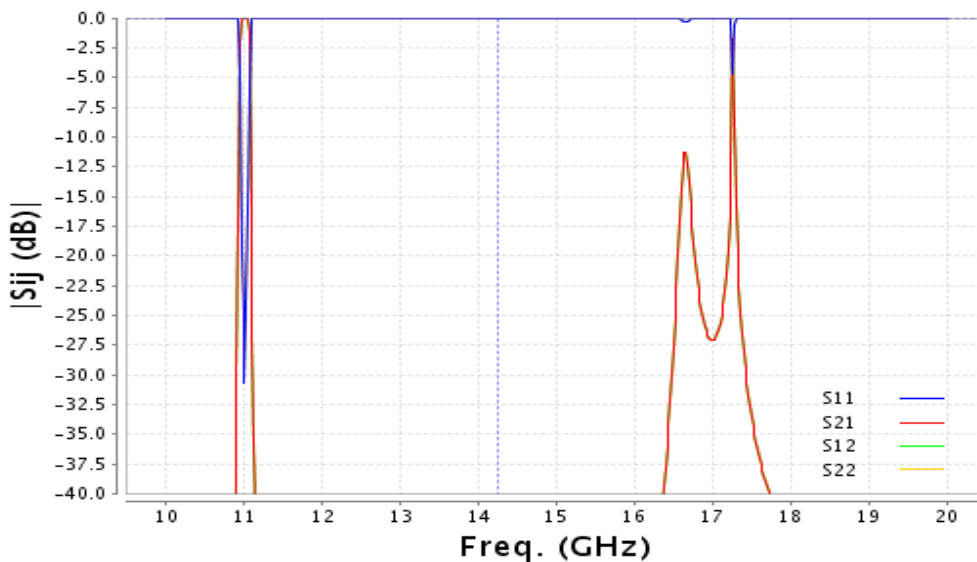


Figure 3.4: Response of the filter with thicknesses of (2, 8, 11)mm (a) Response inside the passband and (b) Response of the filter out of the passband

of the external coupling window. This window is very open (because it has a big thickness), so it has a very strong effect on the *slope parameter* of the adjacent resonator, which is very different to the nominal value of an ideal closed waveguide resonator. This result indicates that it would be interesting to develop techniques for the design of filters, which introduce *slope parameter* corrections for the resonators that have been strongly affected by very wide windows due to the use of large thickness values. In any case, for the study of the spurious band that is the aim of this work, the



(a)



(b)

Figure 3.5: Response of the filter with thickness of (12,9,1)mm (a) Response of the filter inside the passband and (b) Response of the filter out of the passband.

result obtained after the design process is acceptable.

Finally, Fig. 3.5(b) shows the behavior of the filter in the out of band region. Once again, the spurious frequency occurs at lower frequencies because of the use of windows with bigger thickness values. Nonetheless, the introduction of the non-uniform thicknesses reduces the spurious level about -12 dB in the frequency region below 17 GHz. It can also be observed that the reduction of the spurious band is not complete, because there is still a resonance peak around 17.2 GHz. Nevertheless, spurious

bandwidth has been reduced markedly, if it is compared with the spurious band of the reference filter shown in Fig. 3.3(a).

3.3 Spurious reduction using non-uniform cavities

In Chapter 2, it has been explained the main parameters of a filter and it has been reviewed a basic design procedure for waveguide bandpass filter. The design procedure is based on calculating the required values of the impedance inverters from the lowpass prototype elements, and the impedance inverters of ideal resonators.

The filters that have been designed in the previous chapter have the characteristic that all the cavities have the same widths. That is to say, in the impedance inverter and transmission lines model, all the transmission lines have the same characteristic impedance. In this section, it will be reviewed the design of waveguide bandpass filters for the case when cavities have different widths. This means that the characteristic impedances of the terminating transmission lines and of the transmission line resonators, could be different.

Firstly, it will be introduced the filter design procedure when an iris connects resonators with different cavity widths. Because of the different widths, they have different characteristic impedances, therefore the formulas of the impedance inverter (2.38),(2.39) and (2.40) that have been introduced in Section 2.5 suffer slight modifications. The design of the filter using different cavity widths along the filter forces the spurious from each cavity to appear at different frequencies, therefore it is expected to avoid the constructive combination of the spurious band [9]. This effect could help to the previous strategy of changing the thicknesses of irises, to reduce the spurious band.

The filter design procedure that use different cavity widths is similar to the traditional method studied in Section 2.5. In fact, the procedure is the same except for two steps that must be modified. These two steps are the computation of the transmission parameter that is associated to the impedance inverter, and the method to obtain the length of the cavity. Therefore, these two steps will be explained below. For illustration, in Fig. 3.6 I present an example of a filter with different cavity widths in the resonators. In this case, the cavity that has been modified is the central cavity. Actually it does not matter because the procedure is general regardless which cavities are changed.

As it was done in Chapter 2, the dimensions of the filter will be calculated using a structure to compute the dimensions of each iris and the length of each cavity individually. This structure, which represents a coupling window that communicates two cavities, can be represented as shown in Fig. 2.23, if the cavities have the same width; or it can be represented as shown in Fig. 3.7 if the

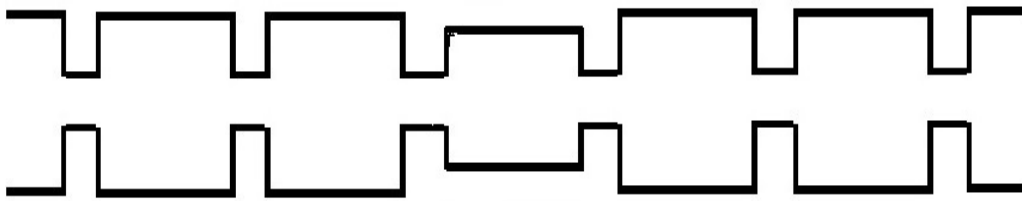


Figure 3.6: Structure of the new type of filter, containing non uniform waveguide cavity widths.

cavities have different widths.

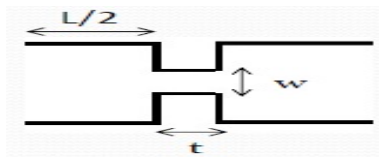


Figure 3.7: Structure of the coupling window for the computation of the iris dimension with two cavities that have different widths.

Fig. 3.7 has the equivalent circuit shown in Fig. 3.8. This equivalent circuit represents the coupling window as an impedance inverter, and the cavities that have different widths as two transmission lines with different characteristic impedances.

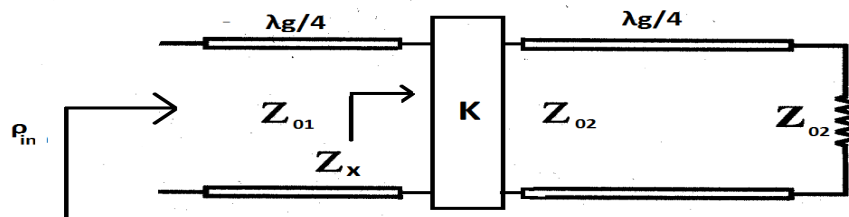


Figure 3.8: Equivalent circuit of the structure of the coupling window for the computation of the iris dimension if the cavities attached have different widths.

Finally, the procedure to design a filter like the filter whose structure is shown in Fig. 3.6 consists of the steps outlined below.

1. Design of lowpass prototype

Lowpass prototype and their formulas is the same as shown in Section 2.3.

2. Computation of g_i elements

Computation of g -elements is the same as shown in Section 2.3.

3. Computation of normalized impedance inverter

In this case the normalization of the impedance inverter is performed in a slightly different way as it was shown in Section 2.5.2. The final scaling is done in the following way:

$$\frac{K_{01}}{\sqrt{Z_{01} Z_{02}}} = \sqrt{\frac{R_A X_1 w}{g_0 g_1}} \quad (3.1)$$

$$\frac{K_{i,i+1}}{\sqrt{Z_{01} Z_{02}}} = w \sqrt{\frac{X_i X_{i+1}}{g_i g_{i+1}}} \quad (3.2)$$

$$\frac{K_{n,n+1}}{\sqrt{Z_{01} Z_{02}}} = \sqrt{\frac{R_B X_n w}{g_n g_{n+1}}} \quad (3.3)$$

Where R_A and R_B are the resistance of the generator and the load impedance respectively, g_i are the values of the lowpass prototype elements and $w = \frac{\text{Bandwidth}}{\omega_0}$ is the fractional bandwidth. X_i is the slope parameter corresponding to the previous cavity and X_{i+1} is the slope parameter corresponding to the next cavity. For example, for the filter shown in Fig. 3.6, the third iris K_{23} is affected by the slope parameter of the standard cavity X_2 and the slope parameter of the cavity with reduced width X_3 . These two same slope parameters are also used in the scaling of the fourth iris. On the contrary, first, second, fifth and sixth irises are only affected by the slope parameter of the standard waveguide. This is because the resonators placed at both sides of these irises have the same width. In other words, for the filter shown in Fig. 3.6 the slope parameters of the resonators attached to these irises satisfy the condition $X_i = X_{i+1}$.

4. Synthesis of dimensions

Once the normalized value of the impedance inverters ($\frac{K}{\sqrt{Z_{01} Z_{02}}}$) are computed by eq. (3.1), eq. (3.2) and eq. (3.3), the next step is to compute the value of the S_{21} parameter as follows:

$$|S_{21}| = \frac{2}{\frac{K}{\sqrt{Z_{01} Z_{02}}} + \frac{\sqrt{Z_{01} Z_{02}}}{K}} \quad (3.4)$$

$$|S_{21}| \text{ dB} = 20 \log_{10}(|S_{21}|) \quad (3.5)$$

Once the scattering parameter $|S_{21}|$ needed to design our filter is known, the procedure to obtain the iris width is the same as the procedure explained in the section explaining the traditional method (Section 2.6.1) but in this case the structure to be simulated is the one shown in Fig. 3.7. The structure of Fig. 3.7 is simulated with a full wave software and the result of this simulation is compared with the theoretical $|S_{21}|$. If this theoretical $|S_{21}|$ value is bigger than the result of the simulation then the iris width has to be decreased, and vice versa. The iris width has to be modified until its simulated $|S_{21}|$ response is equal to the theoretical $|S_{21}|$ (reader is referred

to Section 2.6.1) for more details). On the other hand, Fig. 3.8 shows the equivalent circuit of the structure of the coupling window with two different cavities as shown in Fig. 3.7. This circuit will be analyzed in order to obtain the necessary value of the phases for the calculation of the half lengths of the two cavities attached to a given iris. In this case, the half length of one cavity is different from the other cavity. Therefore we will need two different conditions for the calculation of the two different half lengths. One condition is related to the S_{11} parameter and the other one is related to the S_{21} parameter. When the output port is loaded with the corresponding reference impedance, the input reflection coefficient represents the S_{11} parameter. The input reflection coefficient is computed as

$$\rho_{in} = \rho_x e^{-2\beta l} \quad (3.6)$$

where ρ_x is:

$$\rho_x = \frac{Z_x - Z_{01}}{Z_x + Z_{01}}$$

and Z_x is:

$$Z_x = \frac{K^2}{Z_{02}}$$

Since (Z_{02}) is real, the phase of ρ_x is 0° if $Z_x > Z_{01}$ or 180° if $Z_x < Z_{01}$. In addition, the electrical length of the input transmission line is $-\beta l = -\frac{2\pi}{\lambda_g} \frac{\lambda_g}{4} = -\pi/2$. Using eq. (3.6) the phase of the input reflection coefficient becomes $\rho_{in} = S_{11} = -180^\circ$ if $Z_x > Z_{01}$ or 0° if $Z_x < Z_{01}$.

In case of S_{21} the phase is -90° . This is because the phase introduced by the quarter-wave transmission line is again $-\beta l$, thus $\frac{2\pi}{\lambda_g} \frac{\lambda_g}{4} = \frac{\pi}{2}$. The impedance inverter introduces a phase of $\pi/2$ to the transmitted wave. Finally, summing the phase of each part of the circuit leads to $Ph(S_{21}) = -\pi/2 + \pi/2 - \pi/2 = -\pi/2$.

The technique was explained in section 2.6.2 for the case when the cavities have equal characteristic impedances. In this case the technique is similar, but now it is adapted to the structure of Fig. 3.7, where the length ($L/2$) is the half length of the first cavity and the length ($L'/2$) is the half length of the second cavity having different widths. This structure is simulated with a full wave software, acting on the positions of the reference planes independently (L and L'), until the phase of the transmission parameter that is obtained is $Ph(S_{21}) = -\pi/2$ and $Ph(S_{11} = 0)$ at the design frequency (11 GHz).

Chapter 4

More Illustrative Examples of Spurious Reduction

One of the aim of the project is to reduce the spurious band response for waveguide bandpass filters. With the purpose of illustrating the technique used in this project to reduce the spurious band, a specific filter is studied, implemented in different forms, which will serve as the examples in this chapter. Specifically, the filter that will be designed is a bandpass filter of fifth order, whose central frequency is 11 GHz, its bandwidth is 100 MHz, and its Reflexion level -25 dB. It is made using the waveguide technology and its response is the classic Chebyshev function. The coupling windows are inductive windows for the simplicity of the design.

With the aim to observe the behaviour of the filter using the design strategy explained in Section 3.2, some examples are shown below. Simulations that are shown below are run with the software Fes3D. Firstly, I will present the results for the filter designed by the traditional method in which the thickness of the iris is thin and all the thicknesses are the same along the filter. Secondly, the strategy is to design the filter using different thicknesses for the coupling irises. Thirdly, using different width for the cavities, and finally both of the strategies are combined with the aim to remove the spurious band completely.

4.1 Filters using constant coupling windows thicknesses

First, note that the final values of the impedance inverters when they are denormalized only depend on the slope parameters of the resonators. Consequently, if the widths of the resonators are not modified, the denormalized values of the impedance inverters do not change. Thus, in the two next

examples, namely, the filter using constant irises thickness along the filter and the filters with non-uniform thicknesses in the coupling windows along the filter, have the same impedance inverters, and the corresponding (S_{21}) scattering parameters according to equation (2.44) are: $S_{21\ 1} = -8.6352$ dB, $S_{21\ 2} = -24.8822$ dB, $S_{21\ 3} = -27.9661$ dB where $S_{21\ i}$ is the scattering parameter expressed in dB, associated to the impedance inverter for the i_{th} coupling window.

For the design of filters that have the same waveguide width along the filter, the widths of the impedance inverters are computed with the theory presented in Section 2.6.1, and the lengths of the cavities are adjusted with the theory presented in Section 2.6.2.

However, in this case, with the aim to make easier the design of filters with any combinations of thickness for the irises, I have included an appendix at the end of this document (Appendix 8) where Tab. 8.1, Tab. 8.2 and Tab. 8.3 are tables collecting the dimensions of the irises for different thicknesses, and for the corresponding impedance inverters of the filter under study. Therefore, for the design of a specific filter, these tables can directly be used. Note that these tables have been computed using the theory explained in Section 2.6.1 and Section 2.6.2. These tables specify the values of the width and length of the irises and resonant cavities respectively, for the studied filter. The steps to build a certain filter are, therefore, to choose a specific thickness for the iris, and then to look in the table for the correspondent width and half length for the resonator attached to this iris. The length of the final cavity resonator is actually composed of the two half lengths corresponding to the two irises attached to the corresponding resonator. This will be illustrated with the next example example.

To begin, it will be shown how to build a symmetrical filter whose iris thicknesses are 2 millimeters along the whole structure, due to the fact that this filter will be considered as the baseline filter. This filter has been selected as the reference filter in Section 3 because of its simplicity. The next filters will be compared with this reference filter, with the aim to prove if the final target, that is to reduce the spurious, is achieved.

For the design of a filter whose iris thicknesses are 2 millimeters, we look in the three tables, in the row ($j = 2$), and it is obtained the values for the lengths of resonators and the widths of the irises, namely: $\omega_{1,2} = 8.9182$ mm, $\omega_{2,2} = 5.1217$ mm and $\omega_{3,2} = 4.642$ mm, where $\omega_{i,j}$ is the width of the iris in the i -th position along the filter, and the index j denotes the thickness of the iris in millimeters. The tables also give the half lengths of the resonators attached to each iris. With these

values, the final lengths of the complete resonators can be calculated, resulting in $L_1 = 17.224$ mm, $L_2 = 18.663$ mm and $L_3 = 18.727$ mm. The final design is shown below in Fig. 4.1.

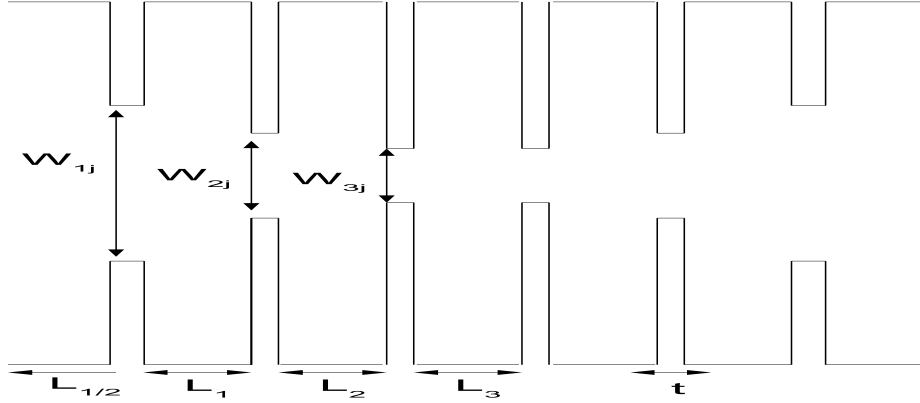


Figure 4.1: Geometry of designed referenced filter.

The behaviour of the reference filter in the fundamental frequency band is shown in Fig. 3.3(a) from Section 3, and the out of band behavior of this filter is shown in Fig. 3.3(b).

The filter above, as could be observed when it was studied in Section 3, meets the specification requirements in the passband. However, it does not achieve any reduction in the spurious level. This is to be expected, because of the simplicity of the design (the filter is uniform in both cavity widths and iris thicknesses).

Thereupon, another filter with constant iris thickness will be simulated below. Due to the fact that the spurious frequencies of the different resonators are more different when the iris thickness is increased to 8 mm, according to Fig. 3.2, the constructive combination of the spurious will be more difficult as compared to the reference filter, that used quite thin irises. Therefore the spurious level could be expected to reduce as compared to the reference filter.

According to this hypothesis, the next filter that will be studied is a symmetrical filter whose iris thicknesses are constant along the filter. However, instead of having a constant thickness of 2 millimeters, the thickness will be increased to 8 millimeters. Specifically, using again the information contained in the tables of Appendix 8, the dimensions of the filter are the following: all iris thicknesses are equal to 8 millimeters, the width of the irises are $\omega_{1,8} = 11.6515$ mm, $\omega_{2,8} = 8.5025$ mm, $\omega_{3,8} = 8.033$ mm; the final lengths of the cavities can be calculated from the half lengths of the resonators given in the tables, resulting in $L_1 = 14.5173$ mm, $L_2 = 16.7266$ mm and $L_3 = 16.918$ mm. The filter

is symmetrical so the lengths of the other cavities are $L_4 = L_2$ and $L_5 = L_1$ whereas the widths of the irises are $\omega_{4,8} = \omega_{3,8}$, $\omega_{5,8} = \omega_{2,8}$ and $\omega_{6,8} = \omega_{1,8}$.

As before, the behaviour of the filter is assessed both inside the passband and in the expected spurious band. Remember that the fundamental passband covers the frequency range from 10.75 GHz to 11.25 GHz, whereas the spurious band extends up to 20 GHz. The results in the fundamental frequency band is shown in Fig. 4.2(a) and the simulation covering the out of band response is shown Fig. 4.2(b).

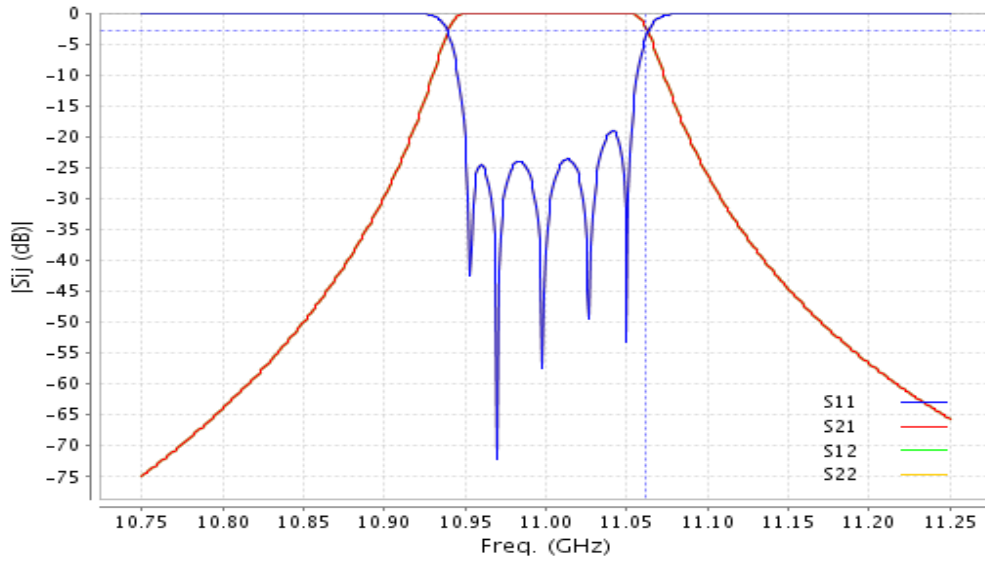
The behaviour of the filter in the fundamental frequency band is good since the filter meets almost completely the target specifications. However, there is a lobe whose reflexion level goes above -25 dB. It may be because of the slope parameter is not equal to the nominal slope parameter used to obtain the value of the impedance inverter, as it has been discussed in Section 3. The spurious band response level has not been reduced as compared to the reference filter. In addition, it can be noticed that the spurious band has been lowered in frequency. Therefore, it is closer to the fundamental passband, which is an undesirable effect. In fact, the spurious response instead of being at frequencies higher than 17 GHz it is now between 16 GHz and 17 GHz.

In spite of this result, I continue with the same strategy of maintaining constant the thicknesses of the irises along the filter. However, I will increase even more the thickness value. In this way I would like to see if the differences in the spurious resonances introduced by the different resonators are increased, and in this way the spurious band is reduced.

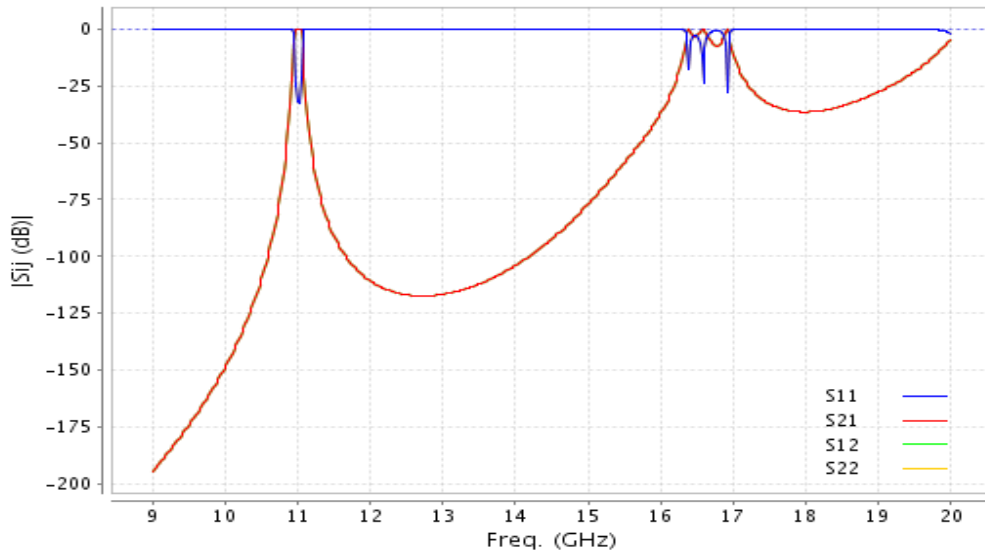
The filter that will be studied next is the filter whose iris thicknesses are 10 millimeters. The dimensions of the filter according to the tables collected in Appendix 8 are: all the thicknesses of the irises equal to 10 millimeters, the width of the irises $\omega_{1,10} = 12.132$ mm, $\omega_{2,10} = 9.2224$ mm, $\omega_{3,10} = 8.771$ mm; the length of the cavities result to be $L_1 = 13.6615$ mm, $L_2 = 16.2387$ mm and $L_3 = 16.61$ mm. It is observed that the cavities with larger irises are shorter than the cavities with shorter irises. This is due to the fact that larger irises need to be wider than shorter irises and the load effect in the cavity is bigger. The simulation results for the fundamental frequency band is shown in Fig. 4.3(a) and the spurious frequency band response is shown in Fig. 4.3(b).

The in-band response of the filter has the same problem as the previous filter, namely that the slope parameters used to compute the impedance inverters of the filter are not the accurate values of the slope parameters in the real waveguide resonators. For this reason there is a reflection lobe that does not meet the requirements. In general, however, the response of the filter is acceptable, because the other specification are fulfilled.

It can be observed in the obtained results, that the spurious band has not been reduced. Further-



(a)

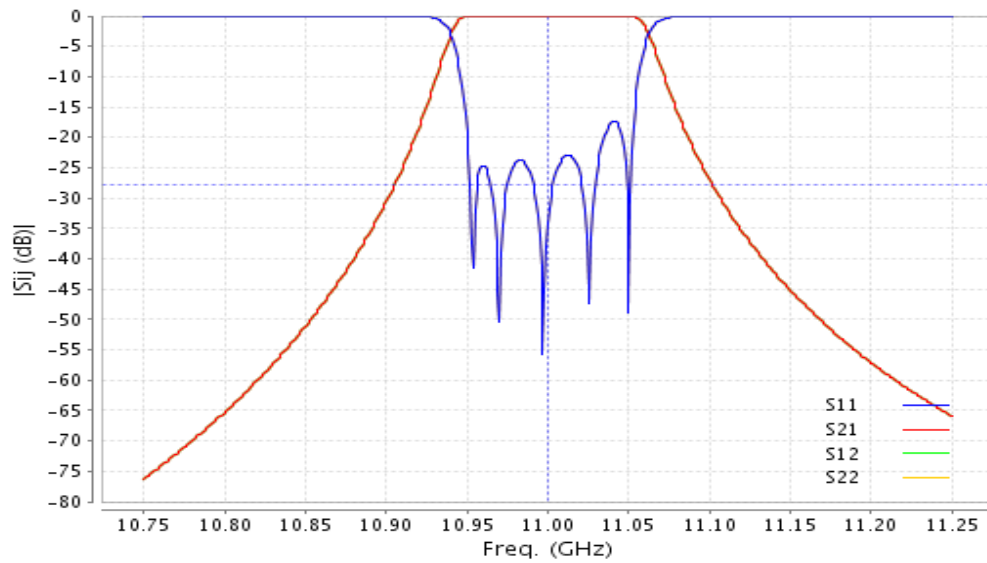


(b)

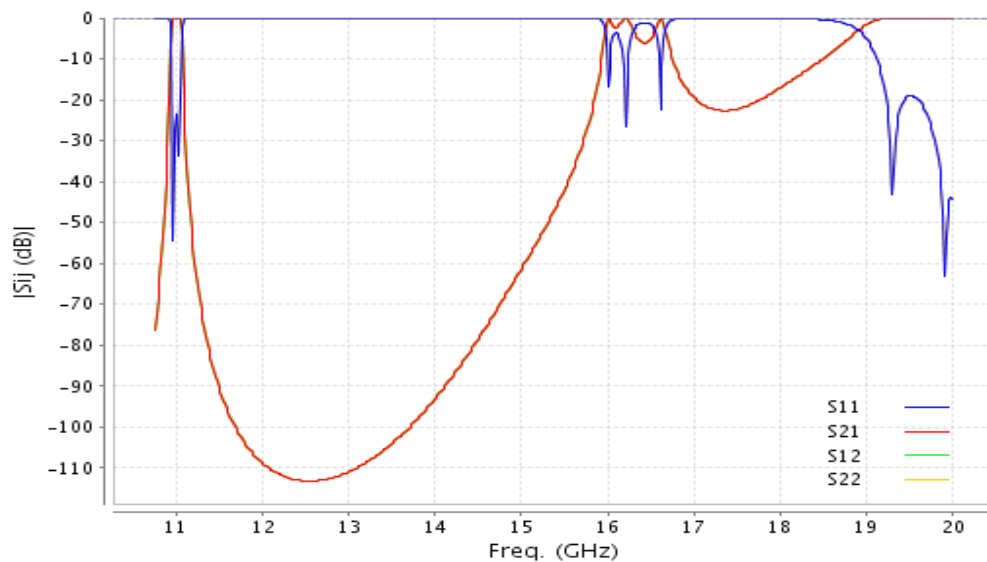
Figure 4.2: Response of the filter that uses constant thicknesses of 8 mm along the filter. (a) Response inside the passband. (b) Response of the filter out of the passband.

more, the spurious is closer to 19 GHz, which is an undesired effect.

In conclusion, various filters with constant thicknesses in the irises along the structure have been studied. The difference between them is that the iris thickness is increased from one filter to the next. In general, by increasing only the iris thickness, the spurious are not removed, and the objective is not achieved. Evenmore, the spurious band approaches the fundamental passband, which is an undesired effect.



(a)



(b)

Figure 4.3: Response of the filter that uses constant thicknesses of 10 mm. (a) Response inside the passband. (b) Out-of-band response of the filter.

Due to this result, it seems necessary to take non-uniform thicknesses of the irises along the filter. In this way the differences between the spurious frequencies of the different resonators will be increased, and the cancellation of the spurious band could improve.

The filters using constant thicknesses along the structure, as introduced in this section, is not effective, since the spurious band is not reduced. Hence, the next step is to simulate a filter with irises of variable thicknesses to introduce larger differences in the spurious bands of the resonators. In this

way the constructive combination of the spurious band is more difficult and the spurious band could be reduced. Therefore, according to this hypothesis in the next section we explore different options introducing non-uniform iris thicknesses.

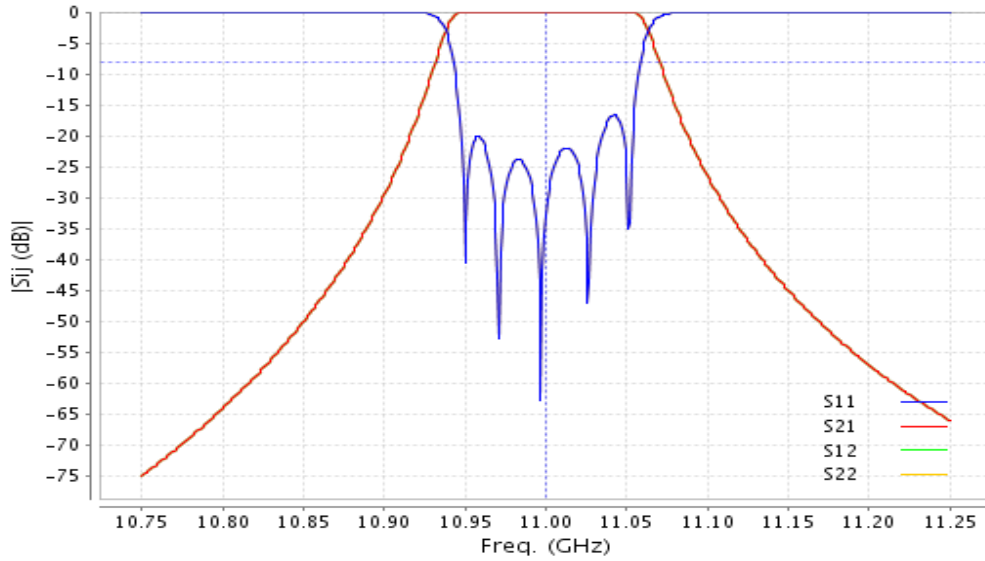
4.2 Filters using non-uniform coupling windows thicknesses along the filter

Now that the behaviour of the filters designed using the same thicknesses of iris along the filter have been studied, it can be concluded that the spurious band reduction must be achieved using other strategies. In fact, it was observed in the previous section that by using thicker but uniform irises, the behaviour of the filter is even worse than using short irises. Therefore, the strategy to be tried now is to change the thickness of the iris along the filter. In this case the thicknesses are different depending on the position of the iris in the filter. The idea is to use different irises along different positions in the filter to avoid the constructive combination of harmonics into a strong spurious frequency band. This strategy has been explained in this project in Section 3 and two examples have been shown. Therefore, the aim of the actual section is to show more examples, following this general strategy, to see if the spurious band can be reduced even more.

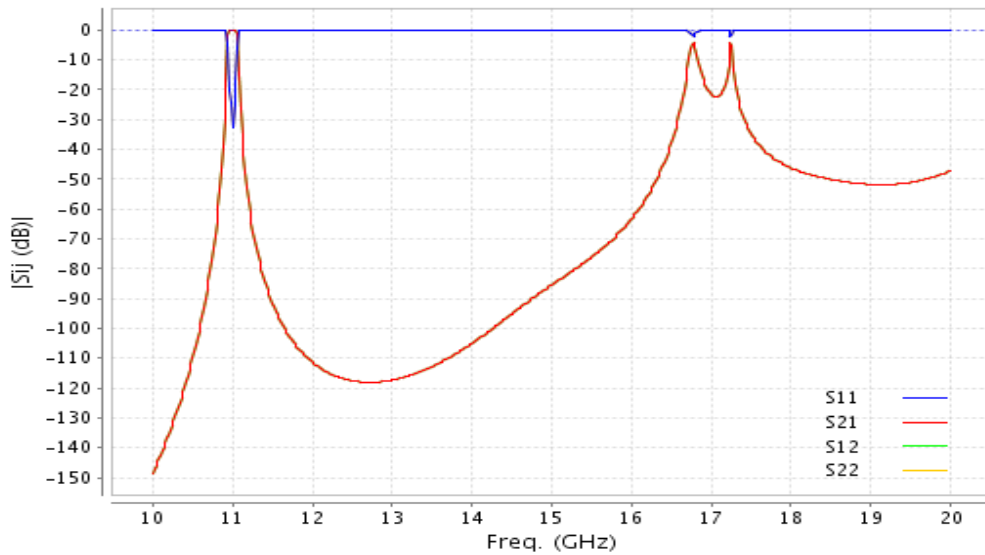
The previous examples (examples of Section 3) followed two strategies, the first one was to use smaller thicknesses for the external coupling windows and bigger thicknesses for the internal coupling windows. The second one was the reverse procedure, namely using bigger thicknesses for the external coupling windows and smaller thicknesses for the internal coupling windows. The examples that will be shown below are: a example that follows the second strategy, a second example with a totally asymmetrical structure, and a third example of a filter that uses a narrow thickness for the first coupling window, a thick iris for the second one, and the third one uses a narrow thickness again.

Then, the first example that has been designed uses coupling windows thicknesses equal to 11 millimeters for the exterior coupling window, 8 millimeters for the second coupling window and 2 millimeter for the most interior coupling window. Specifically, the dimensions of the filter are: $\omega_{1,11} = 12.334$ mm, $\omega_{2,8} = 8.5025$ mm, $\omega_{3,2} = 4.642$ mm; the length of the cavities are $L_1 = 13.7569$ mm, $L_2 = 17.6311$ mm and $L_3 = 18.727$ mm. The behaviour of the filter in the passband can be seen in Fig. 4.4(a).

The simulation results show a filter whose behaviour in the passband does not meet the specifications requirements. The central frequency is a little beneath 11 GHz, and all the reflection lobes have a level higher than -25 dB. This behaviour is logical, taking into account that the external coupling



(a)



(b)

Figure 4.4: Response of the filter that uses thicknesses of (11, 8, 2) mm along the structure. (a) Response in the passband. (b) Response of the filter out of the pass band.

window is a very wide one. Therefore, the nominal slope parameter for the resonator attached to this coupling, is very different as compared to the slope parameter of the real waveguide resonator. In spite of this behaviour in the passband, the filter has reasonable performance, so that it could be used for comparison purposes with respect to the reference filter. The results for this filter out of the pass band show a considerable reduction of the spurious cwbandwidth as shown in Fig. 4.4(b). In fact, the spurious frequency bandwidth has been reduced a lot, and it can be observed that there are only

two remaining resonant peaks.

One of the two peaks is beneath 17 GHz and the other one is slightly above this frequency. Therefore, the resonant peaks are closer to the fundamental frequency as compared to the original baseline filter. However, the bandwidth of the spurious band has been reduced as compared to the same reference filter. If it is compared with the response of the filter shown in Fig. 3.5(a), which was designed in Section 3, the conclusion is that the current example is worse than this previous filter. Although both of them present good results in the reduction of the spurious bandwidth, the filter designed in Section 3 exhibits lower spurious levels than this new filter.

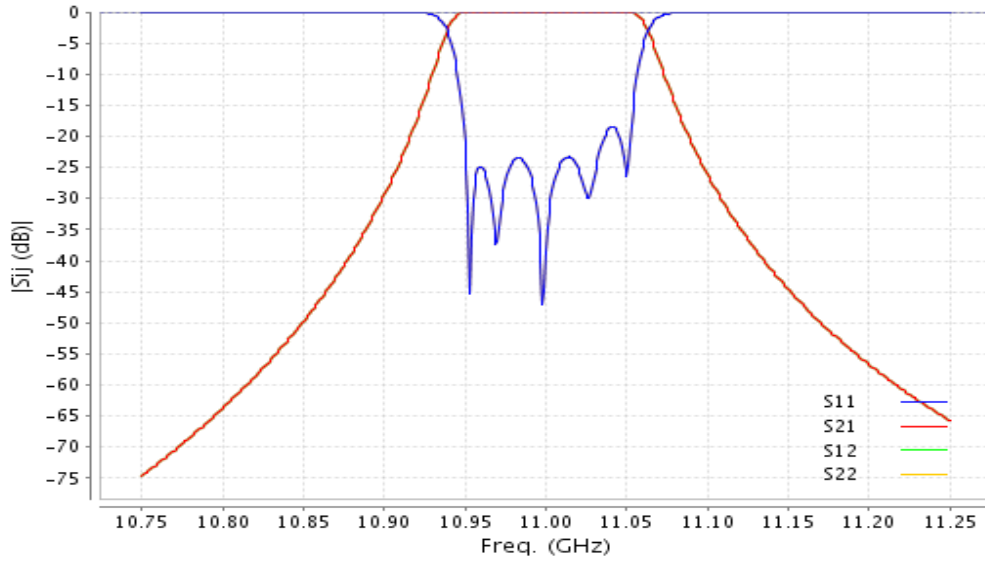
For all the above mentioned filters, the strategy of using big thickness for the external coupling windows and small thickness for the inner coupling windows is a good strategy to, at least, reduce the spurious bandwidth, although this strategy does not remove it completely.

Below, a new strategy is used with the same objective. The new strategy is based on the use of totally different coupling windows along the filter. In this case, all the thicknesses are different and the result is that the filter is totally asymmetric, from input to output. The idea is to use the highest possible number of different thicknesses to avoid the constructive combination of harmonic resonances as much as possible. In this case, the dimensions of the filter are: $\omega_{1,12} = 12.5118$ mm, $\omega_{2,10} = 9.2243$ mm, $\omega_{3,8} = 8.033$ mm, $\omega_{4,6} = 7.1415$ mm, $\omega_{5,4} = 6.5398$ mm, $\omega_{6,2} = 8.9182$ mm; $L_1 = 13.1943$ mm, $L_2 = 16.3927$ mm and $L_3 = 17.227$ mm, $L_4 = 17.714$ mm and $L_5 = 16.8975$ mm. The simulation result in the passband can be observed in Fig. 4.5(a) and the simulation out the passband can be observed in Fig. 4.5(b). The response in the passband is acceptable, although there is a lobe in the reflection level that does not meet the target specifications of -25 dB level. On the other hand, Fig. 4.5(b) shows that the filter reduces the spurious band. Nevertheless, the filter is not good enough to avoid the constructive combination of the spurious band.

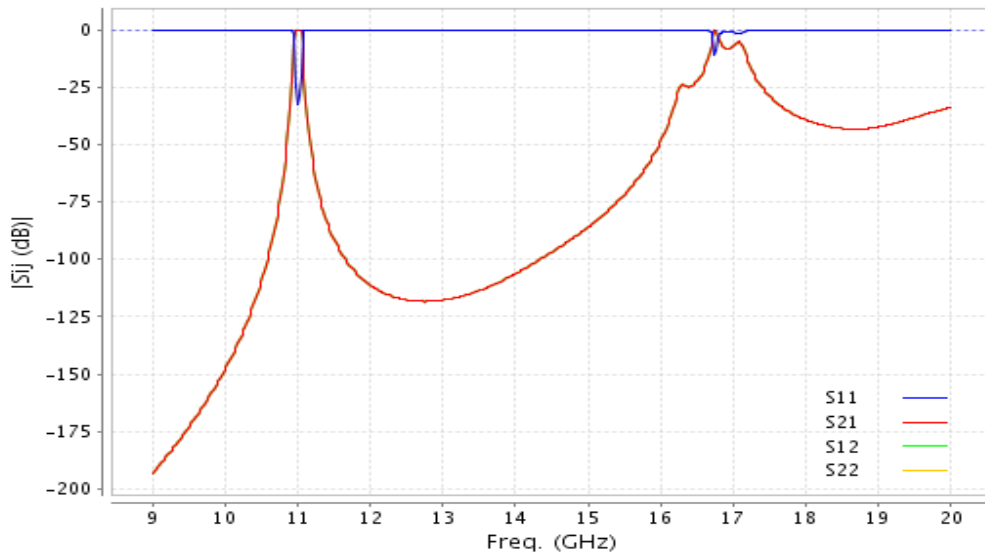
Finally, the strategy that uses a small thickness for the first iris, a big thickness for the second one and a small thickness for the third one again, is used to design the last example of this section.

The simulation results are shown in Fig. 4.6(a) for the response inside the passband and Fig. 4.6(b) for the response out of the passband. The dimensions of the filter are as follows: $\omega_{1,1} = 8.1093$ mm, $\omega_{2,11} = 9.5367$ mm, $\omega_{3,1} = 3.779$ mm, $L_1 = 16.0355$ mm, $L_2 = 17.2776$ mm and $L_3 = 19.0152$ mm.

As can be seen, the fundamental band is not very different from the other examples, that also use non-uniform coupling windows along the filter. Anyway, it can be observed that the spurious band is reduced considerably. There is a resonant peak about 17.3 GHz but the rest of the spurious band has been reduced by a level below -30 dB, what is a good result for the goals of this project.



(a)

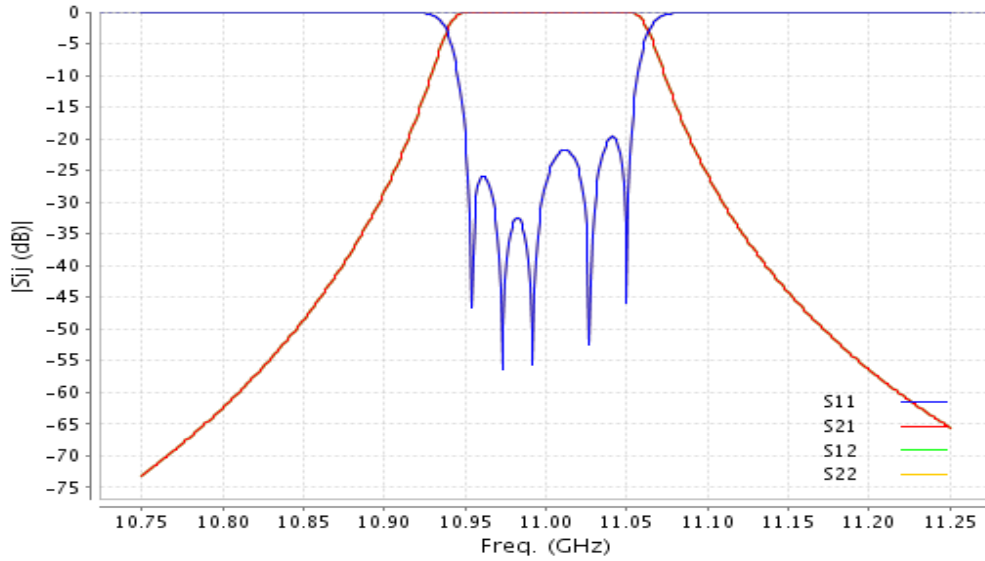


(b)

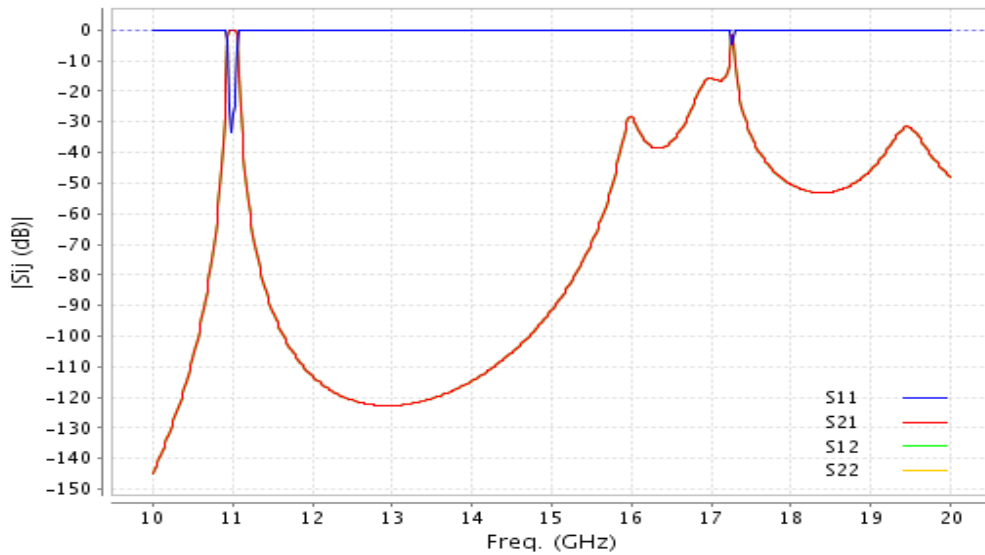
Figure 4.5: Response of the filter that uses non-uniform thicknesses of (12, 10, 8, 6, 4, 2) mm. (a) Response in the passband. (b) Response of the filter out of the pass band.

4.3 Filters using non-uniform cavity width

A different process will be followed to design the filter in this section. This process consists, basically, in using non-uniform widths for the resonant cavities that compose the filter. Actually, the filter is built with resonators that use waveguides whose widths are equal to 19.05 millimeters, except for few specific cavities, that have widths equal to 18 millimeters. The procedure to build a filter with these



(a)



(b)

Figure 4.6: Response of the filter that uses thicknesses of (1,11,1) mm along the structure. (a) Response in the passband. (b) Response of the filter out of the passband.

characteristics has been explained in Section 3.3. As a summary, once the cavity that is going to be different is established, the width of the iris is computed to obtain the desired impedance inverter using equations (3.1,3.2 and 3.3), and the lengths of the cavities are computed to obtain the resonance at 11 GHz, using the procedure described in Section 3.3.

In this case, I will explore three examples to be shown following this strategy. Firstly, the central cavity is changed for the cavity whose width is equal to 18 mm. Secondly, the cavities that are going

to be changed are the first and the fifth cavities. Finally, in the last example of this section, the cavities that are going to be changed are the second and fourth cavities.

The first example, namely the filter whose central cavity presents a different width, has the following dimensions: $\omega_{1,1} = 8.1093$ mm, $\omega_{2,1} = 4.31119$ mm, $\omega_{3,1} = 3.91$ mm, $L_1 = 17.67$ mm, $L_2 = 18.973$ mm and $L_3 = 20.356$ mm. Note that L_3 is the length fo the cavity with different width, and the filter is symmetrical. The simulation results of the filter can be seen in Fig. 4.7(a) for the response inside the passband and the results out of the passband are shown in Fig. 4.7(b).

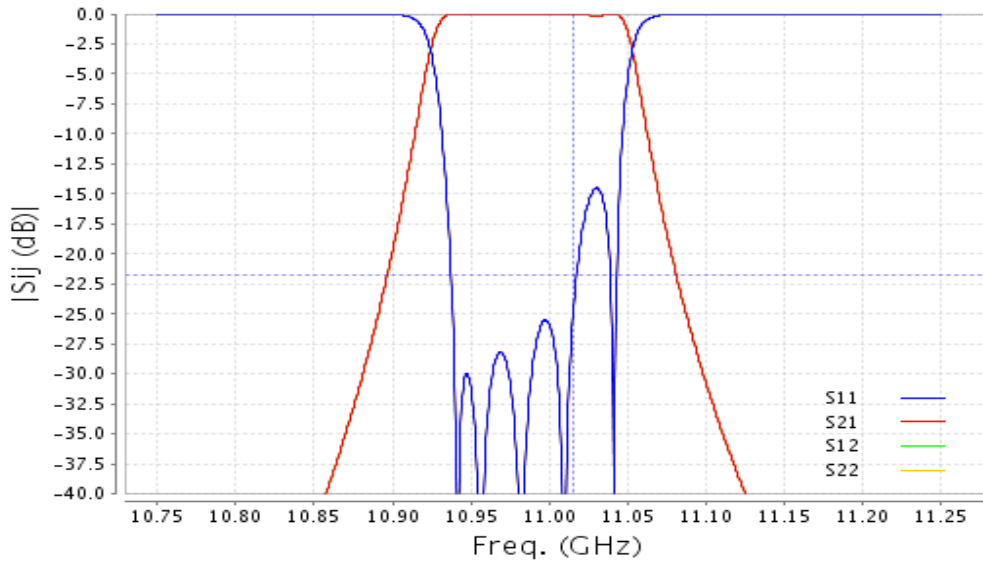
The response of the filter of Fig. 4.7 can be analyzed both inside the passband, and in the spurious band. Inside the passband, the response is not perfectly equi-ripple, but the behavior is acceptable. On the other hand, it can be observed that the spurious has only two resonant peaks. One of them is in 16.5 GHz and the othe one is in about 17.3 GHz. Also, the level of the first peak is quite low, below -17 dB. In general, the bandwidth of the spurious has been largely reduced. Therefore, it can be said that the strategy to change the width of the cavity seems to be a good strategy. With the aim to confirm this hypothesis, it is going to be changed the width of the most external cavities, i.e the first and the fifth cavities.

Changing both the first and the fifth cavities, the dimensions of the filter are as follows: $\omega_{1,1} = 8.2757$ mm, $\omega_{2,1} = 4.311$ mm, $\omega_{3,1} = 3.779$ mm, $L_1 = 18.82$ mm, $L_2 = 18.915$ mm and $L_3 = 19.015$ mm. Note that L_1 and L_5 are the lengths of the resonators with different cavity widths, and the filter is also symmetrical.

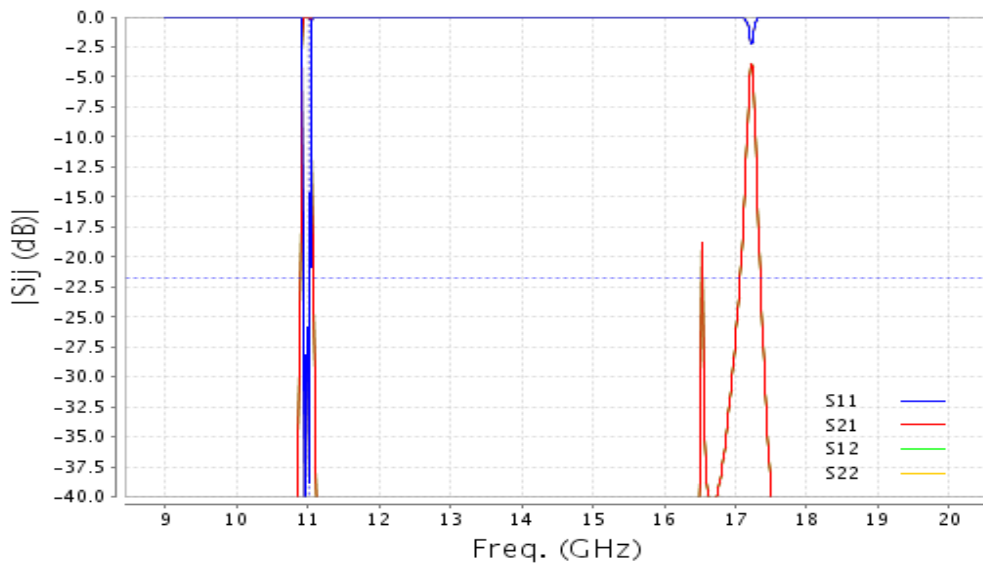
The simulation result inside the passband can be observed in Fig. 4.8(a), and Fig. 4.8(b) shows the response of the filter out of the passband, that can be used to observe the behaviour of the filter in the spurious band.

The new strategy is not good if the cavities that are changed are the most external cavities, as can be observed in Fig. 4.8. The response of the filter in the passband has a good behaviour because it meets the specifications. It is centered in 11 GHz, all the lobes have a reflexion level of at least -23 dB, and the bandwidth is the specified one. The problem is that the behavior of the simulated out of the band (in the range between 17 GHz and 17.4 GHz), is not good because there are three spurious resonant peaks that forms a true spurious band.

Therefore, the next step to check out if the new strategy is able to remove the spurious is based on the change of the second and the fourth cavities. The new dimensions of the filter, which have been computed by the procedure of Section 3.3, are as follows: $\omega_{1,1} = 8.1093$ mm, $\omega_{2,1} = 4.31119$ mm, $\omega_{3,1} = 3.91$ mm, $L_1 = 17.67$ mm, $L_2 = 20.228$ mm, and $L_3 = 18.99$ mm.



(a)

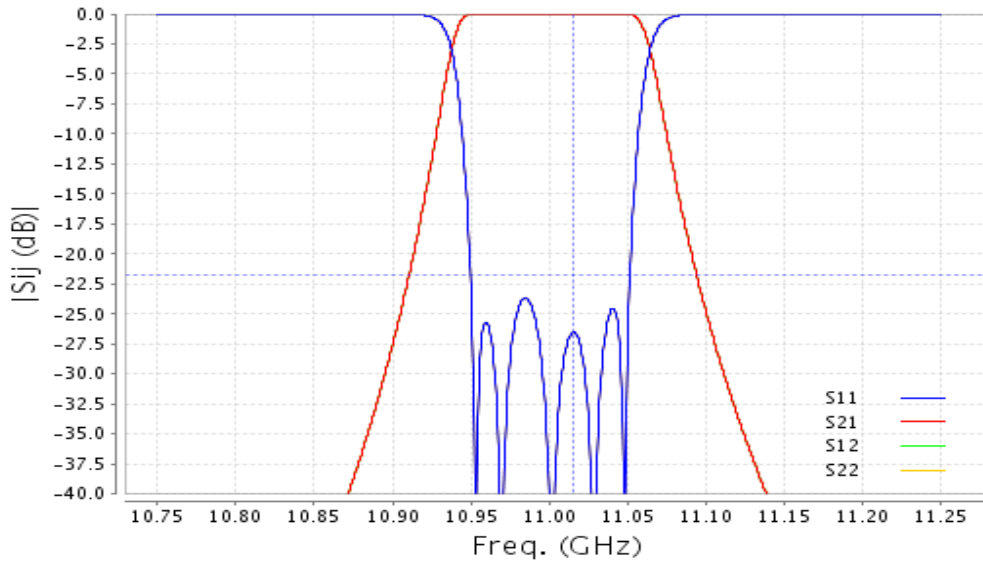


(b)

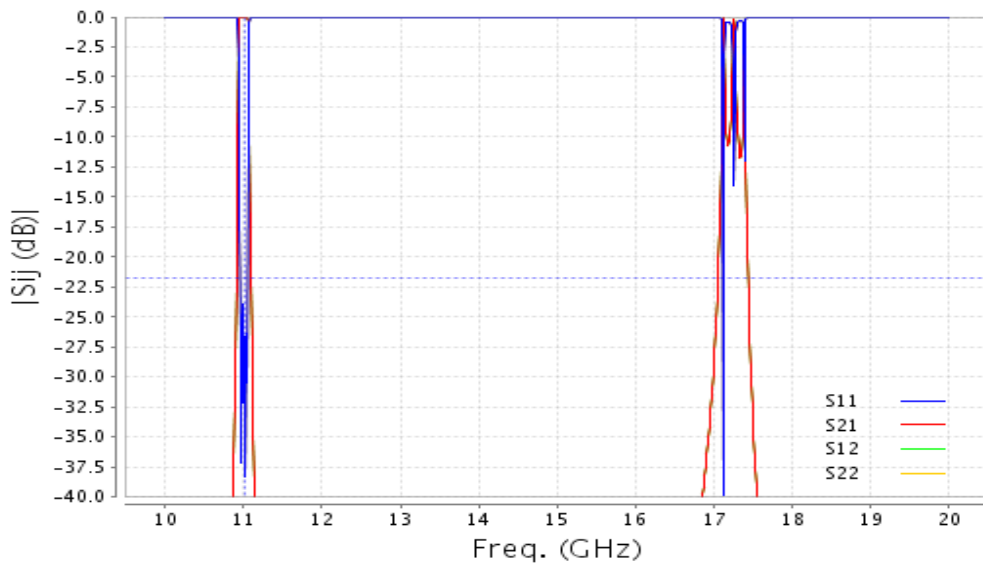
Figure 4.7: Response of the filter that uses thicknesses of 1 mm along the structure and different width for the third cavity. (a) Response inside the passband. (b) Response of the filter out of the passband.

Analyzing the response of the last filter, as shown in Fig. 4.9, it can be seen that the spurious band has been reduced to only two narrow peaks. The first one is in 16.5 GHz and the second one is in 17.3 GHz. Therefore, although with this design the structure has not been able to avoid the construction of spurious frequencies, they have been reduced in bandwidth.

The next step and the last one is based on the idea to combine both of the strategies that have been used in this project. Accordingly, the next examples will consist on filters that will be built using



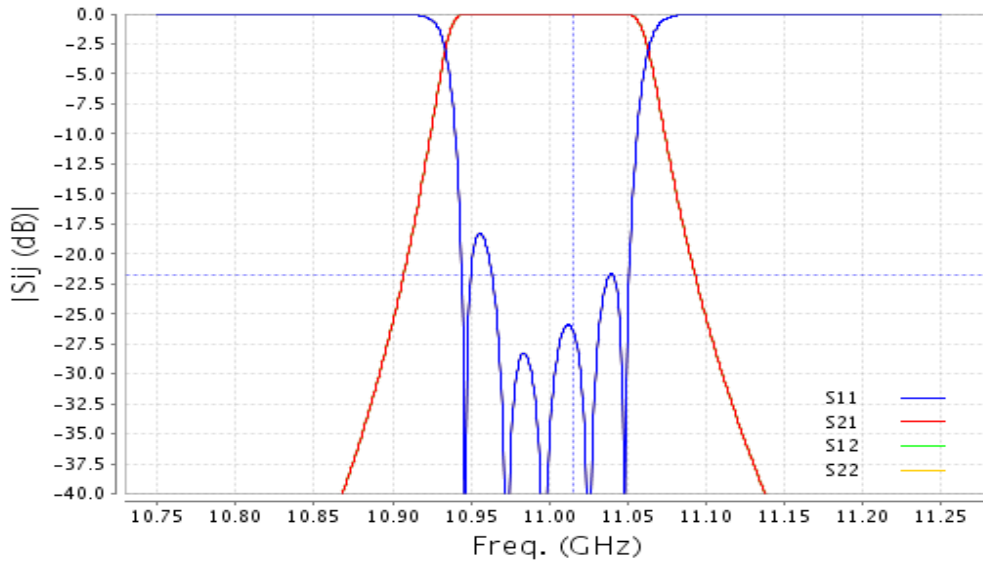
(a)



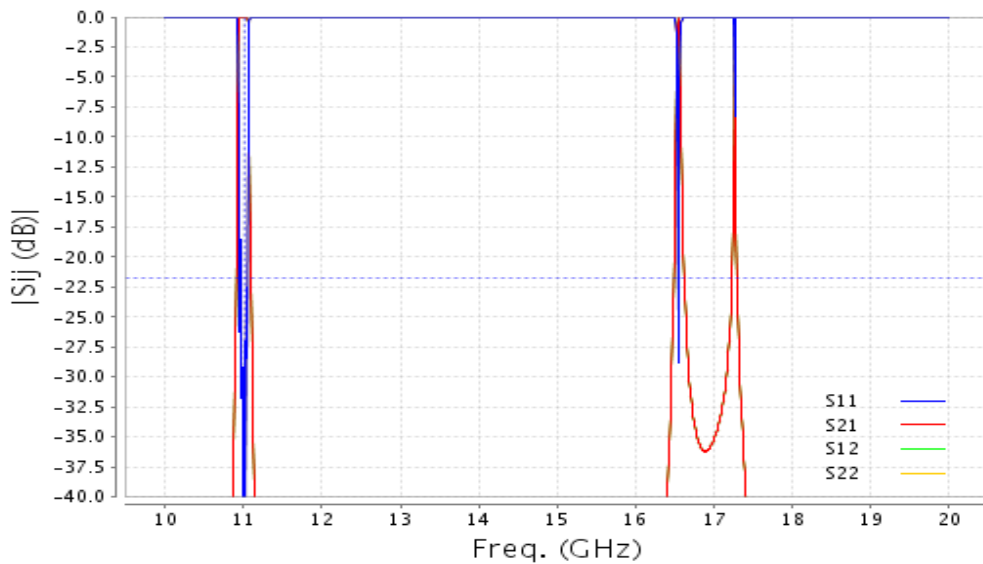
(b)

Figure 4.8: Response of the filter that uses 1 mm thicknesses along the structure, and a different width for the first and the fifth cavities. (a) Response in the passband. (b) Response of the filter out of the passband.

both non-uniform coupling windows and different cavity widths.



(a)



(b)

Figure 4.9: Response of the filter that uses 1 mm thicknesses along the structure and a different width for the second and the fourth cavities. (a) Response in the passband. (b) Response of the filter out of the passband.

4.4 Filters using both non-uniform coupling windows and non-uniform waveguide widths

As stated previously, the final aim of this project is to combine two different strategies. It has been studied the behaviour of filters whose iris thicknesses are different along the structure, and the behavior

of filters with non-uniform cavity widths along the structure. Therefore, this section will be used to study the behavior of filters that are built combining both of them. In this section there will be two examples of filters. Firstly, it will be built a filter using the thicknesses 12 mm, 9 mm and 1 mm because the filter with these irises is known to exhibit good performance. Therefore, the idea is to improve this behaviour by replacing the second and the fourth cavities with other cavities of different widths.

Secondly, the other example will be a filter using the same dimensions of the irises but in this case the filter will be asymmetric, because it will be changed only the width of the second cavity.

The response of the the first example is shown in Fig. 4.10. Its structure is composed by one 18 millimeters cavity and the other are standard cavities of 19.05 millimeters width. The filter is a symmetrical filter with the next dimensions: $\omega_{1,12} = 12.5118$ mm, $\omega_{2,9} = 9.298$ mm, $\omega_{3,1} = 4.7315$ mm, $L_1 = 13.155$ mm, $L_2 = 18.465$ mm, and $L_3 = 18.702$ mm.

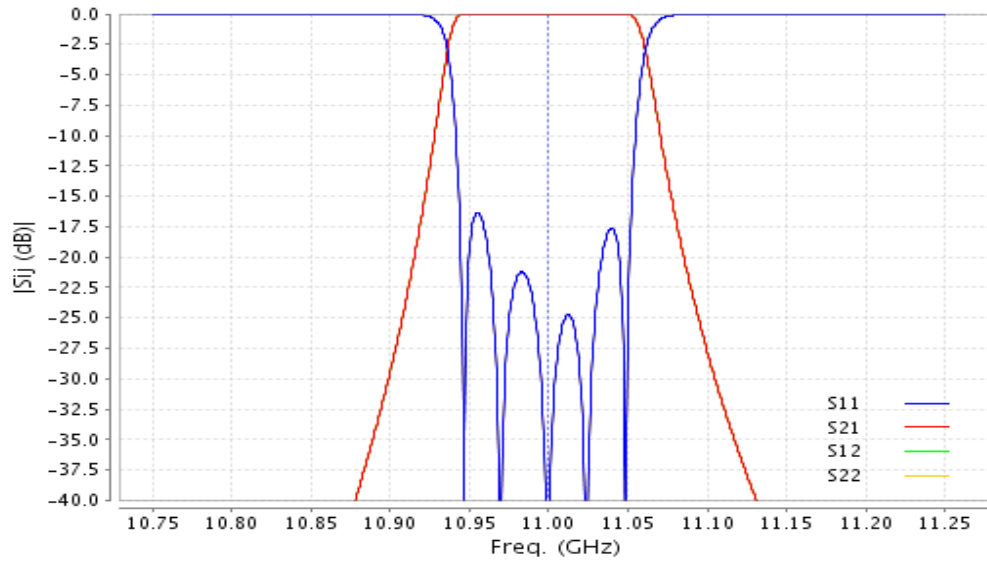
As can be seen in Fig. 4.10(a), the simulated performance is good inside the passband, although all the reflection lobes are not lower than -25 dB, what is one of the main target specifications. Nonetheless it is lower than -20 dB what is good enough to consider the filter as an admissible filter. Additionally, it is centered in 11 GHz and its bandwidth is 100 MHz, which are within the target specifications.

Furthermore, Fig. 4.10(b) shows the behaviour of the the filter out of the passband. It can be observed that the spurious band has been almost eliminated. It remains only a very narrow peak at the frequency of 17.3 GHz. Comparing this behavior with the original filter shown in Section 3, we observe that the spurious band has not been improved considerably. However, the level of the peak in the frequency of 16 GHz has been reduced. In the original filter this level was in -12 dB, and the new filter presents a level of -15 dB.

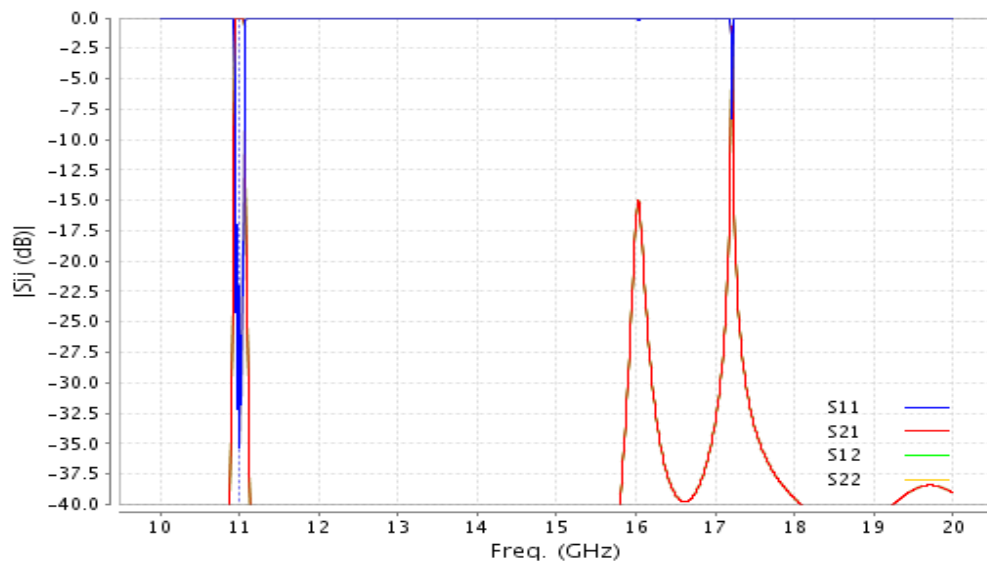
Finally, the last example that is going to be shown in this project is an asymmetrical filter with the second cavity equal to 18 millimeters and the other cavities being standard cavities (19.05 mm width). On the other hand, the thicknesses of the irises that are going to be used are the same thicknesses as in the previous example. Specifically, the new dimensions of the filter are as follows: $\omega_{1,12} = 12.5118$ mm, $\omega_{2,9} = 9.298$ mm, $\omega_{3,1} = 4.7315$ mm, $\omega_{4,1} = 4.7315$ mm, $\omega_{5,9} = 9.2243$ mm, $\omega_{6,12} = 12.5118$ mm $L_1 = 13.155$ mm, $L_2 = 18.465$ mm, $L_3 = 18.72$ mm, $L_4 = 19.2972$ mm and $L_5 = 13.194$ mm.

The behaviour of the filter can be observed in Fig. 4.11 for both the passband and the spurious band. Although the response in the passband is not as good as the others, the spurious band response is the best of all them. In this case, there is a resonant peak but with a really narrow bandwidth. Besides, the rest of the spurious is under -27 dB wich is a really good performance.

4.4. FILTERS USING BOTH NON-UNIFORM COUPLING WINDOWS AND NON-UNIFORM WAVEGUIDE WIDTHS

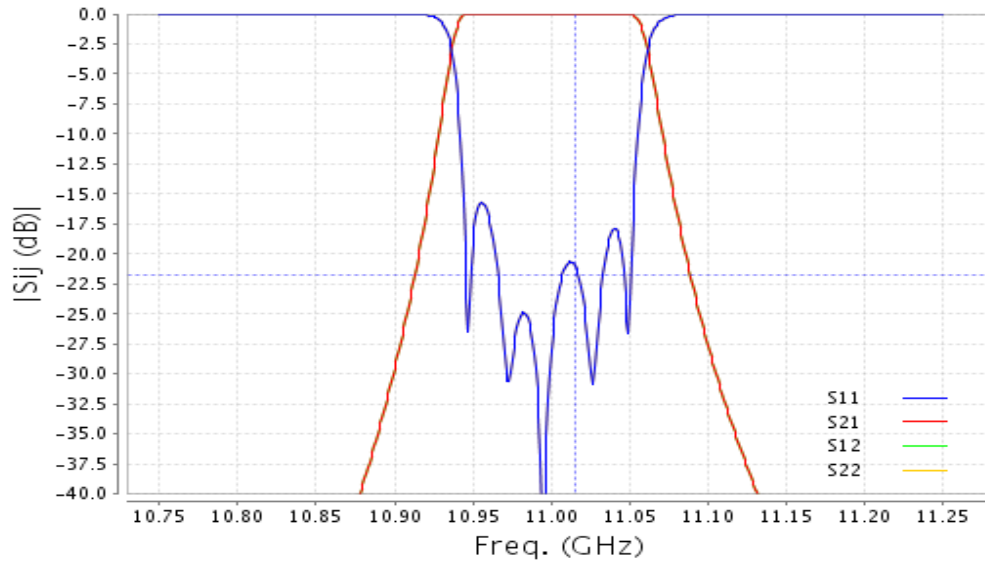


(a)

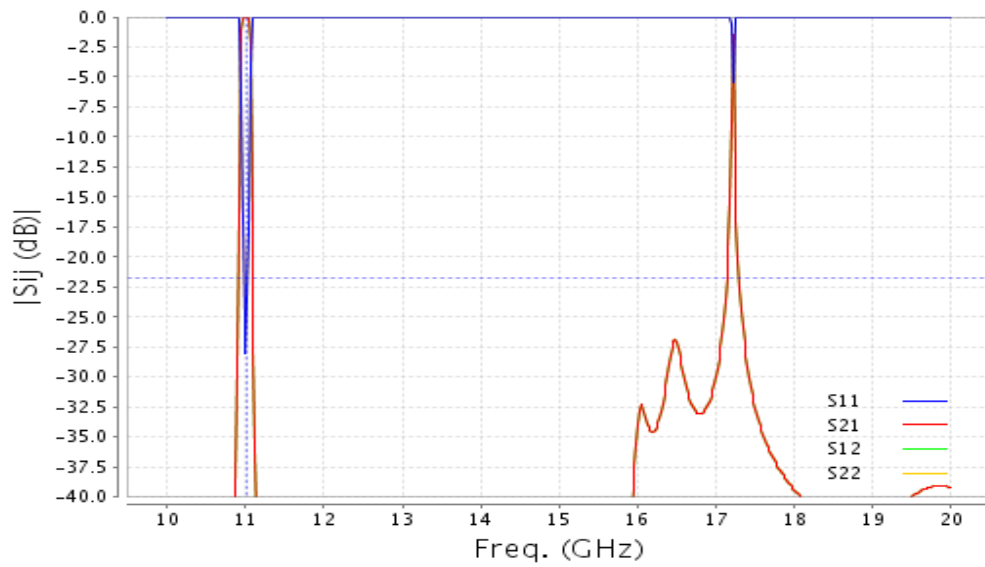


(b)

Figure 4.10: Response of the filter that uses thicknesses of (12, 9, 1) mm and different width for the second and the fourth cavities. (a) Response in the passband. (b) Response of the filter out of the passband.



(a)



(b)

Figure 4.11: Response of the filter that uses thicknesses of (12, 9, 1) mm, and different width for the second cavity. (a) Response in the passband. (b) Response of the filter out of the passband.

Chapter 5

Design of SIW BandPass filter

Waveguide technology has the main advantage over planar transmission structure because of the low loss and its high quality factor. However, there are certain applications where the integration of these components is quite difficult, the solution could be using planar circuits but they usually have high losses. Then, it is born a new concept of substrate integrated waveguide (SIW) in order to meet both specifications, low-cost and high-Q [14], [15].

In this chapter, some considerations that have to be taken into account for designing will be introduced, as well as transitions between the filter implemented with SIW technology and planar technology. In this case, the transition will be between microstrip and SIW. Finally, some experimental results will be shown, and it will be presented a comparison between the simulations of the filters with the full-wave simulator CST and the measurements done of the fabricated structures.

5.1 SIW technology considerations

The structure of a SIW consists of a substrate with top and bottom metal plane and two arrays of via holes that short-circuit both metal planes. An example of a structure of SIW is shown in Fig. 5.1. This structure can be considered as a waveguide where the electromagnetic waves travel through the substrate and are confined by the arrays of via holes that are placed at both sides of the substrate. Therefore, the size of the via holes and the distance between them will play an important role, since a SIW structure will have the same behavior as a rectangular waveguide, as long as two considerations according to these two parameters are complied. These considerations, or restrictions, must be considered in order to avoid a potential radiation [14] and are as follows:

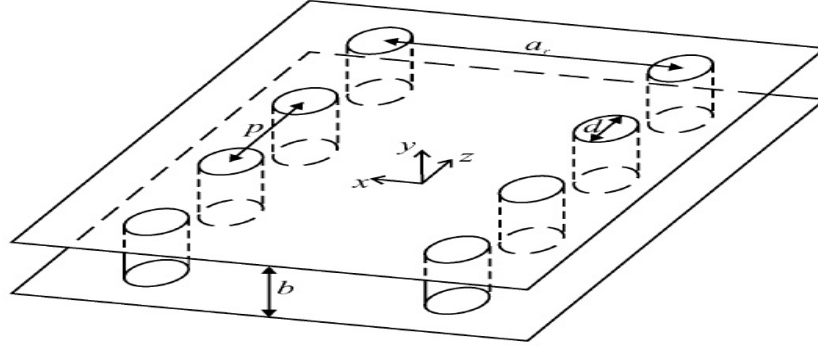


Figure 5.1: Structure of SIW.

1. Via hole diameter

Via hole diameter (d) must be reduced, actually the diameter should fulfill the next relationship:

$$d \leq \frac{\lambda_g}{5} \quad (5.1)$$

Where $\frac{\lambda_g}{5}$ is the wavenumber inside the SIW dielectric substrate and can be computed as the well-known formula:

$$\lambda_g = \frac{c/(f_o\sqrt{\epsilon_r})}{1 - \left(\frac{c/(f_o\sqrt{\epsilon_r})}{2a}\right)^2} \quad (5.2)$$

and c is velocity of light, f_o is the central frequency and ϵ_r is the permittivity of the substrate, a is the width of the waveguide and is calculated from the cutoff as follows:

$$a_{siw} = \frac{1}{2f_{c10}\sqrt{\mu\epsilon}} \quad (5.3)$$

f_{c10} is the cutoff frequency of mode TE_{10} .

2. Pitch

The distance between center of vias (p) is called pitch and is related to the diameter (d) of those vias. The appropriated distance, in order to avoid radiation, can be selected as follows:

$$p \leq 2d \quad (5.4)$$

Choosing properly both the size and spacing of metallic via-holes, leakage loss will be negligible as demonstrated in [14]. The losses of SIW cavity will be determined by the dielectric loss and conductor loss. The conductor loss includes the loss of metallic via-holes and the losses of the bottom and top metal surfaces. Another important parameter is the height of the substrate but this one has no influence into a possible radiation of the structure and only depends on the substrate that we choose.

5.2 Transformation from SIW to Waveguide

A SIW cavity has the same behaviour as rectangular waveguide, however, speaking of designing and computational terms, it is simpler working with rectangular waveguide than SIW, insomuch as it is possible to reuse some of the existing modeling and designing techniques for rectangular waveguide filters. That is why there are some equivalence between both of them that allow us to transform a SIW structure into rectangular waveguide filled with dielectric and vice versa. Formulas to do equivalence between both of them are shown below [11]:

$$a_{RWG} = a\bar{a} \quad (5.5)$$

where a is the width of the SIW cavity and \bar{a} is computed as follows:

$$\bar{a} = \xi_1 + \frac{\xi_2}{\frac{p}{d} + \frac{(\xi_1 + \xi_2 + \xi_3)}{\xi_3 - \xi_1}} \quad (5.6)$$

where:

$$\xi_1 = 1.0198 + \frac{0.3465}{\frac{a}{p} - 1.0684} \quad (5.7)$$

$$\xi_2 = -0.1183 + \frac{1.2729}{\frac{a}{p} - 1.2010} \quad (5.8)$$

$$\xi_3 = 1.0082 - \frac{0.9163}{\frac{a}{p} - 0.2152} \quad (5.9)$$

To transform the dimension of rectangular waveguide filled with dielectric into a hollow rectangular waveguide, next equations must be used:

$$b' = b\sqrt{\epsilon_r} \quad (5.10)$$

$$a' = a_{RWG}\sqrt{\epsilon_r} \quad (5.11)$$

$$d' = d\sqrt{\epsilon_r} \quad (5.12)$$

where b' is the height of the hollow waveguide, a' width of the waveguide and d' is the width of the equivalent iris used in the rectangular waveguide.

An example of Substrate Integrated Waveguide and the equivalent Rectangular Waveguide can be seen in Fig. 5.2.

Once it is obtained the equivalent waveguide, it is only necessary to design the filter using the procedure that has been explained in previous Chapter 2. Finally, the inverse process has to be done, meaning that once the filter has been designed and optimized using the traditional techniques, it is necessary to compute the equivalent dimensions in SIW technology.

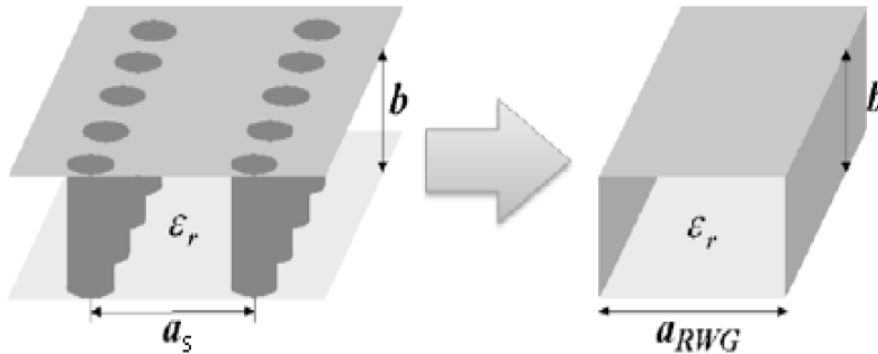


Figure 5.2: SIW and the equivalent rectangular waveguide

5.3 Transition between Substrate Integrated Waveguide and μ Strip

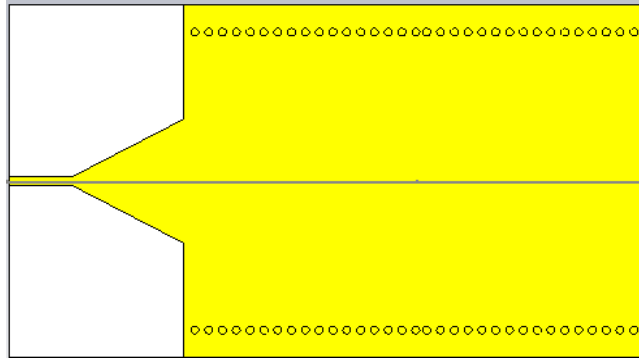
One of the advantages of the Substrate Integrated Waveguide is the relatively easy integration with planar technology. In order to provide a mean to measure the components that have been implemented in SIW or simply, to complete the integration of SIW components with planar circuits, this transition is required. In our case, the transition will be between the SIW bandpass filter and a μ Strip line of standard impedance (50Ω).

Firstly, it will be introduced the more typical transition that can be used and consists only of a tapered μ Strip line [16]. This transition has largely been adopted for two reasons. The first reason is the simplicity of the structure, and due to the simplicity the transition has very low losses. The second one is the bandwidth of the transition, due the tapered shape, the bandwidth is really wide. However, there is an important disadvantage of this kind of structure. This kind of transition tends to be long (about half-wavelength), and its dimensions are typically obtained by means of full-wave simulations.

Secondly, a transition valid for small bandwidth has been chosen, it consists only of a μ Strip line with the impedance desired at input/output, a μ Strip line with the equivalent impedance that better adapt the SIW line, and an impedance inverter to adapt both of them. The performance of this transition is experimentally validated, showing sufficient bandwidth for the required application.

5.3.1 Transition using a tapered μ Strip line

Fig. 5.3 shows the μ Strip-to-SIW transition. It can be observed three section well defined, namely:

Figure 5.3: μ Strip-to-SIW transition1. μ Strip

The first line is a μ Strip whose width w_0 has been computed to obtain the desired impedance at input/output.

2. Taper

This is the transition line that adapt the equivalent impedance of the SIW line with the impedance of the μ Strip line.

3. SIW

This is the SIW line and the dimension w is determined by the cutoff frequency as has been explained previously.

A large difference between the width of the SIW and the width of the μ Strip line will require a long taper. Usually, if the values of both of them are close, a quarter wavelength taper is sufficient to obtain a good return loss. Otherwise, a longer taper will be needed, in any case, the taper length should be chosen as a multiple of a quarter of a wavelength in order to minimize the return loss. The optimum dimensions of the taper, length and width, are obtained using a full-wave simulations. Firstly, it is computed the value of the taper width (w) which minimize the return loss with the structure shown in Fig. 5.4. Once the width has been computed, the next step is to compute the taper length using the structure shown in Fig. 5.3. With the aim to illustrate the design of the taper in a better way, it will be shown a real example that has been designed. The dimensions of the SIW cavity which will be adapted are $w = 31 \text{ mm}$ and $b = 0.508 \text{ mm}$.

Firstly, the width of the taper has been calculated simulating Fig. 5.4 and the results of such simulations are shown in Fig. 5.5. As has been mentioned before (Chapter 1.2), the filter that is going to be implemented with SIW technology is centered at frequency equal to 3 GHz. Consequently, it has to take into account the matching of the transition at 3 GHz to obtain the optimum width.

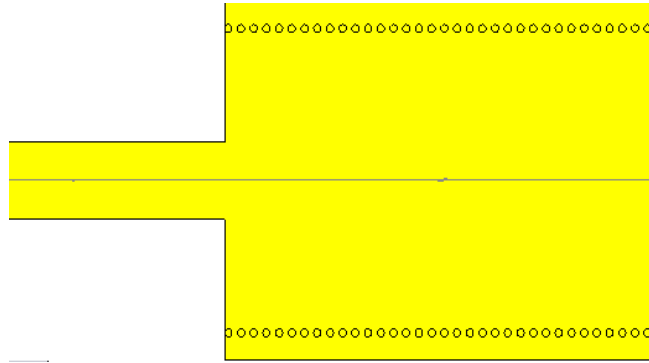


Figure 5.4: Structure to compute the optimum width of the taper

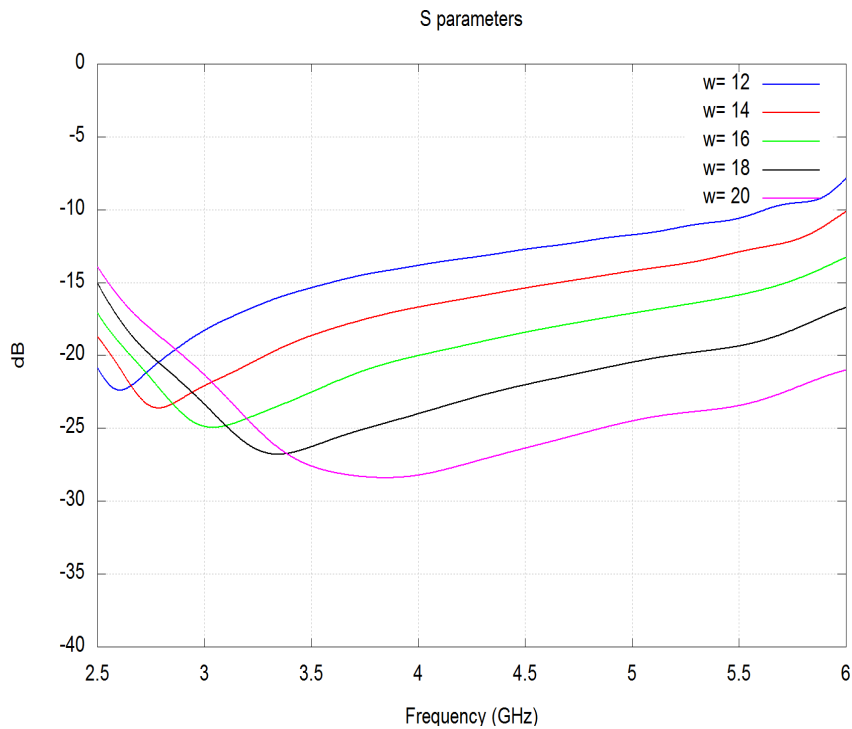


Figure 5.5: Simulations Results of Fig. 5.4

Looking at the simulation results, it can be deduced that the value that we are looking for is a value around 16 millimeters. Running more simulations in order to optimize the value of the width, it is computed a value of 16.2 mm.

Next step is to compute the length of taper. It is simulated Fig. 5.3 with different lengths and it is chosen the length which gives a better matching for the desired frequency.

5.3.2 Transition using an impedance inverter

If bandwidth of the filter is not very wide, it can be used a simple impedance inverter that match the input impedance of 50Ω with the equivalence impedance of the SIW, using a transmission line of length equal to $\frac{\lambda}{4}$. Firstly, equivalence impedance of SIW is calculated as has been seen previously. Once this impedance has been obtained, it is designed the impedance inverter as follows:

1. Calculate impedance of transmission line

Impedance of transmission line is equal to:

$$Z_{in} = \frac{Z_0^2}{Z_L} \quad (5.13)$$

Then, Z_0 that is the impedance of the transmission line is obtained as $Z_0 = \sqrt{Z_L Z_{in}}$ where Z_L is the impedance of SIW and Z_{in} is 50Ω , at least in this case, actually it is the impedance that we would like to obtain at input/output.

2. Width of transmission line

Width of transmission line is computed to obtaine the desired impedance using the well-known formulas [3]:

$$\frac{w}{h} = \begin{cases} \frac{8e^A}{e^{2A}-2} & \text{if } w/h \leq 1 \\ \frac{2}{\pi} [B - 1 - \ln(2B - 1) + \frac{\epsilon_r - 1}{2\epsilon_r} (\ln(B - 1) + 0.39 - \frac{0.11}{\epsilon_r})] & \text{if } w/h \geq 1 \end{cases} \quad (5.14)$$

An example of transition using an impedance inverter can be seen in Fig. 5.6.

5.4 Experimental results

In this section an example of filter built with SIW technology will be shown. The aim is to obtain a filter whose bandwidth is 200MHz, its central frequency is 3 GHz and the order of the filter is four. Using the theory that has been developed previously, the structure of the filter that has been designed can be seen in Fig. 5.7.

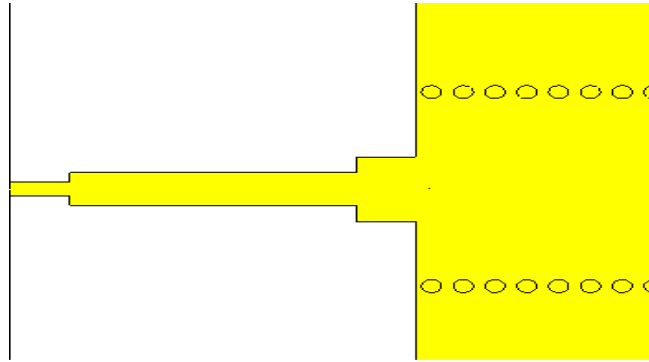


Figure 5.6: Transition using an impedance inverter

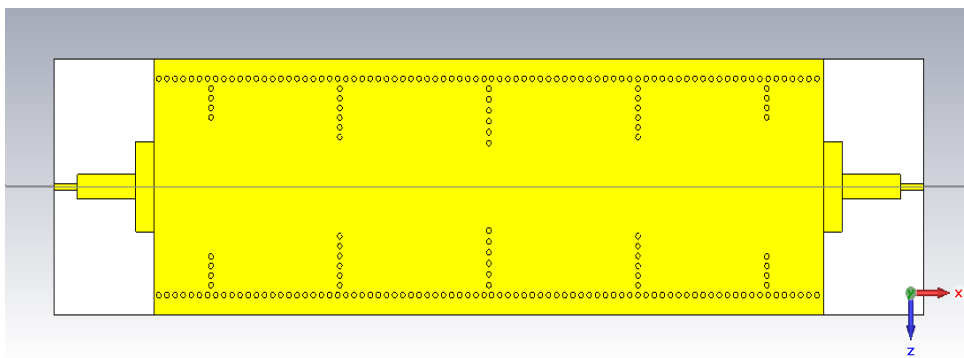


Figure 5.7: Structure of filter

Simulation results of this filter are split into two graphics, one of them shows S parameters and the other one shows the phase of the filter. In this case, the phase of the filter is really important because of the necessity of a linear phase, since the filter is integrated into a radar system, which needs an accurate phase measurement of the targets. Linear phase means that phase response is a linear function of the frequency. This is important to avoid a phase distortion due to the time delay of frequencies relative one to another. A phase distortion could cause errors in the signal processing known as BER (Bit Error Rate).

Finally, S parameters results are shown in Fig. 5.8 and phase results are shown in Fig. 5.9.

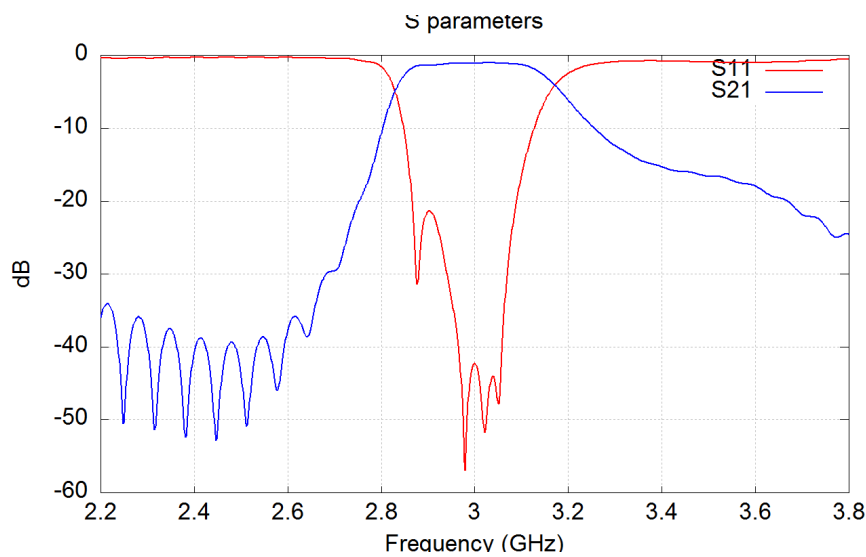


Figure 5.8: S parameters of filter SIW

It can be observed in Fig. 5.8 as the requirements are fulfilled. In Fig. 5.9 can be observed as the phase is almost linear, in the figure has been compared a straight line with the phase and it is good enough to consider it linear.

Therefore, this filter has been manufactured. The results obtained after measurements are shown in Fig. 5.10

Although the behaviour of the filter that has been manufactured is the same as the filter that has been simulated, it can be observed that the frequency has been shifted toward lower frequencies. This effect can be explained by several reasons, eg: substrate roughness, losses or variations of the permittivity... Typically, such a frequency shift is due to a variation in ϵ_r . Therefore, in order to achieve the real value of the ϵ_r , it is modified the value of ϵ_r in the full-wave simulation until the value is changed until both frequency responses are aligned, as can be seen in Fig. 5.11.

Once the new value of the ϵ_r has been calculated, the filter is resized to obtain the response that

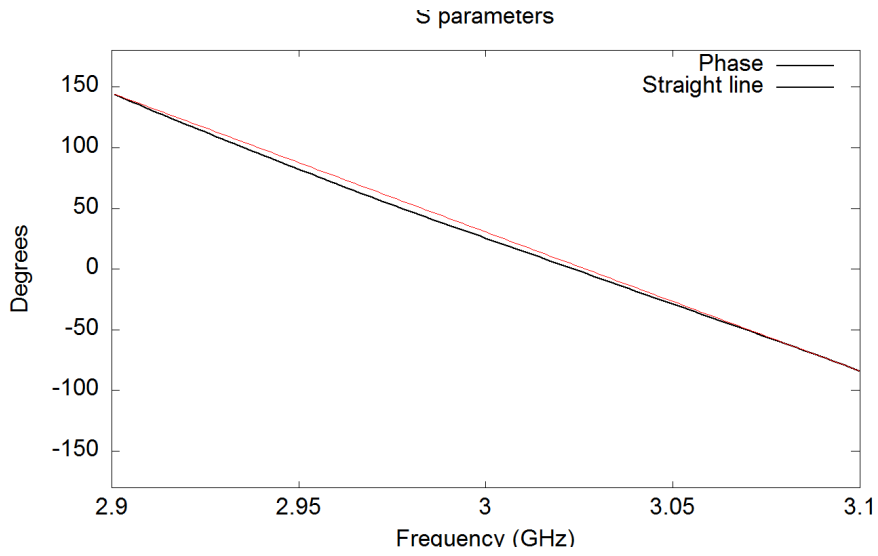


Figure 5.9: Phase of filter SIW

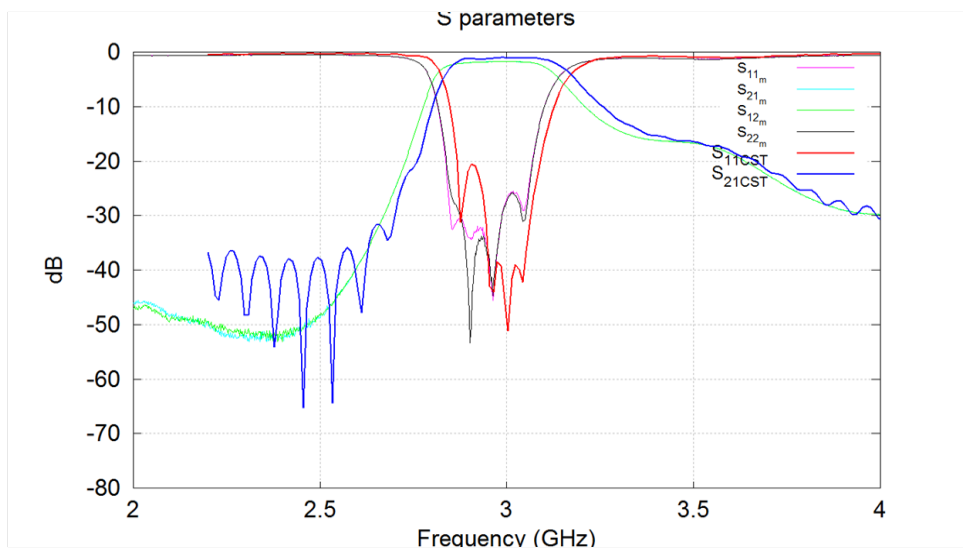


Figure 5.10: Comparison between the filter manufactured and fullwavesimulation

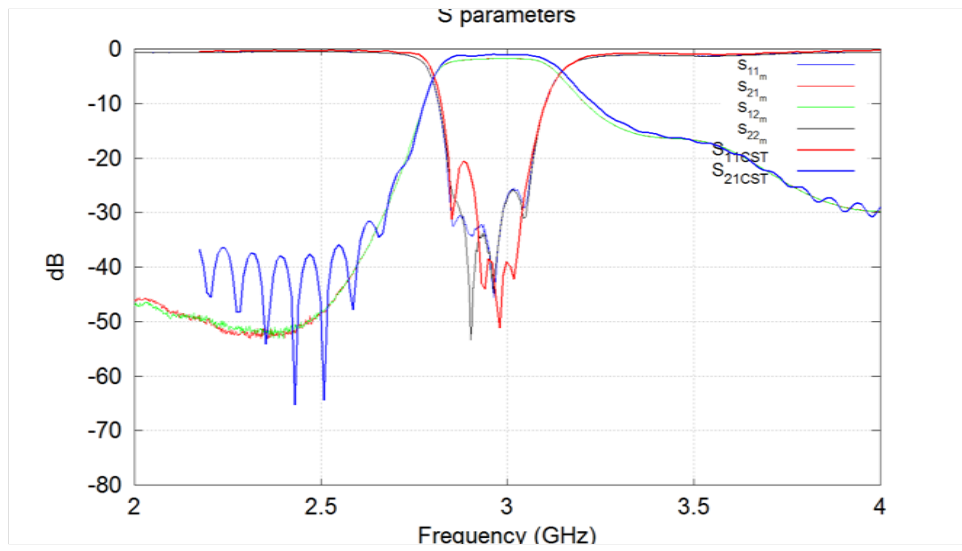


Figure 5.11: Comparison between the filter manufactured and fullwavesimulation with ϵ_r modified

we are looking for. Real and final filter that has been manufactured is shown in Fig. 5.12.



Figure 5.12: Final filter that has been manufactured with ϵ_r modified

Chapter 6

Techniques for size reduction

One of the requirements for the use of a filter into the AESA antenna demonstrator mentioned before, is to use a filter with reduced size. SIW technology has this advantage over traditional waveguide technology. However, for this particular project, the size that has been obtained using SIW technology is not small enough, the size of such a filter is still too big.

Therefore, other technologies are investigated in order to achieve the size reduction without lose the main behaviour of the filter. Basically, two designs have been proposed, firstly, a substrate integrated waveguide cavity loaded with a ring resonator. Secondly, a substrate integrated waveguide cavity loaded with complementary split ring resonator. That way, the final size of the filter has been reduced considerably.

6.1 Substrate Integrated Waveguide loaded with Ring Resonator

The idea of this technique is to use a cavity long enough to have two resonances, namely, f_{101} and f_{102} . Then, a ring resonator is etched on the top layer to perturb the electromagnetic field. These two resonances get closer if the ring becomes bigger. That way, a compact filter can be built.

According to [17], there are some empirical formulas to help with the design of the proposed filter. These formulas are:

$$W_{SIW} = \frac{0.58c}{f_0\sqrt{\epsilon_r}} \quad (6.1)$$

$$L_{SIW} = 1.895 \times W_{SIW} \pm 2d \quad (6.2)$$

$$R_c = 0.26 \times W_{SIW} \quad (6.3)$$

Where c is the light speed in free space, ϵ_r is the relative permittivity of the substrate, d is the diameter of the vias, W_{SIW} is the width of the SIW cavity, L_{SIW} is the length of this cavity and R_C is the radius of the hole etched in the top layer.

This filter presents two main characteristics, one of them is the small bandwidth. In principle, our bandwidth should be about 200 MHz, however this filter has a smaller bandwidth than the target. The filter concept can be still of interest, since it results to a rather reduced structure, actually, the overall size is only 74 mm x 45.2 mm. As has been said previously, the size in this application is quite important, even more important than the bandwidth. Moreover, another important parameter is the losses of the filter that are very low in this precise case.

In order to get a better idea of the filter, the geometry of this one can be seen in Fig. 6.1. In this case, the matching between the SIW cavity and the port of 50Ω is a transition which consists of an impedance inverter matching the 50Ω microstrip and the microstrip that match the impedance of the SIW. Also, the S parameters are shown in Fig. 6.2.

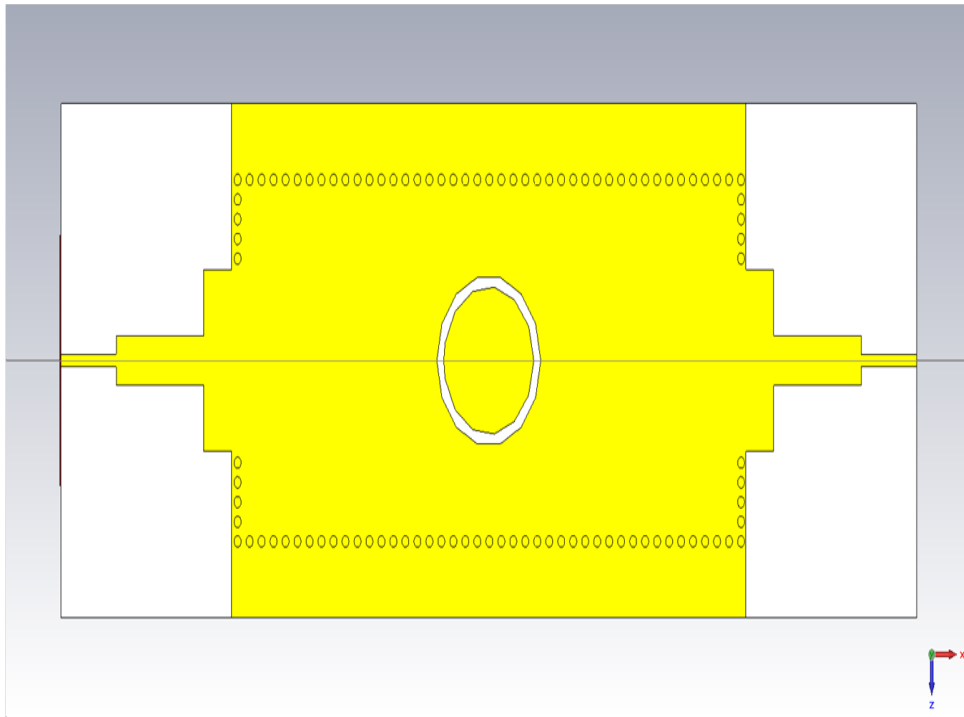


Figure 6.1: SIW cavity loaded with Ring Resonator

An important point that must be taken into account is the row of vias that are added at corner of the SIW. These vias are useful to obtain a better response. On the one hand, it is achieved a sharper skirt and wider stop-band and, on the other hand, it is reduced the insertion loss. Maybe this point is the most critical, at least in this application in which we need the minimum insertion loss.

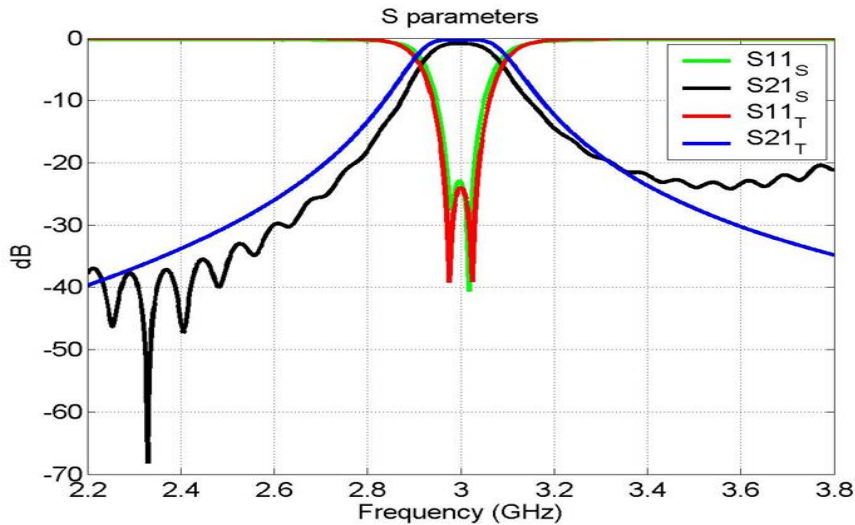


Figure 6.2: S parameter of SIW cavity loaded with Ring Resonator

6.2 Substrate Integrated Waveguide loaded with Complementary Split-Ring Resonator

Complementary Split-Ring Resonators (CSRRs) were introduced by Falcone in 2004 as new metamaterial resonators [18]. The structure of this CSRR and its equivalent-circuit model can be seen in Fig. 6.3. Combining these metamaterial resonators with other planar elements such as shunt stubs or series gaps, it is possible to achieve several microwave devices such as filters, duplexers and couplers.

In this case, it will be used a combination of CSRR and a substrate integrated waveguide to implement a backward-wave transmission below the waveguide cutoff. As has been shown in previous literature [19], Split Ring Resonators (SRRs) provide a stopband behaviour above the cutoff frequency. This behaviour is achieved using SRRs that are magnetically coupled to a waveguide, however if the structure SRR is resonant below the cutoff frequency, the stopband behaviour is switched to bandpass behaviour.

Afterward, this property will be used in order to build a bandpass filter using some resonators that will be coupled in the Substrate Integrated Waveguide [20].

6.2.1 Substrate Integrated Waveguide symmetrically loaded with Complementary Split Ring Resonator

Firstly, it should be said that according to [20] there are four configurations of SIW-CSRR unit cell. Depending on the configuration of the unit cell it is possible to obtain a different behaviour for each

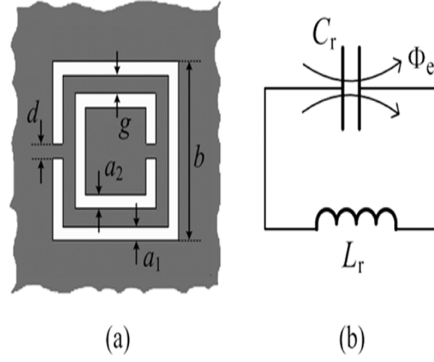


Figure 6.3: Structure of Complementary Split Ring Resonator and its equivalent-circuit model

one. Configurations of the unit cell can be seen on Fig. 6.4 and its different behaviour is shown in Fig. 6.5.

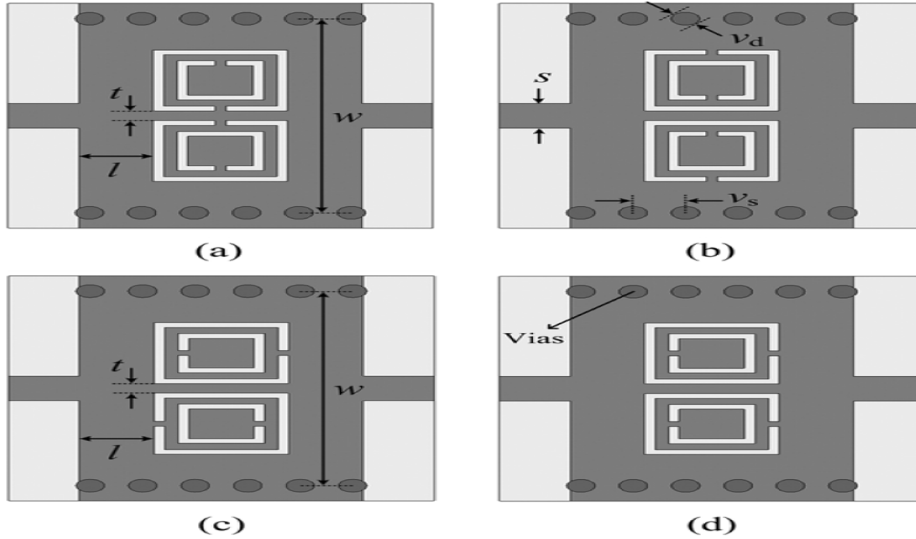


Figure 6.4: Configurations of CSRR unit cell: (a) face-to-face, (b) back-to-back, (c) side-by-side reversely oriented and (d) side-by-side equally oriented

In our case, the configuration that will be used is face-to-face orientation. Consequently, using this configuration, the steps to design the filter with CSRR are as follows:

1. Resonator dimension

First step is to determine the dimension of the first resonator CSRR. There is an equivalent circuit model [21] that is useful to obtain some initial values.

These initial values can be determined because the resonance frequency of the CSRR is given by $f_0 = (L_s C_s)^{-1/2} / 2\pi$, where L_s is the inductance of a single ring with average radioud r_o and width c and C_s is the series capacitance of the upper and the lower halves of the CSRR.

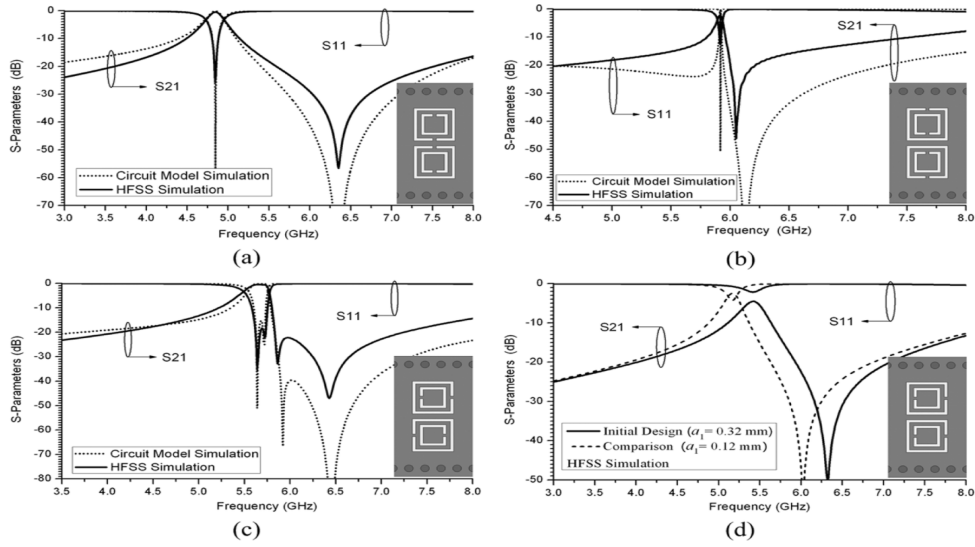


Figure 6.5: Simulations of different Configurations of CSRR unit cell: (a) face-to-face, (b) back-to-back, (c) side-by-side reversely oriented and (d) side-by-side equally oriented

Afterward, CSRR unit-cell is simulated and modified to achieve Q_e which has been determined by the low-pass prototype. Empirical Q_e that is obtained simulating the unit-cell is computed by the next formula:

$$Q_e = \frac{2f_0}{\Delta f_{3db}} \quad (6.4)$$

The modifications that can be done in the CSRR unit-cell are as follows:

- CSRR dimension

Above all, modification of CSRR dimension is important if the resonance frequency is not the frequency that we are looking for. The bigger is the resonator, the lower is the resonance frequency.

- Distance l

Quality factor is practically determined by this distance. If the port is closer to the resonator, Q_e is lower, therefore if we would like a bigger Q_e , we should make the distance l bigger.

- Distance t

This parameter does not influence strongly the response of the resonator, but it modifies slightly the bandwidth. When the distance t is smaller, which means the middle strip is thinner, the bandwidth turns out to be smaller.

2. Coupling coefficients

Once the resonator CSRR dimensions have been determined, the next step is to calculate the distance between both resonators, in order to obtain the desired coupling coefficient from the theoretical model. The structure that has to be simulated can be seen in Fig. 6.6.

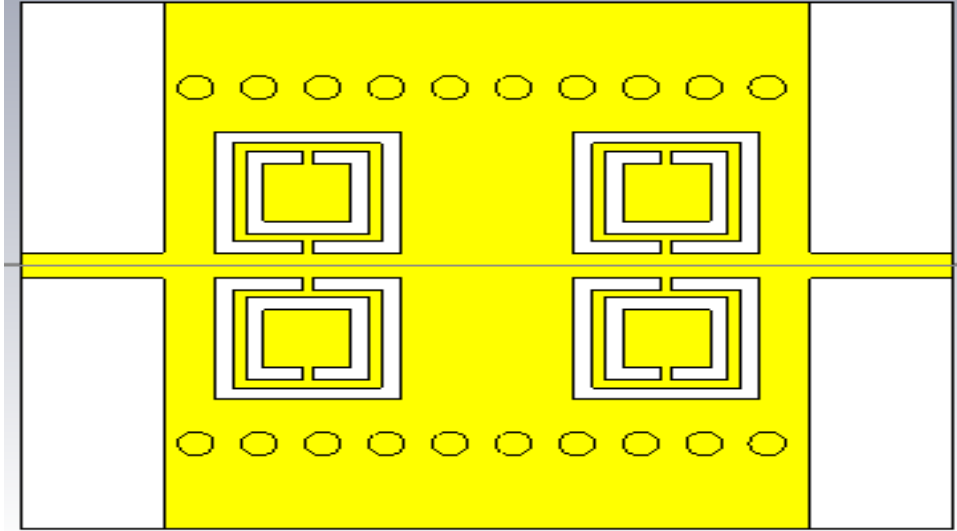


Figure 6.6: Structure of two order CSRR to calculate coupling coefficient

The full-wave simulation results of the structure are shown in Fig. 6.7.

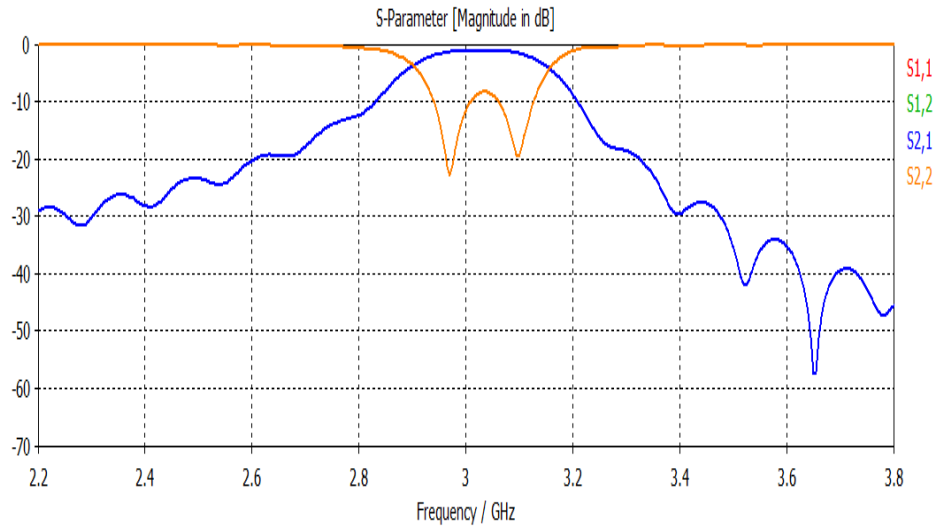


Figure 6.7: Response of two CSRR coupled

Then the coupling coefficient of coupled resonators can be extracted using the following relation:

$$M = \frac{f_1^2 - f_2^2}{f_1^2 + f_2^2} \quad (6.5)$$

Where f_1 and f_2 represents the lower and higher frequency, respectively. Furthermore, it should be taken into account that the closer are the resonators the bigger is the coupling coefficient.

3. CSRR scaled

Last step is to scale the inner resonator in order to adjust its resonance frequency. In that case, the inner resonator has been increased by a factor $k = 1.015$. The structure of the three-stage complete filter is shown in Fig. 6.8.

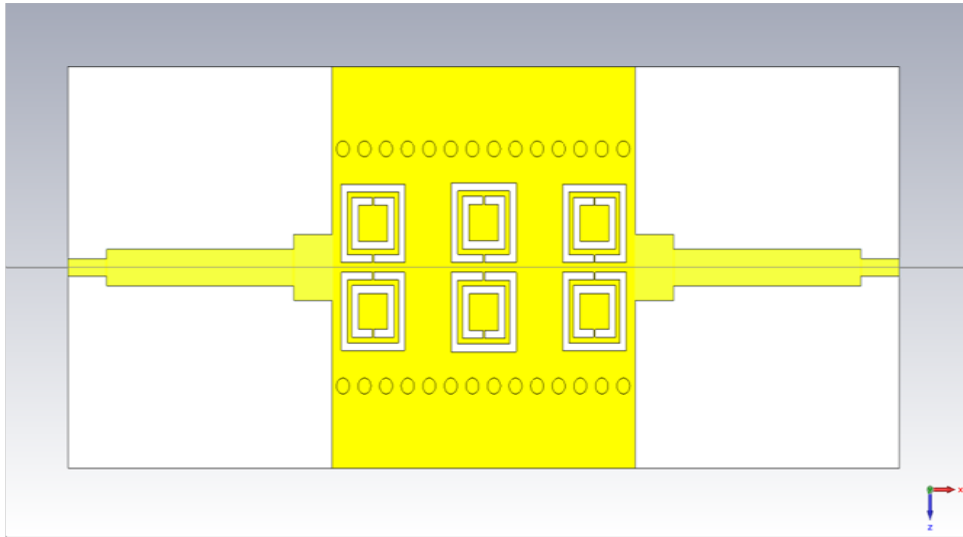


Figure 6.8: Structure of Complementary Split Ring Resonator Filter

The full-wave simulation results of the optimized filter are shown in Fig. 6.9 (S-Parameters) and in Fig. 6.10 (Phase Response).

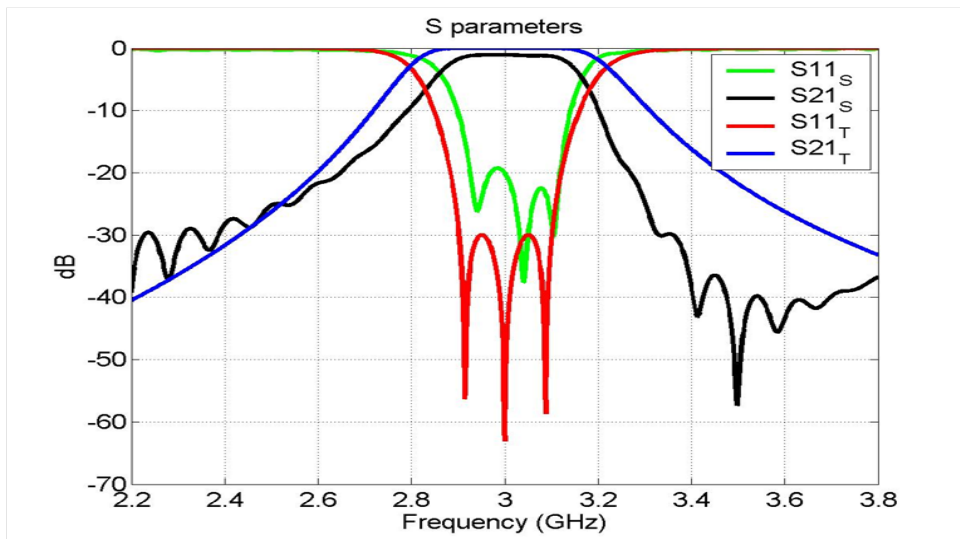


Figure 6.9: S parameter of Complementary Split Ring Resonator Filter

The S-Parameters shown in Fig. 6.9 are compared with the theoretical response of a three order filter whose bandwidth is 200 MHz. The conclusion that we can obtain from this comparison is that the filter has a smaller bandwidth than the initially specified but the rejection of the higher frequencies is stronger than specified. On the one hand, the filter dimensions are very reduced (64.74 mm x 24.2 mm). On the other hand, the insertion losses are relatively high (1.17 dB). However, compared to other technologies, for the given filter order, losses are low and the filter is very compact.

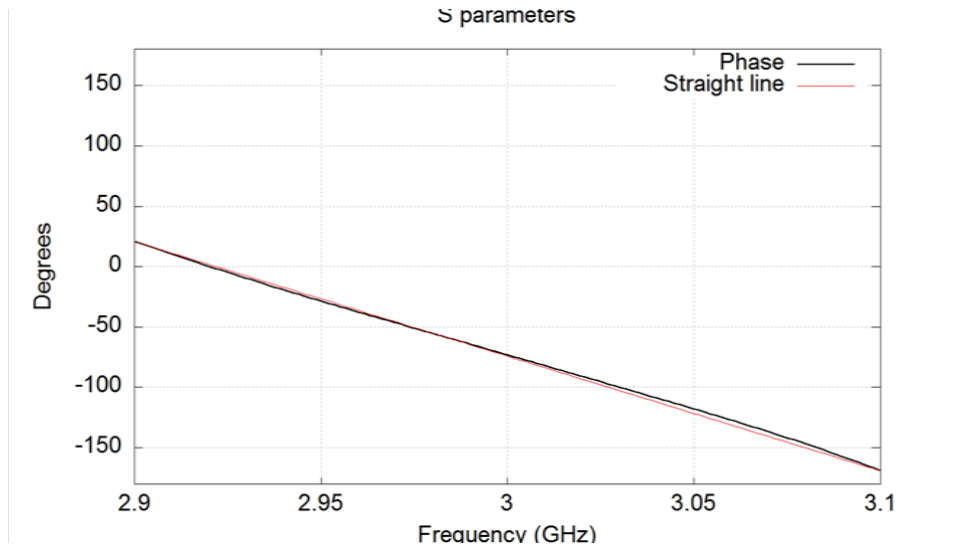


Figure 6.10: Phase of Complementary Split Ring Resonator Filter

In Fig. 6.10 the simulated phase response of the filter is compared to a straight line, showing that it is almost linear.

6.2.2 Substrate Integrated Waveguide Asymmetrically loaded with Complementary Split Ring Resonator

Finally, an example of SIW loaded with CSRR has been used, in order to reduce even more the losses with such reduced size, it is a SIW loaded with CSRR but only in the bottom half. The procedure to design the filter is exactly the same as filter with CSRR in both top and bottom half. Firstly, the resonator is tuned, secondly the coupling coefficient is computed and finally, the center resonator is scaled. The structure of this filter is shown in Fig. 6.11 and its simulation results are shown in Fig. 6.12.

Length of the filter is 61.6 mm and width is 24.2 mm, therefore, the filter dimensions meet with the specifications.

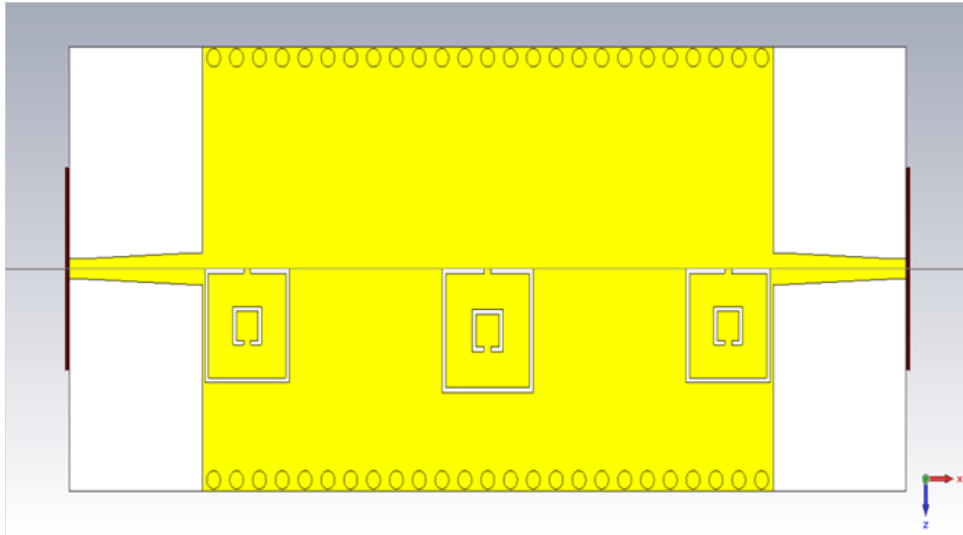


Figure 6.11: Structure of Complementary Split Ring Resonator Filter asimetrically loaded

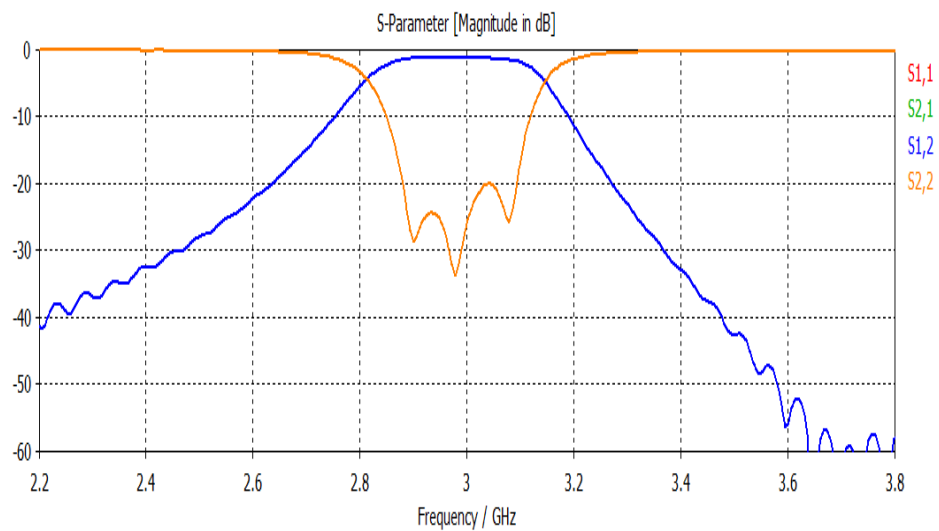


Figure 6.12: S parameter of Complementary Split Ring Resonator Filter asimetrically loaded

Moreover, insertion losses are 1.04 dB, which can be sufficiently low for the intended application. Insertion losses of this filter are 0.13dB less than the previous one where the filter is built with two rows of CSRR. This fact could be determined by the length of the filter, due to this one is shorter than the filter with two rows.

6.3 Intedigital Filter using μ Strip technology

An interdigital filter consists of an array of n TEM-mode or quasi-TEM-mode transmission line that behaves as half-wave resonators in the midband frequency. Each transmission line is short-circuited at one end and open-circuited at the other with alternative orientation [2]. Fig. 6.13 shows a type of interdigital bandpass filter.

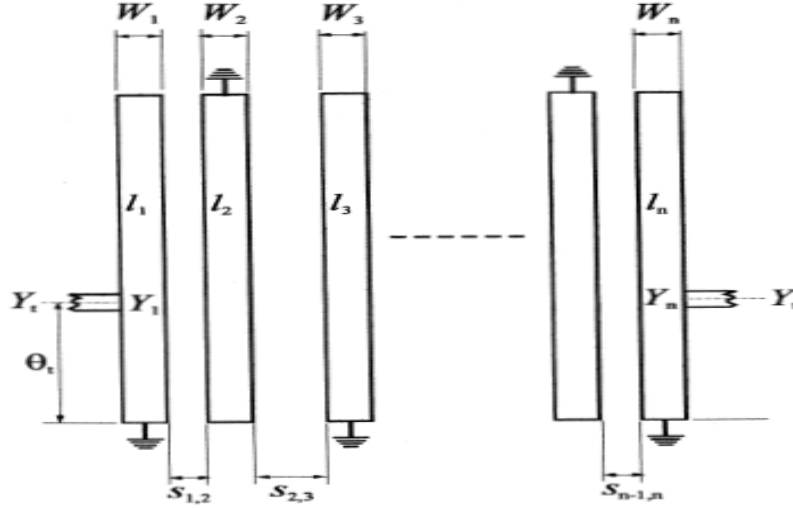


Figure 6.13: General configuration of interdigital bandpass filter

Physical dimensions of the transmission lines can be different, both the lengths ($l_1, l_2 \dots l_n$) and the widths ($W_1, W_2 \dots W_n$) or only the length. In our case case, filter is built with symmetric coupled lines, which means that all resonators have the same line widths. The filter input and output use tapped lines with a characteristic admittance Y_t , which may be set to equal the source/load characteristic admittance Y_0 . An electric length θ_t , measured away from the short-circuited end of the input/output resonator, indicates the tapping position, where $Y_1 = Y_n$ denotes the single microstrip characteristic impedance of the input/output resonator. For the type of bandpass filter with tapped-line I/O in Fig. 6.13 there are design equations given by:

$$\theta = \frac{\pi}{2} \left(1 - \frac{FBW}{2} \right), Y = \frac{Y_1}{\tan \theta} \quad (6.6)$$

$$J_{i,i+1} = \frac{Y}{\sqrt{g_i g_{i+1}}} \quad \text{for } i = 1 \text{ to } n - 1 \quad (6.7)$$

$$Y_{i,i+1} = J_{i,i+1} \sin \theta \quad (6.8)$$

$$C_1 = \frac{Y_1 - Y_{1,2}}{v}, C_n = \frac{Y_1 - Y_{n-1,n}}{v} \quad (6.9)$$

$$C_i = \frac{Y_1 - Y_{i,i-1} - Y_{i,i+1}}{v} \quad \text{for } i = 2 \text{ to } n - 1 \quad (6.10)$$

$$C_{i,i+1} = \frac{Y_{i,i+1}}{v} \quad \text{for } i = 1 \text{ to } n - 1 \quad (6.11)$$

$$Y_t = \frac{Y_1 - Y_{1,2}^2}{Y_1} \quad (6.12)$$

$$\theta_t = \frac{\sin^{-1}(\sqrt{\frac{Y \sin^2 \theta}{Y_o g_o g_1}})}{1 - \frac{FBW}{2}} \quad (6.13)$$

$$C_t = \frac{\cos \theta_t \sin^3 \theta_t}{\omega_o Y_t (\frac{1}{Y_o^2} + \frac{\cos^2 \theta_t \sin^2 \theta_t}{Y_t^2})} \quad (6.14)$$

where FBW is the fractional bandwidth and g_i represents the element values of a ladder type of lowpass prototype filter. C_i ($i = 1$ to n) are the self-capacitances per unit length for the line elements, whereas $C_{i,i+1}$ ($i = 1$ to $n - 1$) are the mutual capacitances per unit length between adjacent line elements. v denotes the wave phase velocity in the medium of propagation. The physical dimensions of the line elements may then be found from the required self and mutual capacitances.

Once the width of the line is fixed and the length is calculated to be half-wave resonator, the final step is to determine the distance between resonators, so the desired coupling is obtained. For the case in which the line widths are equal, coupling is as follows:

$$k_{i,i+1} = \frac{Z_{0ei,i+1} - Z_{0oi,i+1}}{Z_{0ei,i+1} + Z_{0oi,i+1}} \quad (6.15)$$

where:

$$Z_{0e1,2} = \frac{1}{Y_1 - Y_{1,2}}, Z_{0o1,2} = \frac{1}{Y_1 + Y_{1,2}} \quad \text{for } i = 2 \text{ to } n - 2 \quad (6.16)$$

$$Z_{0oi,i+1} = \frac{1}{2Y_{i,i+1} + 1/Z_{0ei,i+1}} \quad i = 2 \text{ to } n - 2 \quad (6.17)$$

$$Z_{0en-1,n} = \frac{1}{Y_1 - Y_{n-1,n}}, Z_{0on-1,n} = \frac{1}{Y_1 + Y_{n-1,n}} \quad (6.18)$$

where $Z_{0ei,i+1}$ and $Z_{0oi,i+1}$ are the even- and odd- mode impedances of the coupled lines associated with resonators i and $i+1$.

In Fig. 6.14 is shown an interdigital bandpass filter in microstrip technology.

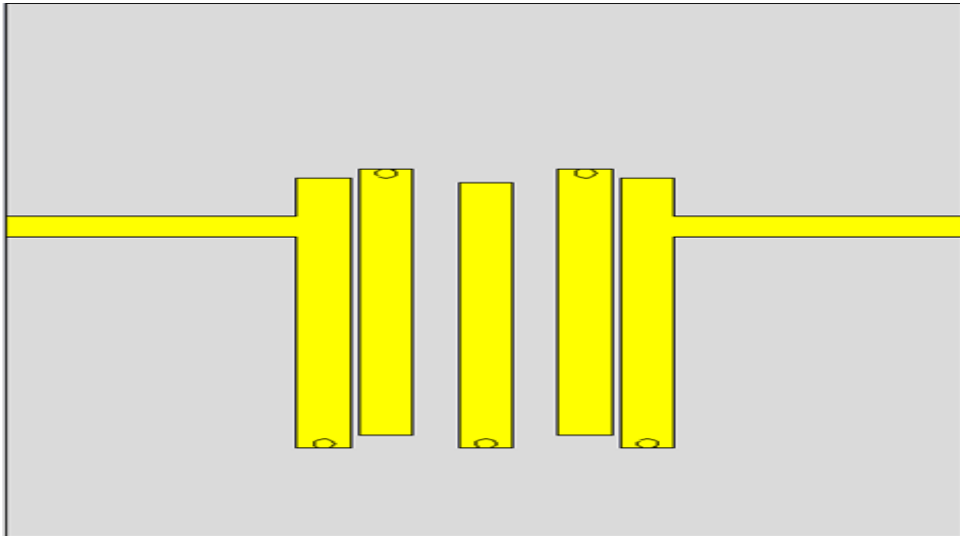


Figure 6.14: Structure of Interdigital Filter

The filter dimensions meet specification comfortably since the size of the filter is only 23.1 mm x 29.05 mm. In Fig. 6.15 is shown the simulation results of the interdigital filter shown in Fig. 6.14. As can be observed, the response is quite good because the rejection out-of-band is below 20 dB, as specified in the design rules. This kind of interdigital filter offers the advantage of the position of the second passband, since the resonators are quarter-wavelength long using the grounding, the second passband is centered at about three times the midband frequency.

However, an important point is the insertion losses. As has been said before, the aim is to achieve the minimum insertion losses. The full-wave simulation results show an insertion loss of about 1.6 dB, and the possibilities to improve them are rather reduced. Consequently, when compared with other technologies, this filter approach has to be dismissed.

The phase of the interdigital filter inside the passband is almost linear as can be deduced observing Fig. 6.16.

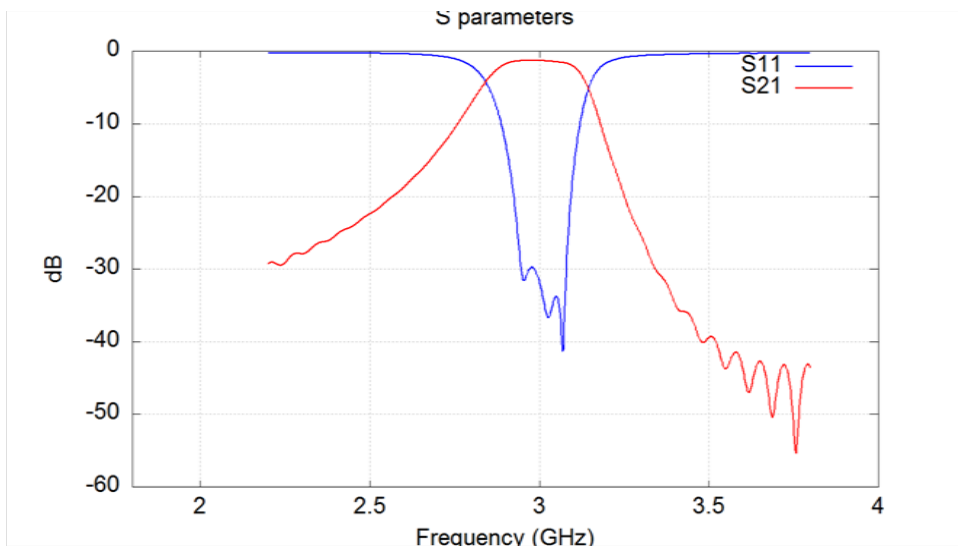


Figure 6.15: S parameter of Interdigital Filter

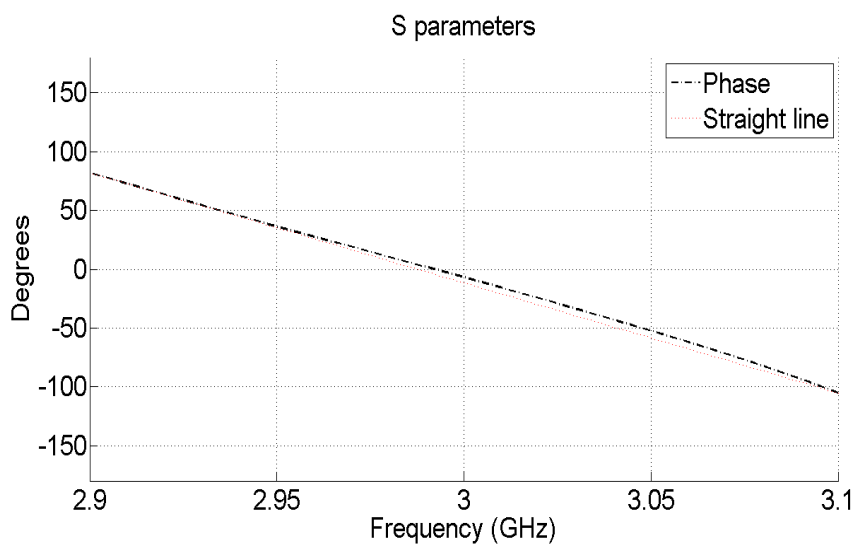


Figure 6.16: Phase of Interdigital Filter

Chapter 7

Conclusions and future work

In this project, two new strategies for the reduction of the spurious level in waveguide bandpass filters has been proposed. The first strategy consists on the design of filters using non-uniform coupling windows along the filter. The second one consist on the design of filters using non-uniform cavities along the filter. In addition, the two strategies are combined, resulting into non-uniform coupling windows with different cavities along the filter.

Using the first strategy proposed, it has been verified that the use of input coupling windows with big thickness and the internal one with small thickness is the best option. Thus, an important reduction of the spurious bandwidth has been achieved, although the spurious is not removed completely. Using the second strategy proposed, it has been verified a that a further reduction is possible. However the reduction is not as significant as in the case of different thicknesses, specially when only one cavity is modified. Finally, using the third and last strategy, it has been verified an important reduction of the spurious bandwidth, achieving attenuation levels of -40 dB for the spurious band although there is a resonant peak that has not been removed.

In addition, filter structures have been investigated using SIW technology, for a specific radar application being developed at the Fraunhofer institute. First, the filter has been designed using SIW technology. The electrical characteristics of the filter are acceptable for the application. However, the size of the structure was large. Due to this fact, some techniques for size reduction were investigated. These alternatives were based on the use of Ring Resonators and Complementary Split Ring Resonators (CSRR) to load SIW cavities. With these techniques the size of the filter has been reduced considerably. Therefore using these alternatives, which are based on metamaterial concepts (Complementary Split Ring Resonator), are proven to be useful.

As future work, it can be of interest to develop accurate circuital models of the SIW filters loaded

with CSRR, since the obtained results are superior and the filter size is very reduced, in comparison to other technologies. Furthermore, with the proper circuital modelling of the filter, it would be possible to design the complete structure without full-wave simulations.

As a final conclusion of the work, it can be observed a quick and visual comparison between different technologies in the next Tab. 7.1.

	Dimensions	Selectivity	Losses	Bandwidth
Traditional SIW Filter	✗ 14.2cm x 4.5cm	✗ Not enough	- 1.08 dB	✓ 200 MHz
SIW Ring Resonator	✓ 7.4cm x 4.2cm	✓ Meet Specifications	✓ 0.87 dB	✗ 57.4 MHz
SIW CSRR	✓ 6.47 cm x 2.44 cm	✓ Meet Specifications	✗ 1.17 dB	✓ 200 MHz
Assymetric SIW CSRR	✓ 6.1 cm x 2.44 cm	✓ Meet Specifications	✓ 1.04 dB	✓ 200 MHz
Interdigital	✓ 2.31 cm x 2.9 cm	✓ Meet Specifications	✗ 1.6 dB	✓ 200 MHz

Table 7.1: Table of the comparison between different technologies

Chapter 8

Appendix

8.1 Table of Dimensions

Tables 8.1,8.2 and 8.3 include the geometric data for all the irises and resonators designed using the procedure described in Section 2.6.2 and 2.6.1. The tables include the data of the irises corresponding to the three impedance inverters of the filter ($i = 1, 2, 3$) and for all the thicknesses of the irises ($j = 1, 2, \dots, 12$). The length specified in these tables is the half length to the iris attached to the corresponding resonator. The length of the final cavity resonator is actually composed of the two half lengths corresponding to the two irises attached to the corresponding resonator.

8.1.1 Table of the first coupling window

Thickness (mm)	Width (mm)	Length of the Cavity(mm)
1	8.1093	8.2655
2	8.9182	7.9545
3	9.58	7.6548
4	10.1324	7.3595
5	10.5994	7.070
6	11.001	6.7880
7	11.349	6.5147
8	11.6515	6.2497
9	11.9063	5.9703
10	12.132	5.7278
11	12.334	5.4893
12	12.5118	5.2606

Table 8.1: Table of the first coupling window

8.1.2 Table of the second coupling window

Thickness (mm)	Width (mm)	Length of the Cavity(mm)
1	4.259	9.4859
2	5.1217	9.2696
3	5.8857	9.1082
4	6.5398	8.943
5	7.1131	8.744
6	7.6266	8.406
7	8.0876	8.435
8	8.5025	8.2676
9	8.8781	8.0997
10	9.2243	7.9337
11	9.5367	7.7700
12	9.8243	7.6088

Table 8.2: Table of second coupling window

8.1.3 Table of the third coupling window

Thickness (mm)	Width (mm)	Length of the Cavity(mm)
1	3.779	9.5076
2	4.642	9.3635
3	5.393	9.2206
4	6.050	9.0733
5	6.626	8.922
6	7.1415	8.768
7	7.6088	8.614
8	8.0330	8.459
9	8.418	8.305
10	8.771	8.150
11	9.095	7.998
12	9.393	7.847

Table 8.3: Table of third coupling window

8.2 Code of Matlab to compute the impedance inverters

```

%Specifications of the filter
RL = -25;
BW = 2*pi*100e6;
wo = 2*pi*11e9;
wa = (wo-BW/2);
wb = (wo+BW/2);
lambdac = 2*0.01905;
wc = 2*pi*3e8/lambdac;
n = 5;

%It is computed the elements g
Beta = log(Lar/17.37);
gamma = sinh(Beta/(2*n));
a = zeros(1,n);
b = zeros(1,n);
g = zeros(1,n+1);
go=1;
for k = 1:n
    a(k) = sin((2*k-1)*pi/(2*n));
    b(k) = gamma^2 + (sin(k*pi/n))^2;
end
g(1)=2*a(1)/gamma;
for k = 2:n
    g(k) = 4*a(k-1)*a(k)/(b(k-1)*g(k-1));
end
if rem(n,2) ~= 0
    g(n+1) = 1;
else
    g(n+1) = (coth(Beta/4))^2;
end
g = abs(g);

%It is computed the impedance inverters
c = 3e8;
ko1=1/sqrt(go*g(1));
w = BW/wo;
lambdaa = 2*pi*c/wa;
lambdab = 2*pi*c/wb;
lambdao = 2*pi*c/wo;

```

```
lambdaga = lambdaa/(1-(wc/wa)^2)^(1/2);
lambdagb = lambdaab/(1-(wc/wb)^2)^(1/2);
lambdago = (lambdaga+lambdagb)/2;
x = pi/2*(lambdago/lambdao)^2;
Ko1 = ko1*sqrt(w*x(1));
K = zeros(1,n);
k = zeros(1,n);
for i = 1:n
    k(i) = 1/sqrt(g(i)*g(i+1));
end
for j = 1:n-1
    K(j) = w*sqrt(x(j)*x(j+1))*k(j);
end
K(n) = k(n)*sqrt(w*x(5));

%It is computed S21
S21 = zeros(1,n);
S21(1)=20*log10(2/(Ko1+1/Ko1));
for z = 2:n+1
    S21(z) = 20*log10(2/(K(z-1)+1/K(z-1)));
end
```

Bibliography

- [1] Seymour B. Cohn, Ralph Levy, *History of Microwave Passive Components with Particular Attention to Directional Couplers* IEEE Transactions on Microwave Theory and Techniques, Vol MTT-32, No.9, September 1984.
- [2] J.S. Hong, M.J. Lancaster, *Microstrip filters for RF/Microwave Applications*, John Wiley & Sons, 2001, USA.
- [3] David M. Pozar, *Microstrip Engineering*, Addison-Wesley, 1990.
- [4] Felice Maria Vanin, *Dimension Synthesis for Rectangular Inductive Iris Filters*, ESTEC
- [5] Wolfgang Menzel, Andreas Muller, Frank Bogelsack, “A Capacitively Coupled Waveguide Filter with Wide Stop-Band,” *Proceedings of 33rd European Microwave Conference*, Munich, 9th October 2003.
- [6] Wolfgang Menzel, Andreas Muller, Frank Bogelsack, “A Capacitively Coupled Waveguide Filter with Wide Stop-Band,” *Proceedings of 33rd European Microwave Conference*, Munich, 9th October 2003.
- [7] Ivan Arregui, et al., “A Compact Design of High-Power Spurious-Free Low-Pass Waveguide Filter,” *IEEE Microwave and Wireless Components Letters*, Vol. 20, No. 11, pp. 595–597, November 2010.
- [8] L. Ge, J.P. Wang and Y.-X. Guo, “Compact microstrip lowpass filter with ultra-wide stopband,” *Electronics Letters*, Vol. 46, No. 10, pp. 689-691, May 2010.
- [9] G.L. Matthaei, Leo Young, E.M.T Jones, *Microwave filters, impedance matching-networks and coupling structures*, Artech House, 1980, Boston, Massachusetts, USA.
- [10] Alan V. Oppenheim, Ronald W. Schaffer *Discrete-Time Signal Processing* Pearson.

- [11] Li Yan, Wei Hong, Guang Hua, Jixin Chen, Ke Wu and Tie Jun Cui. *Simulation and Experiment on SIW Slot Array Antennas* IEEE Microwave and Wireless Components Letters. VOL. 14, NO. 9, SEPTEMBER 2004.
- [12] Seymour B. Cohn, "Direct-Coupled-Resonators Filters," *Proceedings of the IRE*, vol.45 , no. 2, pp. 187-196, Feb. 1957.
- [13] C. Vicente, et. al., "FEST3D - A Simulation Tool for Multipactor Prediction," *International Workshop on Multipactor, Corona and Passive Intermodulation in Space RF Hardware*, ESTEC, Noordwijk, The Netherlands, pp. 11-17, Sept. 2005.
- [14] Dominic Deslandes, "Accurate Modeling, Wave Mechanism, and Design Considerations of a Substrate Integrated Waveguide" *IEEE Transactions on Microwave Theory and Techniques*, VOL. 56, NO. 6, June. 2006.
- [15] Feng Xu and Ke We, "Guided-Wave and Leakage Characteristics of Substrate Integrated Waveguide" *IEEE Transactions on Microwave Theory and Techniques*, VOL. 53, No. 1, January 2005
- [16] Dominic Deslandes, "Design Equations for Tapered Microstrip-to-Substrated Integrated Waveguide Transitions" *IEEE Letters*
- [17] Changjun Liu, Kama Huang, "A Compact Substrate Integrated Waveguide Band-pass Filter" *Progress In Electromagnetics Research Symposium Preceedings, Cambridge, USA, 2010*
- [18] F. Falcone, T. Lopetegi, J.D. Baena, R. Marques, F. Martin, and M. Sorolla, "Effective negative- ϵ stopband microstrip lines based on complementary split ring resonators" *IEEE Microwave Wireless Components Letter*, Vol. 14, no. 6, pp 280-282, Jun. 2004
- [19] J. Bonache, F. Falcone, T. Lopetegi, J. Garca-Garca, R. Marques, F. Martin, and M. Sorolla, "Spurious Passband Suppression in Microstrip Coupled Line Band Pass Filters by Means of Split Ring resonators" *IEEE Microwave Wireless Components Letter*, Vol. 14, no. 9, pp 280-282, Sept. 2004
- [20] Yuan Dan Dong, Tao Yang and Tatsuo Itoh, "Substrate Integrated Waveguide Loaded by Complementary Split-Ring Resonators and Its Applications to Miniaturized Waveguide Filters" *IEEE Transactions on Microwave Theory and Techniques*, VOL. 57, NO. 9, September 2009
- [21] Juan Domingo Baena, Jordi Bonache, Ferran Martn, Ricardo Marqus Sillero, Francisco Falcone, Txema Lopetegi, Miguel A.G. Laso, Joan Garca-Garca, Ignacio Gil, Maria Flores Portillo and

Mario Sorolla “Equivalent-Circuit Models for Split-Ring-Resonators and Complementary Split-Ring Resonators Coupled to Planar Transmission Lines ” *IEEE Transactions on Microwave Theory and Techniques*, VOL. 53, NO. 4, September 2005